Spring 1988

Dynamics of the solar atmosphere: Spicules and fibrils

Alphonse Christopher Sterling
University of New Hampshire, Durham

Order Number 8816700

Dynamics of the solar atmosphere: Spicules and fibrils

Sterling, Alphonse Christopher, Ph.D.

University of New Hampshire, 1988

U·M·I
300 N. Zeeb Rd.
Ann Arbor, MI 48106

PLEASE NOTE:

In all cases this material has been filmed in the best possible way from the available copy. Problems encountered with this document have been identified here with a check mark __✓__.

1. Glossy photographs or pages _____
2. Colored illustrations, paper or print _____
3. Photographs with dark background _____
4. Illustrations are poor copy _____
5. Pages with black marks, not original copy __✓__
6. Print shows through as there is text on both sides of page _____
7. Indistinct, broken or small print on several pages __✓__
8. Print exceeds margin requirements _____
9. Tightly bound copy with print lost in spine _____
10. Computer printout pages with indistinct print _____
11. Page(s) _____ lacking when material received, and not available from school or author.
12. Page(s) _____ seem to be missing in numbering only as text follows.
13. Two pages numbered _____. Text follows.
14. Curling and wrinkled pages _____
15. Dissertation contains pages with print at a slant, filmed as received __✓__
16. Other _____

_____

_____

DYNAMICS OF THE SOLAR ATMOSPHERE: SPICULES AND FIBRILS

BY

ALPHONSE CHRISTOPHER STERLING
B.S., California Institute of Technology, 1981

DISSERTATION

Submitted to the University of New Hampshire
in Partial Fulfillment of
the Requirements for the Degree of

Doctor of Philosophy
in
Physics

MAY, 1988

This dissertation has been examined and approved.

Joseph V. Hollweg
Dissertation director, J.V. Hollweg
Director, Solar-Terrestrial Theory Group
Research Professor of Physics

Terry G. Forbes
Research Associate Professor of Physics

John A. Lockwood
Professor of Physics

Harvey Shepard
Harvey Shepard
Chairman, Physics Department
Professor of Physics

Robert E. Simpson
Robert E. Simpson
Associate Professor of Physics

December 18, 1987
Date

To my mother and father -

two of the hardest working persons I know.

ACKNOWLEDGEMENTS

The work for this dissertation has been supported by the NASA Graduate Student Researchers Program under grant NGT-29-004-800, the NASA Solar-Terrestrial Theory Program under Grant NAGW-76, and by NASA Grant NSG-7411. I thank the staff of the University of New Hampshire Research Computing Center for the use of their PRIME computing facilities. I am grateful to many collegues, instructors, staff members, and friends who have assisted me in various ways during the years of my graduate studies; a partial list of these individuals follows. I owe a special thanks to Tom Milliman and John Perko, who have helped me overcome many computer problems. Persons who have assisted me with the scientific aspects of this dissertation include Terry Forbes, Phil Isenberg, Martin Lee, John Mariska, Bernard Roberts, and Chuck Smith. I am grateful to Kathy Theall, who in addition to typing much this dissertation, has given me reliable assistance in many instances. I thank Pat Stevenson and Dot Kittredge for handling much of the paper work associated with my studies. I acknowledge the Physics Department librarian, Becky Marden, for her assistance, conversation, and infinite patience when I would return books late. Many of the accurate figures of this work have been drafted by Sherry Palmer and Bob Weidknecht. Several others, including Chih Ping Ping, Jim Connally, Craig Pollock, and Parameswaran Sreekumar, have given me guidance and suggestions throughout the years. Most of my

gratitude, however, is reserved for my research advisor, Joseph Hollweg. He has enriched my life with cookouts, Thanksgiving dinners, sailing, and solar physics.

Table of Contents

List of Tables

List of Figures

ABSTRACT

DYNAMICS OF THE SOLAR ATMOSPHERE: SPICULES AND FIBRILS

by

Alphonse Christopher Sterling
University of New Hampshire, May, 1988

Numerical and analytical studies of MHD waves on magnetic flux tubes are applied to problems of the solar atmosphere. In particular, theoretical analysis of the chromospheric features known as spicules and fibrils are undertaken. The thesis consists of three principal segments:

(i) A preexisting spicule model is extended and developed. In the model, a series of rebound shocks propagating on a vertical magnetic flux tube results in chromospheric material with spicule-like properties below a raised transition region. The model emphasizes dynamic motions and shock heating, but excludes radiative and ionization losses. At long times, the model approaches a new hydrostatic equilibrium with the transition region remaining raised, and with a region of shock-heated chromosphere below it. The variation of the model properties in response to different initial parameters is investigated. One conclusion is that the model is capable of generating structures with properties consistent with

observations of spicules (with the exception of temperature) when only the dynamics is considered.

(ii) An analytical study is performed using linearized MHD equations to demonstrate that spicules may act as resonance cavities for MHD Alfven waves propagating along a vertical magnetic flux tube. When the resonances are excited, large amounts of wave energy from the photosphere and lower chromosphere can propagate into the spicule. This may result in the observed heating, fading, and twisting motions of spicules. It is assumed that the wave energy can be dissipated as heat via a turbulent cascade which follows a Kolmogorov spectrum.

(iii) The spicule model used in the first segment of the thesis is applied to a magnetic field geometry which is vertical through the photosphere and chromosphere, turns horizontal in the low corona, and eventually turns vertical again and extends into the outer corona. Radiative and ionization losses are again omitted. A structure develops on the horizontal segment which may be identifiable with a fibril, but a full spicule does not develop. At long times, the fibril and short spicule remain extended, and a standing wave develops on the flux tube.

INTRODUCTION

At first glance the sun appears to be a quiet, featureless globe. A more detailed examination, however, reveals a highly dynamic object which supports a variety of phenomena such as sunspots, plasma loops, and jets of gas. This myriad of features has kept the imaginations of astronomers and astrophysicists captivated throughout the histories of their disciplines. The sun is a natural object of intense interest to these scientists because it is the nearest star to earth, and the only one at present which can be studied in great detail. Additionally, the dynamics of the sun's features results from the interaction of the plasma, which makes up its atmosphere with the ubiquitous magnetic field; thus the sun is a natural laboratory for the physicist interested in plasmas and magnetohydrodynamics (MHD).

After thousands of years of speculation, hundreds of years of telescopic observations, and decades of newer observing techniques, including observations from space, a general picture of the sun and its workings is emerging. This thesis deals with spicules and fibrils. These features are a major aspect of the puzzle since they exemplify the complex nonlinear dynamics of energy and mass transport in the solar atmosphere.

The general goal of this thesis is to develop aspects of a theoretical model for spicules and fibrils. These phenomena, and indeed solar atmosphere dynamics in general, are controlled by nonlinear processes. Detailed investigations of such processes necessitates the use of computers. Thus a major portion of the work presented here is numerical. However, several problems have also been solved analytically, both to complement the numerics and to develop a new theoretical idea for heat and energy transport in spicules.

The dissertation will commence with a review of spicule and fibril properties and theoretical models in the first chapter. After some mathematical and MHD development in Chapters 2 and 3, new work and development on a current spicule model will be discussed in Chapter 4. A new idea for transferring energy and heat into spicules will then be presented in Chapter 5. Finally, some of the ideas developed with the spicule model of Chapter 4 will be modified to examine the possibly related fibril-type structures in Chapter 6.

As a prelude to the forthcoming chapters, the current understanding of the sun will be sketched in this Introduction. The dynamics of interest in this thesis is that which is present in *quiet sun* regions. These are regions which are most common on the sun, and lack the more peculiar features of *active regions*, such as sunspots, plages, etc.

Some general studies of the sun are Jordan (1981), Priest (1982), and Sturrock et al. (1986). Also see the centennial volume of Solar Physics (1985). On a somewhat simpler level, there is Giovalnelli (1984). Among the earlier texts are Zirin (1966) and Gibson (1972); these books contain valuable information on the tactics of the solar physicist, although some of the ideas they present are dated.

Overview of the Sun

The sun is a ball of gas composed mainly of hydrogen. It has a radius $R_0 = 6.96 \times 10^{10}$ cm to the surface seen with the unaided eye. Since it is in general not possible to observe photons originating below the surface, current ideas on the structure of the interior are due almost exclusively to theories developed to conform with observable features on the surface. In contrast to the interior, there exists a wealth of detailed observations of the sun from the surface outward, and so it is possible to give a much more descriptive survey of the solar atmosphere.

Solar Interior

Figure I.1 displays the solar interior. The core is the location of the source of energy. A consequence of the gravitational attraction of the sun's large mass is the production of extremely

high temperatures ($\approx 2 \times 10^7$ K) and pressures in the core. These conditions are amenable to the production of energy in the form of photons and energetic particles, including neutrinos, via thermonuclear reactions. Photons first diffuse away from the core by being randomly absorbed and re-emitted (radiated) by surrounding material. The region of the interior where this mode of energy transport occurs is called the *radiative zone*. The temperature and density decrease with distance from the solar center, and eventually the conditions require energy transport primarily via convection, i.e., mass motions. This occurs from about .75 R_0 to 1.0 R_0, in a region referred to as the *convection zone.* Upon reaching the surface, the convection manifests itself as the granulation (see Priest 1982, Fig. 1.8) and supergranulation (see Gibson 1972, Fig. 2.11).

One way in which the solar interior is directly observed is via observations of neutrinos produced in the core. The observed fluxes of these particles, however, do not coincide with the fluxes predicted by theory. This lacuna has been discussed extensively in the literature, and is known as *the solar neutrino problem.* (See reviews by Bahcall 1985 and Newman 1986 and references therein.) It is possible that the resolution to this dilemma between observation and theory resides in the field of elementary particle physics, but one cannot rule out the possibility of an error in our understanding of the energy production mechanism in the solar interior. We are therefore cautioned against believing that our picture of the sun is complete.

Photosphere

Moving outward from the interior and through the convection zone, the density of the solar sphere continues to drop to a point where the photons from the interior are not readily absorbed or scattered by the surrounding media. They escape into space much more freely at this boundary. Energy is once again carried outward mainly by the photons. Thus the surface, known as the *photosphere* (from the Greek word for light), is formed.

The photosphere represents the first of three principal layers of the *solar atmosphere*. One of the defining characteristics of the three atmospheric regions is the temperature. Figure I.2 shows the temperature as a function of radius for the solar atmosphere. At the base of the photosphere the temperature is $T \cong 6000$ K. The temperature continues to drop above the surface until a minimum value of some 4300 K is obtained at a height of approximately 500 km above the surface. (In this thesis, the term 'height' always refers to distance above the photospheric surface.) This level is referred to as the *temperature minimum*. At higher heights, atmospheric heating processes become dominant, and the temperature begins to rise with height. In the *chromosphere*, the second region of the solar atmosphere, the temperature is roughly 10^4 K. After some 2000 km the temperature again rises dramatically, going from 10^4 K to 10^5 K in a few hundred km. This

jump occurs in the *transition region* . The third principal layer of the solar atmosphere is the *corona*, a very hot (10^6 K), tenuous extended region above the transition region.

The most obvious feature of the photosphere is the *photospheric granulation*. Seen in white light, there are about a million granules on the sun at any time. The lifetime for an individual granule is about 8 minutes, and their diameters range from about 800 to 1500 km. Granules seem to be composed of hot upflowing material in their centers, and cooler downflowing material at their boundaries. Some granules, known as *exploding granules*, darken in their centers and expand radially at the end of their lives; recent high resolution observations by Title et al. (1987) suggest that exploding granules are quite common.

In addition to the granulation, there exists other scales of granulation visible in the photosphere. Among these is the *supergranulation*, with cell diameters ranging from 20,000 to 54,000 km and lifetimes of 1-2 days. Upward motions of 0.1 km s^{-1} at cell centers, horizontal outward flows of 0.3 or 0.4 km s^{-1}, and downward flows at the cell boundaries of 0.1 to 0.2 km s^{-1} are observed.

High resolution photographs of the photosphere reveal tiny bright elements concentrated at the supergranule boundaries. By comparing these photographs with magnetograms, it is seen that these features, called *network bright points*, are correlated with

regions of intense magnetic fields. Furthermore, little or no photospheric magnetic fields are found away from the bright points. This one to one correspondence between magnetic fields and bright points has led to the suspicion that the bright points are the channels for the magnetic flux exiting the convection zone. These magnetic channels, or flux tubes, have diameters of around 150-300 km (or perhaps smaller) and field strengths of 1 - 2 kilogauss. It is probable that the fluid motions of supergranules push these magnetic flux tubes to the supergranule boundaries. (The magnetic fields spread out above the photosphere; the average magnetic field strength of the sun in higher atmospheric layers is about a gauss.)

A review of quiet sun photospheric granulation and network bright points has been recently published by Muller (1985).

Chromosphere and Transition Region

The chromosphere ('color' sphere) is so named because it was first noticed as a red flash around the limb of the sun just before and just after the total phase of solar eclipses. The red color is attributed to the predominance of radiation in wavelengths in the red end of the spectrum, primarily that due to the n=3 to n=2 transition in atomic hydrogen (this is the H_α transition). The chromosphere is opaque when observed in this spectral line, and consequently, telescopes equipped with H_α filters will only see down to the chromosphere. Much of what has been learned about this

region of the sun's atmosphere has come from such H_α observations. Other spectral lines, such as Ca II, are also formed in and used in the study of the chromosphere.

The chromosphere is highly structured and nonuniform. This can be seen in the limb view in Figure 1.13a of Priest (1982). The jet-like features are the spicules, first described 110 years ago by Secchi (1877), and named for their appearance by Roberts (1945). These objects have lifetimes of five to ten minutes and reach a maximum height of some 10000 km. Spicules are an enigma in several respects; e.g., their upward velocities are non-ballistic, they have temperatures comparable to or higher than those of the chromosphere (implying the existence of some heating source), and they often fade from view after achieving their maximum height. A complete model of spicules will have to account for these and other observations outlined in the first chapter.

In disk views of the chromosphere (Priest 1982, Fig. 1.13b), the *chromospheric network* becomes visible; this network coincides with supergranule boundaries seen in the photosphere. Also visible is a multitude of fine structure, much of which can be seen at the perimeter of supergranule cells. This fine structure is composed of features which are generally dynamic, and often jet-like, in nature. Included among these features are bright and dark objects, known as the *bright mottles* and the *dark mottles*, which seem to be similar to the spicules seen on the limb. Which, if any, of these features correspond to the spicules has not been determined with certainty.

It seems likely that either the bright or dark mottles, or both, manifest themselves as spicules when viewed at the limb. Making a one to one correspondence between the limb and disk features is difficult because of the short lifetime of the features compared to the rotation period of the sun (26-30 days).

Fibrils are another chromospheric feature visible on the disk (see, for example, Bray and Loughhead 1974, Plate 5.1). They also are dynamic phenomena, and share similarities with the (dark) mottles. The axes of fibrils are basically horizontal, whereas those of mottles and spicules are predominantly vertical. The observed properties of spicules and fibrils, and the major theories regarding them will be discussed in the first chapter. New ideas on these features will be developed in the succeeding chapters.

The standard quasi-empirical model of the chromosphere yields a temperature structure which starts to rise with height after the temperature minimum, as shown in Figure 1.2. (See Pheuman and Orrall 1986.) This model is only quasi-empirical since some physical assumptions, such as hydrostatic equilibrium, are used. The energy requirements for the chromosphere are $\approx 4 \times 10^{6}$ erg cm^{-2} s^{-1} (Withbroe and Noyes 1977); this corresponds to a volumetric heating rate of $\approx 10^{-2}$ erg cm^{-3} s^{-1}. (Active regions are more energetic, requiring 2×10^{7} erg cm^{-2} s^{-1}.)

Theoretical attempts to understand the quasi-empirical model rely on the existence of the hot corona above the chromosphere. (As

will be discussed shortly, the source of the coronal heating is a key question.) One approach to developing a theoretical model (see Priest 1982) demands that most of the heating input from the lower atmosphere be balanced by radiation losses. Acoustic waves are believed to contribute to the heating at these lower levels. The resulting temperature profile increases only relatively slowly with height below about 2000 km. However, the radiative loss rates are a strong function of temperature - they are very low at lower temperatures, but increase dramatically in the neighborhood of 10^4 K. A result is that at around 2000 km, the energy balance changes drastically. The temperature has gradually climbed to a point where the radiation losses are large enough to dominate the input heating. In order for energy balance to be maintained, an additional source is required. This source is heat from the much hotter corona above. The flow of coronal heat down into the upper chromosphere is maintained by a large temperature difference in a very narrow region. This results in the transition region. (It must be pointed out that alternative interpretations of the transition region also exit; e.g. Dowdy, Rabin, and Moore 1986, Rabin and Moore 1984, and Antiochos 1984.)

The chromosphere and transition region are very dynamic, with evidence for fluid motions throughout. Much of this motion is deduced by observing the doppler shifts of appropriate spectral lines. It is via such doppler shift observations that the existence of downflows of hot (radiating in the ultraviolet) material in the transition region have come to be known. These *ultraviolet*

downflows may play a major role in the heating of the upper chromosphere and transition region. It has also been suggested that these flows are due to the return of spicule material to the lower solar atmosphere. This suggestion will be returned to later in this dissertation. Additionally, non-thermal broadening of spectral lines (see discussion in the review on the transition region by Mariska 1986) implies the existence of unresolved velocities toward and away from the observer, and may be indicative of turbulence (Hollweg 1984a, 1985).

Corona

The outermost major layer of the sun's atmosphere is the corona. Once only visible during total solar eclipses, the corona is now studied by using coronographs, i.e. telescopes fitted with occulting disks to obscure the sun's brighter surface. These give observations of Thomson scattered photospheric radiation off of free coronal electrons. The corona emits (rather than scatters) prominently in X-rays and UV due to its high temperature. However, the earth's atmosphere is opaque to X-ray and UV radiation, and so coronal observations in these wavelength ranges have had to await the advent of the space age. A large body of X-ray and UV coronal data was obtained by the *skylab* space station in the early 1970's. These observations, along with those of other satellites, have yielded fresh insight into the structure and dynamics of the corona. Among the structures found are bright loops of dense plasma, and

large dark regions of less dense corona known as *coronal holes*. By matching coronal images with magnetic field topologies computed from measured photospheric fields, evidence has been obtained that the coronal loops represent regions of closed magnetic field lines and the coronal holes represent regions where the magnetic fields open out into space. The solar wind high-wind stream detected near the earth seem to originate in the coronal holes (Zirker 1977).

As mentioned above, the temperature of the corona is very high, 1-3 x 10^6 K. The source of the coronal heat has been a major question in solar physics since its recognition in the 1930's. A precise answer to this question is still unknown, but much progress toward a solution has been made. Most of the current research into this question revolves around the use of the magnetic field as a medium for the transport of mechanical energy from the photosphere and/or the convection zone into the corona, and its conversion into thermal energy. Older ideas involving the transfer of energy from the lower atmosphere via sound waves are losing favor, since it appears that sufficient energy fluxes do not exist in sound waves (Athay 1986, Athay and White 1978, 1979; Bruner 1978). Coronal energy requirements are given by Withbroe and Noyes (1977) to be 3 x 10^5 erg cm^{-2} s^{-1} in quiet regions and 8 x 10^5 erg cm^{-2} s^{-1} in coronal holes. (Active regions require 10^7 erg cm^{-2} s^{-1}.)

Goals of Chromospheric Research

The above brief overview has omitted much of what is known about the sun. Part of this results from restricting the discussion to the quiet sun. But also ignored are questions about solar cycles, the generation of magnetic fields in the sun, and the relationship of the sun to other stars. This dissertation will not address any of these important questions; the emphasis is on the dynamics of spicules and fibrils. Still, even in this seemingly limited domain, some contributions to key questions in solar physics can result. Some specific suggested questions for chromosphere and transition region research to address are (paraphased from Athay 1985):

> (i) What are the primary mechanisms for heat deposition and energy transport?
> (ii) Once energy is dissipated from the primary heating mechanism, what is its disposition? What fraction is radiated locally and what fraction is transported elsewhere before being radiated? Also, what are the roles of flows in energy transport?
> (iii) What gives rise to the mass flows? How much of it is inherent in the heating mechanisms and how much simply arises from pressure gradients due to differential heating?

The chromosphere appears to be largely governed by discrete fine structures near the limit of earth based telescopic resolution. So in order to address the questions above, this *chromospheric fine structure* cannot be ignored. Spicule-like structures, whether in the

form of bright or dark mottles, fibrils, or spicules, seem to dominate the chromosphere's fine structure. Also, the energy requirements for spicules are comparable to those of other solar atmospheric features. (However, globally the overall energy budget of spicules is smaller than that of other atmospheric regions, since the spicules only cover one percent of the solar surface at a given time.) Even stronger statements can be made regarding the effects of chromospheric fine structure on the overall mass balance of the sun, since the total mass flux in spicules exceeds that of the solar wind by a factor of a hundred (see Chapter 1). Consequently, the study of spicules and fibrils is vital to an understanding of the chromosphere, as well as other regions of the solar atmosphere. Finally, the study of spicules may help in a more general understanding of the sun via insight into solar nonlinear dynamics. Spicules are highly nonlinear phenomena, as exemplified by there velocities (25 km s^{-1}) which are supersonic compared to the sound speed of spicules ($\approx$ 10 - 20 km s^{-1}). Such nonlinear behavior may be common on the sun.

This dissertation's contribution to solar physics is minute. Major dynamical phenomena of nature are not often understood overnight - or even over a six-year period. It is only hoped that this work will further the progress toward long sought explanations of the workings of the sun.

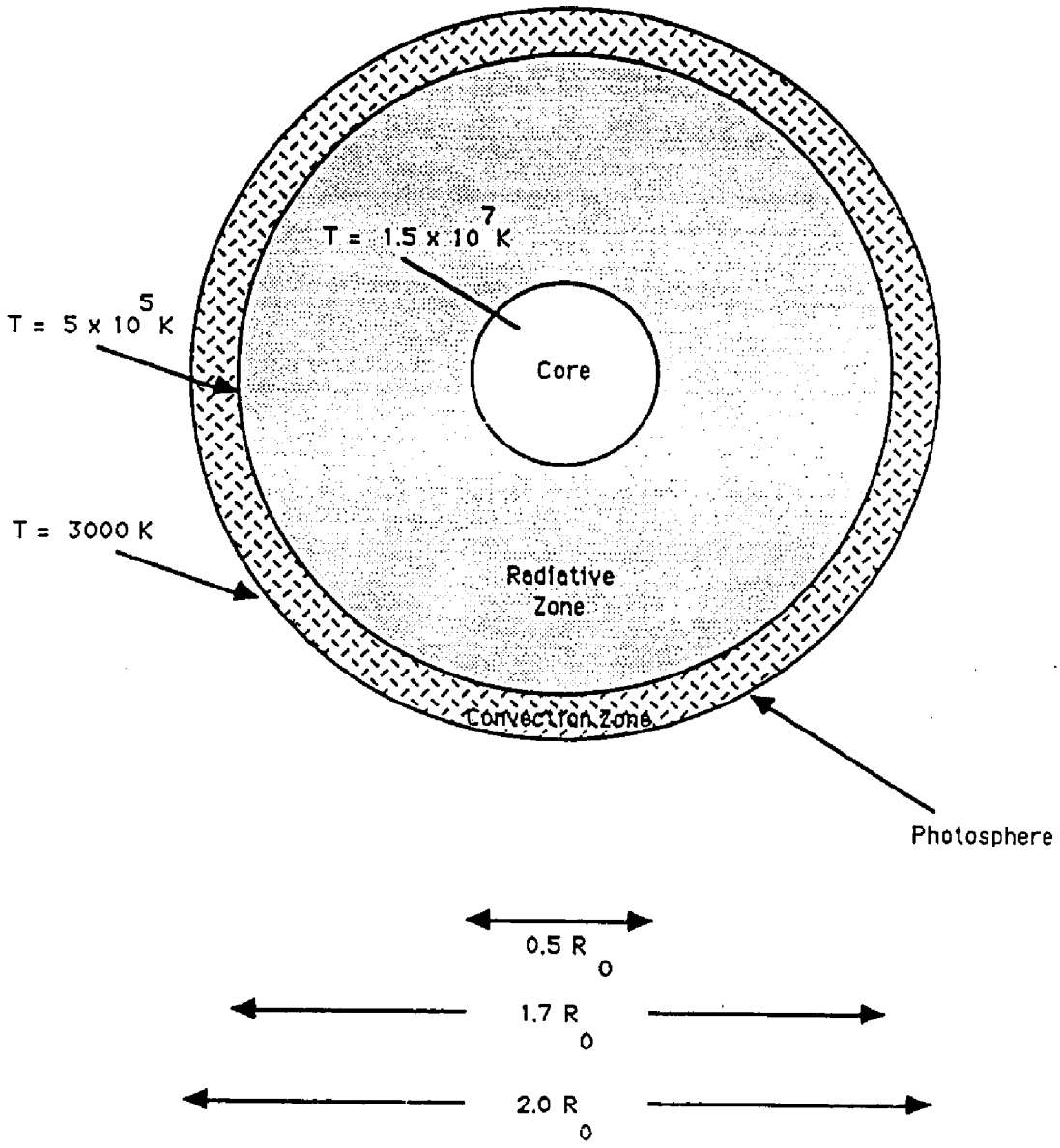

Fig. I.1. The solar interior. Indicated temperature and distances are approximate.

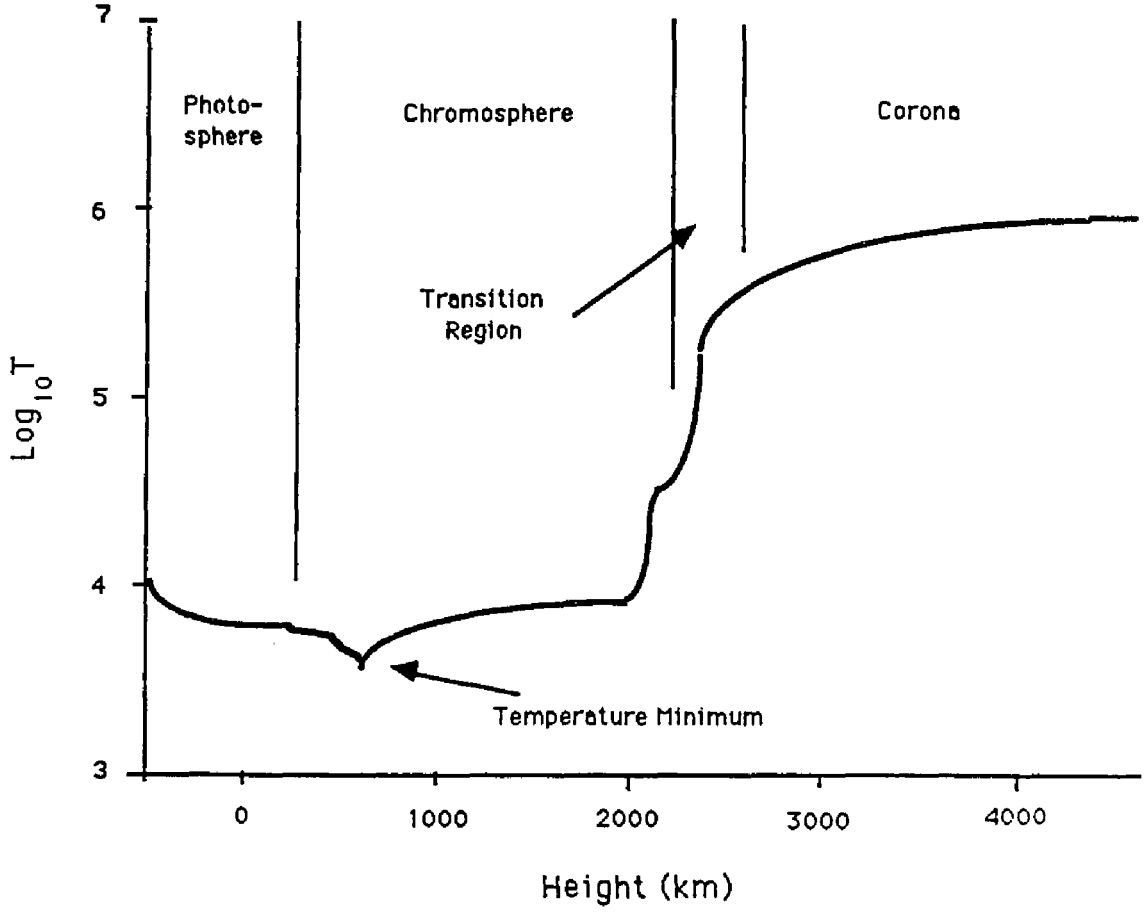

Fig. I.2. Schematic of temperature vs. height in the solar atmosphere. The major divisions of the atmosphere are labeled.

CHAPTER 1

CHROMOSPHERIC FINE STRUCTURE: OBSERVATIONS AND THEORY

In this chapter the observed properties and theories of formation of spicules and fibrils will be reviewed. Other reviews can be found in Athay (1976), Beckers (1968, 1972), Bray and Loughhead (1974), and Michard (1974).

Observations

Spicules

General Features

As noted in the Introduction, the spicules appear to be jets of gas emanating from the chromosphere. At any given time, they cover approximately one percent of the solar surface. Observation of spicules is complicated by the fact that their diameters, usually reported to be around 1000 km, place them at or near the limit of resolution for earth based telescopes. There are reports of a small decrease in spicule diameter with height (Beckers 1968; Lynch, Beckers, and Dunn 1973); this may result from the spicule becoming

more transparent at greater heights, however, rather than from a true physical diameter decrease (Lynch, Beckers, and Dunn 1973).

The spicules reach a range of heights, with reported maxima averaging 6500 to 9500 km, and they often have non-vertical orientations. The height values are somewhat subjective, as the spicules may not have a sharp upper boundary. The top is generally defined to be where the spicule becomes invisible. Spicules appear to be much denser than the surrounding medium at all heights (Michard 1974). Typical values for density are $3.7 - 0.5 \times 10^{-13}$ g cm^{-3} (bottom to top), compared to approximately 8×10^{-16} g cm^{-3} in the surrounding corona. The density and temperature profiles of spicules are relatively flat compared to those of the chromosphere.

Beckers (1972) notes that spicules near the solar poles seem to follow the polar (coronal) rays. This is consistent with the view of spicule formation along magnetic fields. Further support for the association of spicules with magnetic fields comes from observations of the solar disk. Such observations reveal a concentration of chromospheric fine structure, presumably spicules, at supergranule boundaries - the magnetic field is enhanced in these regions.

Spicule Motions

The motions of spicules seem to be complex, and in any case, are not well understood. Movies made in H_α indicate that their tops rise with an upward velocity of around 25 km s^{-1}. Several observers report this upward velocity to be constant over a large distance, despite the presence of the competing effect of gravitational deceleration (see Beckers 1968, 1972). Some reports based on doppler measurements are consistent with the 25 km s^{-1} velocities (Beckers 1968, 1972), while other doppler measurements suggest more complex motions, at times resulting in reversal of sign in velocity (Zirker 1967, Beckers 1968, Mamedov and Orudzhev 1978). In any case, it seems highly unlikely that vertical spicule motion is ballistic. Indeed, ballistic motion with an initial upward velocity of 25 km s^{-1} would lead to a maximum height of only 1200 km. There have been reports of horizontal motions of spicules, indicating shaking transverse to the axis (Pasachoff, Noyes, and Beckers 1968; Nikolskii 1970; and Weart 1970; Mamedov and Orudzhev 1983).

Some observers report a slight inclination to spicule emission line spectra. An often stated interpretation of these tilts is a spinning or twisting motion in spicules (e.g., Beckers 1968; Livshits 1967; Pasachoff, Noyes, and Beckers 1968), which can be as large as 30 km s^{-1}.

Spicules achieve their maximum heights after some five minutes. After this time, the spicule may fall back along the same path over which it evolved, or it may fade from view along its entire length. This fading has raised the question of the fate of spicules;

in particular, do they dissolve into the corona, leave the sun, or return to the surface? Insight into this question is gained by examining the mass flux, F, in spicules:

$$F = \rho V f$$

where ρ is the density in the spicule, taken to be 10^{-13} g cm^{-3} ; V is the upward velocity of the spicule (25 km s^{-1}); and f is the fraction of the sun's surface covered by spicules, taken to be f = 0.006 (Beckers 1972). The value of F is then on the order of 10^{-9} g cm^{-2} s^{-1}. The solar wind mass flux is two orders of magnitude smaller at 10^{-11} g cm^{-2} s^{-1} (Axford 1985). Thus the spicule mass is not leaving the sun. Since the mass of the corona does not increase dramatically over time, the implication is that at least 99 percent of the material in spicules returns to the solar surface. The nature of this return is, however, unknown. A hypothesis to be discussed in Chapter 5 is that spicules often return to the solar surface after being heated to a high enough temperature to preclude emission in chromospheric spectral lines - this would explain their apparent fading prior to falling.

Energy Considerations

If spicules form out of material ejected from the chromosphere then some heating is taking place during their generation since their inferred temperatures are in the range 10,000

- 16,000 K, which is hotter than the lower chromosphere. Moreover, energy must be supplied to the spicule in order to overcome the cooling of the gas which would be expected during an adiabatic expansion. Even without the heating, the energy requirements for spicule formation are formidable. As a rough estimate of the energy flux density needed to create a spicule of length L = 7000 km in a time $\tau \approx 5$ minutes, noting that the energy is mostly gravitational, write

$$\frac{\partial}{\partial t} \int_{\text{bottom}}^{\text{top}} E_{\text{grav}}\, dz \approx \frac{1}{\tau} L\, \rho\, g_0\, h_{\text{average}}$$

$$= (7 \times 10^8 \text{ cm}) \cdot (300 \text{ s})^{-1} \cdot (10^{-13} \text{ g cm}^{-3}) \cdot (2.7 \times 10^4 \text{ cm s}^{-2})$$

$$\cdot (3.5 \times 10^8 \text{ cm})$$

$$= 2.2 \times 10^6 \text{ erg cm}^{-2} \text{ s}^{-1}.$$

This value is greater than the coronal energy losses in both quiet sun and coronal hole regions (Withbroe and Noyes 1977), and it is comparable to the heating requirements, about 4×10^6 erg cm^{-2} s^{-1}, of the quiet chromosphere. (The losses in coronal active regions are somewhat higher, at 10^7 erg cm^{-2} s^{-1}.) Additional energy, about 10^6 erg cm^{-2} s^{-1}, would be needed to heat the spicule. Still more energy would be needed to balance radiation losses. This demonstrates that the spicule energy source is a major problem in solar atmospheric

physics on a par with the more famous "coronal heating" and "chromospheric heating" problems.

Mottles

As mentioned in the Introduction, the disk of the sun displays features called mottles. The mottles are clustered around supergranule boundaries, and are similar to the spicules in that they are elongated, jet-like structures. As for the dark mottles, their lifetime is 10 minutes or somewhat smaller, and their average size is about 800 x 10000 km. The properties of the bright mottles are similar, except they have shorter lengths.

The bright mottles are less numerous than the dark mottles. There is currently some feeling in the solar physics community that the dark mottles (as observed in the wings of H_α) represent a large portion, and perhaps the bulk of the spicule population (Michard 1974, Athay 1986). This interpretation receives some support from Gaizauskas (1984), who has followed a grouping of spicules (but not individual spicules) onto the solar disk and found them to manifest themselves as a group of dark mottles there. However, Dere, Bartoe, and Brueckner (1983) have a dissenting view; they measure dark mottle velocities to be smaller than those of the spicules. The bright mottles have also been associated with spicules (e.g. Bhavilai 1965), while some favor the idea that the bright mottles correspond to the bases of spicules (e.g., Beckers 1972). It seems clear that at

least some of the mottles are disk manifestations of the spicules, but the precise details of the correlations are still wanting.

Ultraviolet features

In recent years, a group of observers at the Naval Research Laboratory (NRL) has undertaken a series of observations of the sun at ultraviolet wavelengths. The instrument used, the High Resolution Telescope and Spectrograph (HRTS), was flown on a series of rocket flights and the Spacelab 2 mission aboard the space shuttle (Dere, Bartoe, and Brueckner 1983, 1984, 1986). Withbroe (1983) has also conducted ultraviolet observations of the sun using equipment aboard Skylab. These flights have revealed the existence of ultraviolet features with properties similar to those of spicules and dark mottles. Thus it appears that spicules exist at temperatures of the order of 10^5 K also.

Fibrils

Fibrils appear on the chromospheric disk as long, low-lying structures. They are often seen diverging from the network into the cell centers (Athay 1986). Fibrils are most easily seen in solar active regions, and most of the detailed studies of their properties have involved these active region fibrils (Foukal 1971a,b; Marsh

1976). They are also reportedly visible in more general regions of the chromosphere (Giovinelli 1974, 1975; Athay 1985).

Bhavilai (1965) and Gaizauskas (1985) state that fibrils sometime appear to be composed of several sections joined together to form one long object. Foukal (1971b) reports the size of fibrils to be 15000 km, in general agreement with the measurements of others (Bray and Loughhead 1974). Foukal also indicates that the top of the horizontal section of fibrils as being 4000 km above the surface. This agrees with Athay (1976) who states that they are no more than some 6000 km high. These fibril height estimates are obtained by observing them at the solar limb in H_α. Although some fibrils seem to be a part of a loop structure (e.g., Bahvilai 1965), Athay (1986) states that their terminal point opposite the network end of the fibril is unknown.

There is little agreement among observers on the details of fibril properties. The magnetic field strength along which they presumably exist, for example, is given as greater than 100 G by Foukal (1971b), while Pikelner (1971b) deduces magnetic field strengths of only 1-2 G. The plasma motions along fibrils are also uncertain. Athay (1976,1986) contends that network fibril flows are generally from the cell center into the network, whereas Marsh (1976) reports no preferential flow direction. Foukal (1971b) gives fluid motions on fibrils to be 20-30 km s^{-1}, fibril densities to be greater than 10^{-13} g cm^{-3}, and temperatures to be greater than 25000 K. Marsh (1976) found velocities of 34 km s^{-1}, while Pikelner

gives densities of 8×10^{-15} g cm^{-3} and temperatures of 18000 K at a height of 4000 km.

Fibril lifetimes are given as 1-20 minutes by Foukal (1971b). Marsh (1976) obtained similar results. Both observers noted a tendency for longer fibrils to be longer lived. The Marsh (1976) data seems to be composed of (at least) two subgroups of fibrils, as pointed out by Athay (1986). One of these groups consists of shorter objects which may be identical to the mottles, while the longer objects may be the "true" fibrils.

What can be said with some confidence about fibrils is that they are key elements of the chromospheric structure and they seem to be indicative of the existence of horizontal magnetic fields.

Theoretical models

This section will deal with models of spicules and fibrils. Mottles will not be treated per se, as the question of the disk representation of spicules and mottles is heavily dependent upon the physics of radiation transfer and spectroscopy. These subjects are outside the scope of the present work, and will not be investigated in this thesis. However, it is probable that any of the spicule models could be developed into a model of mottles. It is also probably true that any of the spicule theories can be adapted to fibrils.

There have been a variety of spicule models presented over the years. Earlier reviews and discussions of several of the models have been published by Beckers (1968, 1972), Bray and Loughhead (1974), and Campos (1984). This section will summarize the older models, and review newer, numerical models.

Spicule models

a) Shock Theories

The idea that spicules result from the passage of shock waves in the chromosphere has been advanced by several workers. The earliest proposals by Unno and Kawabata (1955) and Uchida (1961) dealt only with hydrodynamic shocks. The incorporation of magnetic fields in shock wave theories of spicules was suggested by Uchida (1961), and advanced by Osterbrock (1961) in the first MHD theories of spicules. The advantage of MHD theories is that they provide a natural explanation for the observed association of spicules with the supergranule boundaries, where the chromospheric magnetic field is enhanced. Parker (1964) and Wentzel and Solinger (1967) identified the spicule with the gas behind the shock. This idea has difficulties explaining some general features of spicules, such as their relatively constant velocity and their abrupt disappearance at the end of their lives. Gibson (1972) also points out that the Parker (1964) model fails to explain the flat temperature profile of

spicules. The shock mechanism may work in the chromosphere, but not in the corona, since shocks would heat the coronal gas so that the spicule would be hotter than the corona. Also, shocks would only allow the ratio of spicule to coronal densities to reach 4 (if the ratio of specific heats is 5/3). In fact, spicule and coronal temperatures are 10^4 and 10^6 K, respectively, and the ratio of their densities is 10^3.

b) Thermal Instability

There have been suggestions that spicules are driven via thermal instabilities in the solar atmosphere. Kuperus and Athey (1967) argue that radiative losses (in the lower transition region) alone cannot balance the downward heat conduction flux from the hot corona. They suggest the kinetic transport of chromospheric gas in the form of spicules as an additional energy sink. Kopp and Kuperus (1968) extend this idea to the magnetic solar atmosphere. In their picture, the imbalance between the conductive flux from the corona the and the radiation exists only above the supergranule boundaries where the magnetic field is concentrated. The excess energy is manifested in spicule motions. Over the supergranule cells, however, nearly horizontal (canopy-like) fields restrict the conductive fluxes and the kinetic motions in the chromosphere so that the conductive fluxes can be balanced by radiation; thus no spicules are required as energy sinks in these regions.

Some physical insight as to how the thermal energy could be transformed into spicule motions can be drawn from a numerical model by Bessey and Kuperus (1970). They deposited heat in a model isothermal solar atmosphere, resulting in a pressure gradient which gave rise to a driving force on the chromospheric material. Unfortunately, it is difficult to relate the results of this model to the solar atmosphere, since the model neglects several key ingredients. These include magnetic field, the true temperature structure (and the transition region in particular), radiative losses, and ionization losses. Further numerical calculations, amended to include some of the listed omissions, could perhaps produce a plausible spicule model, although such a model would probably be similar to the models discussed in section h below. However, Beckers (1972) points out that the lower transition region model suggested by Kopp and Kuperus (1968) (a predecessor to the model of Gabriel 1976) conflicts with observed transition region spectral line emissions. Also, Jordan (in proceedings to a talk by Withbroe 1976) has stated that observations indicating that radiation losses are more important than heat conduction in coronal holes rules out the proposal of Kuperus and Athay (1967). Rabin and Moore (1980) reach a similar conclusion, since a spicule generating mechanism based on heat conduction from the corona fails to explain the relative similarities of spicules in quiet sun and coronal hole regions despite the fact that the conduction flux is substantially lower in the coronal holes.

Thermal instabilities have also been suggested as spicule sources by Defouw (1970) and Hood and Priest (1980). No predictions of specific structure resulting from these suggestions were made.

c) Magnetic Reconnection

Another class of spicule theories employs magnetic annihilation via reconnection as the driving force for spicules (Pikelner 1969, 1971a; Uchida, 1969). These theories are based on observations of magnetic neutral points in the chromospheric network (Bray and Loughhead 1974), which are interpreted as regions where the reconnection and subsequent spicule generation occurs. In the Pikelner model, supergranulation fields of opposite polarity are pressed toward each other by photospheric granule motions. This results in compression of plasma gas between the fields, and the subsequent heating of this gas. The compression simultaneously induces cooling of the gas via radiation. This destroys the hydrostatic equilibrium in the region between the field lines; the response is that the cooled compressed gas falls and the field lines closest to each other will reconnect. Some of these field lines will reconfigure themselves and rise upward in response the the magnetic forces (see Figure 1.1). The region between the field lines becomes evacuated (i.e. the gas pressure is reduced) and the magnetic field lines again move closer, inducing a repetition of the process. This continues until all the field in the region is

annihilated. This theory would not generate spicules below a height of about 1000 or 2000 km, since magnetic pressure would not be able to force the fields together owing to the greater gas pressure at lower heights. Such a mechanism may be consistent with observations of gaps at the base of spicules (Gaizauskas 1984).

Blake and Sturrock (1985) have performed a one-dimensional numerical simulation of the Pikelner type mechanism. Using a simple magnetic field geometry, they find that the kinematic aspects of spicules can be reproduced. A key feature is the "self stabilizing" feature of the acceleration of the model, which keeps the gas velocity nearly constant during the growth and decay phase of the model spicule. This stability arises because strong magnetic fields lead to an increase in plasma velocity and a resulting decrease in gas density. This density reduction decreases the magnetic field strength (since it is "frozen in"; see Chapter 2), leading to a decrease in the acceleration. Conversely, when the magnetic field becomes too weak, the plasma decreases its speed, leading to an increase in plasma density, resulting in an increase in magnetic field strength, and a consequent increase in acceleration.

A modification to the Pikelner mechanism suggested by Blake and Sturrock (1985) is that the spicule trajectory is determined by a second set of magnetic field lines situated transverse to the driving reconnected field lines. They further claim that such a field configuration is suggested by a surge (chromospheric jet structure of a larger scale than spicules) observation displayed in the same

paper. (They pursue the possibility that spicules and surges are driven by similar mechanisms.)

A difficulty with the magnetic reconnection scenarios is that spicules seem to be more common than magnetic field neutral points in the supergranulation network (Beckers 1972). It is possible, however, that the required field polarity reversals and neutral points exist on scales smaller than the resolution of the observations. The work of Blake and Sturrock (1985), while enlightening, has to be developed further before close comparisons with spicules can be made. Their work is limited to cold spicules; thus there is no discussion of predicted temperature profiles or heating. It would be difficult to carry out numerical or analytical calculations with the magnetic field geometry suggested by Blake and Sturrock, as such a task would require three-dimensional considerations.

d) Model of Athay (1984)

Athay (1984) views spicules as the manifestation of one leg of a mass flow cycle involving the corona, transition region, and chromosphere. The ultimate driving mechanism is a set of large amplitude fluctuations, in both space and time, of the heating rate in magnetic flux tubes. The cycle begins with mass downflow from the corona instigated by a heating decrease along a magnetic flux tube. When the heating is decreased, the temperature drops, leading to an

increase in plasma density under the assumptions of pressure balance and frozen in field conditions. The radiation rate is proportional to the square of the density, thus the temperature drop results in the gas radiating away more heat, and becoming denser, leading to even more radiation, and so on. This cooled (temperature $T= 10^5$ K), dense coronal gas will then flow down along the field lines. Left behind by the downflowing plasma will be an evacuated flux tube. Athay then assumes that a larger heating rate is restored to the flux tube. The heating induces a large pressure gradient near the base of the flux tube. This pressure gradient drives an upflow. It is anticipated that the gas will move upward with a velocity at or greater than the sound speed, and that the pressure gradient will be subhydrostatic, as is the case in spicules. So there is a possibility that the rising gas will resemble spicules. Numerical studies substantiating or rejecting these ideas have yet to be performed.

This proposal by Athay (1984) is attractive in that the atmosphere is assumed to be highly inhomogeneous- this may be in line with observations such as those discussed by Dowdy, Rabin and Moore (1986). Moreover, the idea of constant changing of the temperature structure in the model seems natural in view of the dynamic and ever changing nature of the lower solar atmosphere. Additionally, Athay points out that the model offers a natural explanation for the apparent paucity of spicules in active regions, where consistent higher heating rates may prevent downflows in the first leg of the cycle. Also, spicules would avoid low magnetic field areas, such as supergranule cell centers, since there would be no

easy channel for the fluid motions. Another possible success of the model is that it may offer an explanation to another outstanding enigma in solar physics-the emission measure structure of the lower transition region. (Briefly, emission measure gives an indication of the amount of material emitting radiation at a given temperature. Standard models of the transition region fit observed emission measure curves for temperatures greater than approximately 2.5 x 10^5 K, but fail at lower temperatures. See Athay 1982.) However, other models which invoke a spicule producing source at the base of the flux tube (c.f. Chapter 4), and assume the material to return to the photosphere via the ultraviolet downflows may explain the emission measure profile equally well.

The mechanism still leaves open the question of the nature of the flux tube heating source. Additionally, the mechanism seems to require a closed circuit between the corona and the chromosphere, and thus seems to fail to offer an explanation for the observations of spicule-like structures on small loops which have been observed by some (Moore 1986). Another question is whether or not there is enough mass in the corona to support this mechanism (see next section).

e) Coronal Condensation

Krat and Krat (1971) and Mamedov and Orudzhev (1978) have explored the possibility that spicules originate from a condensation

of coronal plasma. If the original coronal gas has some angular momentum, then Krat and Krat note that the condensation could result in the observed rotation of spicules. They also suggest that the mechanism would not necessarily contradict the apparent upward motions of spicules observed on the limb, since these observations may represent a progressive cooling of spicules form the base upward. These papers do not present any elaboration of the suggested mechanism, so no comparisons with observed spicule properties can be made.

A key question to be raised regarding any theory of spicule formation out of the corona is whether or not there exists enough mass in the corona to supply the mass of spicules. That this is a question of serious concern can be seen from the following estimate. Let the total mass of the quiet sun along a spicule-supporting magnetic field column be M_c. Then,

$$M_c = \int_{bott}^{top} A_c \rho_{0c} e^{-z/\Lambda_c} dz$$

where A_C is the cross-sectional area of the magnetic field column, ρ_{0c} is the mass is the mass density at the base of such regions, Λ_C is the scale height, z is vertical height, 'bott' and 'top' are the z value of the base and top of the corona, respectively. Now if most of the coronal mass is within a few tenths of a solar radius of the surface, the gravitational acceleration can be approximated as constant, g = 2.72×10^4 cm s^{-2}, in estimating the integral. So,

$$M_c \approx A_c \rho_{0c} \Lambda_c \left(e^{-bott/\Lambda_c} - e^{-top/\Lambda_c} \right)$$

If the first exponential is taken to be 1, and the second 0, then

$$M_c \approx A_c \rho_{0c} \Lambda_c$$

The density of spicules is relatively constant over their heights, so the spicule mass is just $M_s \approx A_c \rho_{os}$ (height) = A_c (10^{-13} g cm^{-3}) (10^9 cm) = $10^{-4} A_c$ grams. So $M_s/M_c \approx 10^{-4} / \rho_{0c} \Lambda_c$. The scale height for the ionized corona is $\Lambda_c = 2kT/gm_H$, where k and m_H are the Boltzmann constant and the hydrogen mass, respectively. Taking a temperature of 10^6 K, one has $\Lambda_c = 6 \times 10^4$ km. Using $\rho_{0c} = 8 \times 10^{-16}$ g cm^{-3} (see, for example, Priest 1982), yields $M_s/M_c \approx 20$. Thus it is difficult to see how the corona could be the mass source for spicules.

f) Twisted Flux Tubes

Tsirul'nik (1983) has attempted to describe spicules in terms of the untwisting of magnetic flux tubes. He numerically solved the nonlinear MHD equations and found that some of the energy used to maintain the twists was transformed into mass upflows. For moderate initial twists in the field ($B_X/B_Z \leq 1$), he finds that spicule-like structures are generated. A slow shock is found to

form at the base of the flux tube. The shock leads to some shock heating. The dissipation of the shock may lead to additional heating of the gas. However, Tsirul'nik (1983) fails to include the expansion of the magnetic flux tube with height in the chromosphere, thus a major difficulty with the model is that large magnetic fields (B_z = 1000 G) are assumed, whereas network fields are, as discussed in the Introduction, thought to be at least an order of magnitude weaker. It is not clear if the shocks provide enough heating to overcome the adiabatic cooling associated with the expected flux tube expansion. Tsirul'nik also neglects dissipation terms in his equations. Thus even more extreme conditions would be required to drive real spicules by this method. Finally, it is not clear how the initial twists would be maintained on open field lines, or how the untwisting of the field lines would be initiated whether they are open or closed.

g) Acoustic Gravity Wave Model of Campos (1984)

Campos (1984) has constructed an analytical model of spicules as acoustic gravity waves channelled along magnetic field lines. The waves would be driven by photospheric motions with periods of 300s. (The sun oscillates at this period due to the "5-minute oscillations.") Campos demonstrates that such waves can carry the required mass flux into the upper atmosphere, even allowing for the possible large evanescence of the waves in the chromosphere. He calculates the mass flux by multiplying the density perturbation

associated with the waves by the velocity of granular motions in the photosphere. A temperature profile for the model spicule is generated by balancing the dominate heating source, viscous damping, with the dominant energy loss mechanism, thermal radiation. The height of the spicule is identified as the viscous dissipation height, which coincides with the height over which the acoustic gravity waves propagate prior to steepening into shocks. Campos claims that the shocks induce the spicule material to break magnetic confinement. The upward velocity of the spicule is identified as the phase velocity of the acoustic gravity waves; this velocity is greater than the sound speed.

The Campos (1984) model results agree well with observations. However, the effects of the waves on the transition region were not discussed. More detailed (perhaps numerical) models may show the solar atmosphere to respond to the acoustic gravity waves in a manner similar to the rebound shock model, discussed in the next section. The spicule would then consist of the material below an uplifted transition region raised by the acoustic gravity waves, in preference to the acoustic gravity wave model where the spicule consists of the waves themselves.

h) Nonlinear Numerical Models

Recent nonlinear models of spicules explain the observed spicule properties with varying degrees of success. These theories

all involve identifying material below a raised transition region as the spicule. Hollweg, Jackson, and Galloway (1982) consider the role of nonlinear Alfven waves and fast shocks in lifting the transition region. Their model yields density profiles which resemble those of spicules, but the calculated temperatures are much too low due to the nearly adiabatic cooling of the chromospheric material below the raised transition region.

This low temperature problem also occurs in the spicule model of Suematsu et al. (1982). They consider the role of a single upward propagating slow shock in lifting the transition region. The shock results from a sudden pressure enhancement at the base of a magnetic flux tube with constant cross section.

The model due to Hollweg (1982) overcomes the temperature problem by utilizing a train of acoustic shocks to heat the chromospheric gas beneath the uplifted transition region. The shock train results from a single initial impulsive energy source at the base of the model (at photospheric levels). In linear theory, the impulse response (see Chapter 3) of the lower solar atmosphere consists of a wavefront followed by an oscillating wake as has been known for a long time (e.g., Morse and Feshbach 1953; Stein and Schwartz 1972; Rae and Roberts 1982). The wake arises as follows. Some of the material displaced upward by the initial wavefront falls due to gravity. The momentum of this falling material results in compression of the material in the atmosphere below it. The compressed material then "rebounds," generating a new wave. This

process repeats several times, giving rise to the oscillating wake. Nonlinearly, the wavefront and wake steepen into a shock train. The shocks resulting from the wake are therefore be referred to as "rebound shocks." The shocks are channeled along a strong magnetic field of varying cross section and repeatedly interact with the transition region, resulting in an upward velocity of the transition region which is roughly constant, and in substantial chromospheric heating. This is a significant departure from the model of Suematsu et al. (1982) which considers only a single shock interaction and thus induces ballistic motions of the transition region and insufficient heating. The model due to Hollweg (1982) will subsequently be referred to as the *rebound shock model.*

Observations of velocity variations in spicules noted in the above section on spicule motions may be consistent with time-dependent acceleration induced along the axis of the spicule in association with the wake, as predicted by the rebound shock model.

i) Other Suggestions

There have been additional suggestions for spicule generation. An idea presented by Schatten and Mayr (1986) is that spicules are material ejected from the convection zone via the intense magnetic flux tubes at the surface. They explore this idea by considering "solar wind" solutions for material flows on the subsurface magnetic flux tubes. It has also been suggested that spicules can

result from the propagation of *solitons* on magnetic flux tubes (Roberts 1983). Both of these suggestions must be developed into models which can be compared with spicule observations.

This concludes a rather extensive review of the many published spicule producing suggestions and models. Without higher resolution observations, it is difficult to rule out any specific theory, although some stand on stronger ground than others. In Chapter 4, the rebound shock model (section h) will be extended and elaborated upon. This will include a study of its long-time behavior, and a study of the model's sensitivity to input parameter variations. Among the results will be that the model is capable of producing spicules with many features in common with the observations. Of course not all observed spicule features will be reproduced. This need not unduly worry the theorist. Paraphrasing Francis Crick (?), no theory need fit all the data, since some of data are wrong.

Fibril models

While there have been many attempts to model spicules, theoretical models of fibrils are quite scarce, and to the author's knowledge, there has been only one attempt to create a numerical model of fibrils.

Pikelner (1971b) studied the absorption of fibrils when seen against the solar disk, and their emission when seen at the limb. In

this way he deduced several properties of a model fibril. Foukal (1971b) suggested that the Parker (1964) shock mechanism for producing spicules may be applicable to fibrils. Furthermore, he notes that the since magnetic fields are stronger in fibrils than in spicules (according to his measurements), the shock mechanism may be, if anything, more appropriate for fibrils than spicules.

Marsh (1976) has suggested a very simple fibril producing mechanism involving flows along a straight, but inclined, rigid magnetic flux tube. If material is impulsively injected into the tube at a velocity v_0, and decelerates only under the influence of gravity, then the lifetime (the time for the fibril to extend and retract) is given by

$$\tau = \frac{2 v_0}{g} \sqrt{1 + \left(\frac{2 g l}{v_0^2}\right)^2} \qquad (1.1)$$

where l is the maximum projected length of the fibril.

Using a velocity v_0 = 34 km s^{-1}, Marsh (1976) found that the lifetime verses length behavior of the model fibril predicted by equation (1.1) is in good agreement with the observed data.

Suematsu (1985) developed a nonlinear numerical model of fibrils based on the Suematsu et al. (1982) spicule model (see Section h above). The model is also similar to the spicule model due

to Hollweg (1982). Suematsu modified the spicule code for application to a low-lying magnetic loop. The loop starts in the photosphere, rises up through the chromosphere and transition region into the corona, then descends into the transition region and ultimately into photosphere again at the far end of the loop. Suematsu found that, as in the spicule case, the transition region is lifted by shocks resulting from an impulsive pressure pulse in the photosphere. The chromospheric material behind the displaced transition region moves along the loop into the corona, producing fibril-like structures. The shock continues along the loop ahead of the displaced transition region and is partially reflected by the the transition region at the far end of the loop. It turns out that the reflected shock does not disrupt the model fibril significantly. The coronal material between the two transition regions is nearly adiabatically compressed by the model fibril, and promotes the retraction of the fibril even when it goes beyond the apex of the loop.

A shortcoming of the Suematsu (1985) model is that the predicted temperatures are only about 1000 K, which is much lower than observed values. The rebound shocks which led to the temperature increase in spicules in the work of Hollweg (1982) do not play an important role in the Suematsu (1985) work since the rebound shocks which developed along his loops were too weak to make a significant contribution to the dynamics of the system. The consequences of the low temperatures are even more serious in light of the fact that the system studied neglects dissipation.

In chapter 6 of this thesis, a new nonlinear numerical model for fibrils will be developed. It is to be based on the Hollweg (1982) work on spicules, and thus shares features with the Suematsu (1985) work. The new work involves the study of acoustic waves on a flux tube which is initially vertical, then turns horizontal for a distance, and finally turns vertical again and heads out into the outer solar atmosphere. It will be seen that this geometry leads to some physical results different from the loop model of Suematsu (1985).

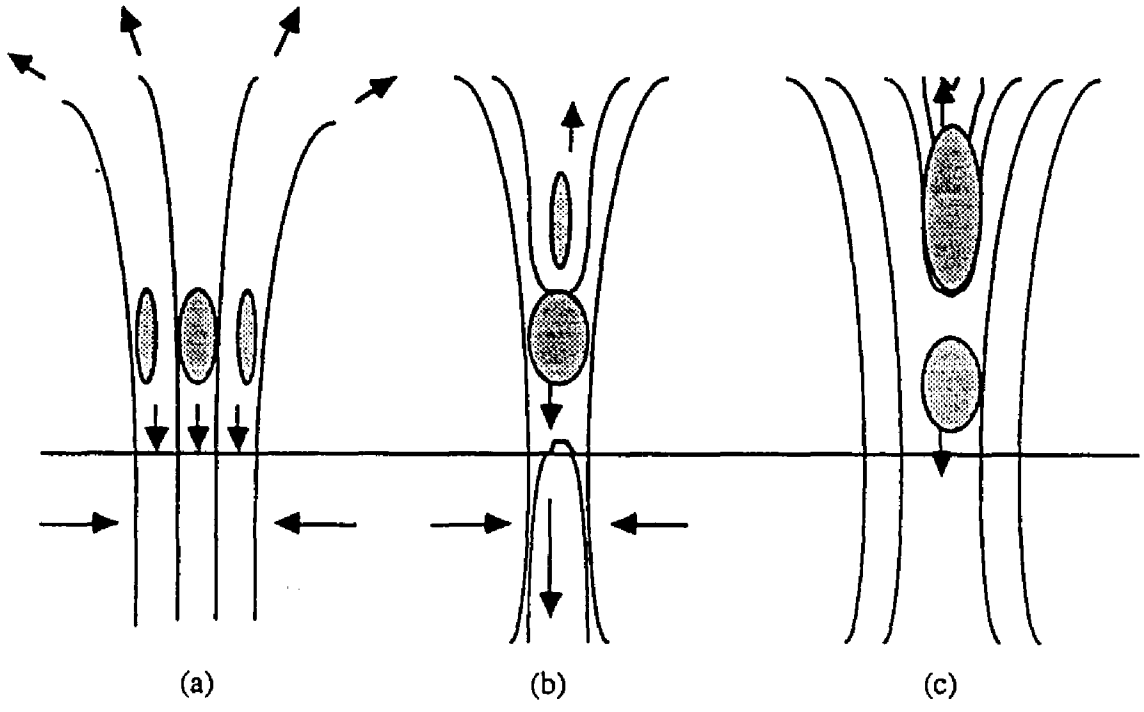

Fig. 1.1. Spicule producing mechanism of Pikel'ner (1971).Magnetic fields pressed together in (a) lead to heating and subsequent radiation, cooling, condensation, and fallingof plasma. This is accompanied be field line reconnection and the ejection of material upward, (b) and (c), giving rise to a spicule.

CHAPTER 2

THE EQUATIONS OF MHD

Introduction

The study of solar physics requires a discussion of energy, momentum, and mass transfer in a plasma. A description of these phenomena can be carried out for the solar atmosphere, viewing it as an ionized fluid capable of supporting waves and interacting with magnetic fields. Such a view is taken in the discipline of magnetohydrodynamics (MHD) applied to the sun.

The equations of MHD are similar to those of fluid dynamics. The difference resides in the additional driving forces in the MHD equations due to the electrical and magnetic character of the MHD fluid.

The three basic MHD fluid equations are statements of the conservation of mass, momentum, and energy. With the addition of Maxwell's equations and an equation of state, the discipline of MHD can be completely formulated. In this chapter a description of each of the three fluid equations will be given, along with a discussion of some MHD consequences of Maxwell's equations. Additionally, the basic physics of shocks propagating parallel to a magnetic field will

be discussed; such shocks occur in the numerical calculations of Chapters 4 and 6.

References for this material are numerous; some examples are Chen (1974), Ferraro and Plumpton (1961), and Priest (1982). Other references will be cited in the text.

The MHD Fluid Equations

In this thesis, spicules and fibrils will be viewed as flows guided by magnetic field lines. Along with the general MHD equations, the equations for flow along a magnetic flux tube with varying cross-sectional area, A, will be written in a standard "conservation form" which is convenient for numerical solution via a "flux-corrected transport," or FCT, code.

The Mass Conservation Equation

The first MHD fluid equation to be discussed is the mass conservation equation. Given a fluid in a volume V, conservation of mass demands that the decrement of the amount of material (of density ρ) in V be equal to the surface integral of the flux out of V. Thus

$$\frac{\partial}{\partial t}\int_V \rho \, dV = -\int_S \rho \, v \cdot dS. \qquad (2.1)$$

The volume V is bounded by the closed surface S. Employing Gauss' law, (2.1) can be written

$$\int_V \frac{\partial \rho}{\partial t} dV = -\int_V \nabla \cdot (\rho v) \, dV \qquad (2.2)$$

where the derivative and integral can be interchanged on the left hand side (LHS) if the volume element is fixed. The integrands can be combined under one integral,

$$\int_V \frac{\partial \rho}{\partial t} + \nabla \cdot (\rho v) \, dV = 0. \qquad (2.3)$$

Since this result holds for an arbitrary volume, the integrand must vanish, and the most general form of the mass conservation is obtained:

$$\frac{\partial \rho}{\partial t} + \nabla \cdot (\rho v) = 0. \qquad (2.4)$$

For the purposes of this thesis, a useful form of the mass conservation equation can be obtained directly from (2.1). Consider a "tube" of velocity vectors, analogous to a "magnetic flux tube." The tube's cross-sectional area will be denoted A, and its length will be denoted ds, where s is distance along the velocity vector. Thus dV =

A ds. The integral on the right-hand side (RHS) of (2.1) is, to first order in ds, just [∂(ρvA)/∂s]ds, where v is the s-component of v. Thus (2.1) becomes

$$\frac{\partial}{\partial t}(\rho A)+\frac{\partial}{\partial s}(\rho v A)=0 \qquad (2.5)$$

where A may be a function of s and t. Equation (2.5) is in the conservation form referred to above. In this form one finds on the LHS a time derivative of some quantity plus a space derivative of the flux of that quantity. The sources appear on the RHS; in this case the sources are zero.

The Maxwell equation $\nabla\cdot\mathbf{B} = 0$ may be treated in the same way. The result is

$$\frac{\partial}{\partial s}(B A)=0 \qquad (2.6)$$

where A and s now refer to the magnetic flux tube, and B is the s-component of **B**. If v and B are everywhere parallel, then (2.5) and (2.6) combine into

$$\frac{\partial}{\partial t}\left(\frac{\rho}{B}\right)+\frac{\partial}{\partial s}\left(\frac{\rho v}{B}\right)=0. \qquad (2.7)$$

The Momentum Conservation Equation

The MHD momentum conservation equation is a statement of Newton's second law:

$$\rho \frac{Dv}{Dt} = \textbf{Forces per volume.} \qquad (2.8)$$

where r and v are functions of space and time.

The upper case D's of (2.8) represent the derivative in the frame of reference of the moving plasma. This is the *convective derivative* and may be written

$$\frac{DG}{Dt} = \frac{\partial G}{\partial t} + (v \cdot \nabla) G \qquad (2.9)$$

for an arbitrary vector quantity G. Equation (2.9) can be derived in a straightforward fashion by regarding the LHS as the total derivative of G, and applying the chain rule. The physical interpretation of (2.9) is that the first term on the RHS is the variation in time of the quantity G itself, i.e. the intrinsic time change in G. The second term represents the change in G due to its movement through a gradient at velocity v.

Next, the forces of equation (2.8) will be considered. By analogy with hydrodynamics, forces which are important are those due to gravity, ρg, and pressure gradient, -∇P. The only other force of concern in this thesis is the Lorentz force

$$\mathbf{F}_L = \frac{1}{c}\mathbf{J} \times \mathbf{B} \qquad (2.10)$$

where c is the speed of light and J is the current density. The forces due to the electric field have been neglected; according to the principle of quasineautrality, this is an excellent approximation in the solar atmosphere.

Collecting together the terms in the above paragraphs, equation (2.8) is

$$\rho \frac{\partial \mathbf{v}}{\partial t} - \rho\ \mathbf{v} \times (\nabla \times \mathbf{v}) + \rho \nabla \frac{v^2}{2} = -\nabla p + \rho \mathbf{g} + \frac{1}{c}\mathbf{J} \times \mathbf{B} \qquad (2.11)$$

where a vector identity has been used to give the second and third terms on the LHS.

Equation (2.11) can be put into "conservation form" by invoking the "thin flux tube approximation." Consider a magnetic flux tube. The plasma can flow freely along the magnetic field lines, and the flux tube can also expand or contract in time in response the various forces acting on it. The plasma is tied to the magnetic field in virtue of the "frozen-in theorem" (see below), and the expansion or contraction will induce velocity components normal to **B**. However, if the tube is very thin, then the normal velocity component due to expansion or contraction will be negligible in comparison to the field-aligned part of the flow. In that case it is possible to retain

terms involving $\partial A/\partial t$ while dropping terms which explicitly involve the normal velocity components. This is thin flux tube approximation, and it allows the following procedure to be followed. Dot (2.11) with the unit vector along the magnetic field lines, $\hat{s}$, giving

$$\rho \frac{\partial v}{\partial t} + \rho v \frac{\partial v}{\partial s} = - \frac{\partial p}{\partial s} + \rho g_s \qquad (2.12)$$

Multiplying (2.12) thru by A and combining with (2.5) yields

$$\frac{\partial}{\partial t}(\rho v A) + \frac{\partial}{\partial s}(\rho v^2 A) = - A \frac{\partial p}{\partial s} + \rho g_s A \qquad (2.13)$$

where again A is a function of s and t. The momentum equation as derived here has two source terms on the RHS. For the numerical calculations of Chapters 4 and 6, and the analytical calculation of Chapter 3, an additional force term will be added to the RHS. This additional term will result in an additional term in the energy equation (2.20) to be derived in the following section. The analysis involving the additional force term is straightforward and will not be included in this chapter.

The Energy Conservation Equation

The first equation used in the development of the energy conservation equation is the adiabatic heat equation. This equation is a statement of the conservation of entropy (Priest 1982),

$$\frac{D}{Dt}(p/\rho^{\gamma}) = 0 \tag{2.14}$$

where $\gamma = c_p / c_v$ is the ratio of specific heats. Combining (2.14) with (2.4) and (2.9) yields

$$\frac{\partial p}{\partial t} + \nabla\cdot(pv) + (\gamma - 1)\, p\nabla\cdot v = 0. \tag{2.15}$$

Making geometrical simplifications like those made for the mass and momentum equations, the heat equation (2.15) is

$$\frac{\partial}{\partial t}(p\,A) + \frac{\partial}{\partial s}(p\,v\,A) = -(\gamma - 1)\,p\,\frac{\partial}{\partial s}(v\,A). \tag{2.16}$$

It is important to note that (2.16) has assumed that A is independent of time, implying that the magnetic field is rigid. Thus terms involving variations of the magnetic energy will not be included. This means that only hydrodynamic motions guided by a rigid magnetic field will be considered. Justification for this procedure will be given below.

Now the momentum equation will be modified to a form which makes a statement about kinetic energy. Multiplying (2.13) by v and subtracting $v^2/2$ times (2.5) yields

$$\frac{\partial}{\partial t}\left(\frac{1}{2}\rho v^2 A\right) + \frac{\partial}{\partial s}\left(\frac{1}{2}\rho v^3 A\right) = -A\left(v\frac{\partial p}{\partial s} - \rho v g_s\right) \qquad (2.17)$$

Combining this with (2.16) gives the desired form of the MHD energy conservation equation:

$$\frac{\partial}{\partial t}(E A) + \frac{\partial}{\partial s}(E v A) = \rho v g_s A - \frac{\partial}{\partial s}(p v A) \qquad (2.18)$$

where

$$E = \frac{1}{2}\rho v^2 + \frac{p}{\gamma - 1} \qquad (2.19)$$

The physical interpretation of (2.18) can be realized after introducing the gravitational potential, ϕ, via $g_s = -\partial\phi/\partial s$. Some manipulation of (2.18) then yields

$$\frac{\partial}{\partial t}(\varepsilon A) + \frac{\partial}{\partial s}(\varepsilon v A) = -\frac{\partial}{\partial s}(p v A) \qquad (2.20)$$

where

$$\varepsilon = \frac{1}{2}\rho v^2 + \frac{p}{\gamma - 1} + \rho\phi \qquad (2.21)$$

This implies that ε, the sum of the kinetic, thermal, and gravitational energies, changes in response to the work done on the

fluid by the pressure, p, which appears as a source term on the RHS of (2.20).

Note that the momentum equation has ignored viscosity. Similarly, the energy equation has ignored viscosity and other entropy-producing terms such as heat conduction, joule heating, and radiation. It will be assumed that this approximation is valid everywhere except at shocks, where steep gradients develop and viscosity or heat conduction can become important. However, the shocks will be handled in a different manner, as will be seen in the final section of this chapter. The effects of heat conduction and radiation have been examined numerically by Mariska and Hollweg (1985), for flow conditions related to the spicule flows which are to be studied here. They found that the dissipative effects of heat conduction and radiation reduced the velocity amplitudes by about a factor of two. The heat conduction and radiation did not fundamentally alter the basic dynamics of the problem. In this thesis, it will be assumed that the basic dynamics can be adequately explored via the vastly simpler (from the numerical standpoint) dissipationless equations.

The Frozen In Theorem

A basic consequence of MHD, known as the Frozen In Flux Theorem, follows when the electrical conductivity can be considered infinitely large. The theorem asserts that the plasma and magnetic

field lines move together in the following sense: Consider an arbitrary closed curve C, and let the magnetic flux encompassed by C be Φ. Now follow the motions of the parcels of gas originally lying on C. At some later time these parcels define a new curve C_1. Then the magnetic flux encompassed by C_1 will still be Φ. Thus motions along the field are allowed without constraint, but motions transverse to the field must be accompanied by transverse motions of the field lines, and vice versa. If this were not true, then the current associated with moving a conductor across the magnetic field lines would be infinite, if the conductivity is infinite. The resulting emf would immediately restore a situation where there is no motion across the field lines. One argument demonstrating this theorem will be given here. See also Priest (1982), Roberts (1967), and Parker (1979).

Ohm's law can be stated

$$\mathbf{J} = \sigma \left(\mathbf{E} + \frac{\mathbf{v} \times \mathbf{B}}{c}\right) \tag{2.22}$$

where J is the current density and σ is the electrical conductivity. When combined with the Maxwell induction equation

$$\nabla \times \mathbf{E} + \frac{1}{c}\frac{\partial \mathbf{B}}{\partial t} = 0, \tag{2.23}$$

equation (2.22) becomes

$$\frac{\partial \mathbf{B}}{\partial t} = \nabla \mathrm{x}\ (\mathbf{v} \times \mathbf{B}) \tag{2.24}$$

under the assumption of infinite conductivity. This can be converted to a statement about magnetic flux by integrating over a surface S:

$$\int_S \frac{\partial}{\partial t}\mathbf{B}\cdot d\mathbf{S} - \int_S \nabla \mathrm{x}(\mathbf{v}\mathrm{x}\mathbf{B})\cdot d\mathbf{S} = 0. \tag{2.25}$$

Via Stokes' theorem, this is

$$\int_S \frac{\partial}{\partial t}\mathbf{B}\cdot d\mathbf{S} - \oint_C \mathbf{v}\mathrm{x}\mathbf{B}\cdot d\mathbf{l} = 0, \tag{2.26}$$

The first integral is the time derivative of the magnetic flux due to changes of B with time, while the second is the rate of change of the magnetic flux across S due to the movement of the boundary of S at velocity v. (See Priest 1982 for a more detailed discussion of the second integral.) Thus (2.26) says that the total time derivative of the magnetic flux is zero, and so the total magnetic flux is constant in time and the frozen in statement is substantiated.

The equations given above have assumed that v and B are everywhere parallel. This assumption is allowed by the frozen-in theorem, since motion along B is unconstrained. However, it has also been implicitly assumed that there are no motions across B, since the cross-sectional area, A, of the flow tube or magnetic flux tube was assumed to be independent of time. This is only an

approximation, which requires further justification. One approach is as follows: Suppose the pressure inside a flux tube is enhanced, due to the passage of a sound wave for example, by Δp. To restore pressure balance with its surroundings, the tube will expand decreasing both its thermal pressure p and magnetic pressure $B^2/8\pi$. The tube will again be in equilibrium with its surroundings when

$$d\,(p + B^2 / 8\,\pi) = -\,\Delta p$$

or

$$dp + B\,dB / 4\,\pi = -\Delta p \tag{2.28}$$

If the tube simply expands laterally one has

$$\frac{dB}{B} = \frac{d\rho}{\rho} \tag{2.29}$$

in virtue of the frozen-in theorem. And if the expansion is adiabatic one has

$$\frac{dp}{d\rho} = \frac{\gamma p}{\rho} \tag{2.30}$$

Putting this all together gives

$$\frac{dB}{B} = -\frac{\Delta p}{\rho}(v_A^2 + c_s^2)^{-1} \tag{2.31}$$

where v_A and c_s are the Alfven and sound speeds, respectively:

$$v_A^2 = B^2 / 4\pi\rho \tag{2.32}$$

$$c_s^2 = \gamma p / \rho \tag{2.33}$$

Now Δp will generally be less than or comparable to p itself, and one then has, roughly,

$$\frac{|dB|}{B} \lesssim \frac{c_s^2}{v_A^2 + c_s^2} \tag{2.34}$$

In the solar magnetic flux tubes it is observed that $v_A^2 \approx c_s^2$ in the photosphere, but $v_A^2 \gg c_s^2$ in the chromosphere and corona. Thus $|dB|/B$ will be small in the chromosphere and corona, and the magnetic field can be approximated as being rigid there. Fortunately, the interesting dynamics to be explored in this thesis occurs in the chromosphere, and it is anticipated that the rigid field assumption is a good one.

Equations (2.5), (2.13), and (2.18), along with the frozen in flux condition (which will be assumed valid) comprise the basic tools to be used in the subsequent chapters.

Shock Analysis

Shocks are an important element of the numerical models developed in Chapters 4 and 6. Therefore, an overview of shock properties will be given here.

A shock forms from the steepening of a large amplitude wave. By "large amplitude" it is meant large enough for nonlinear features of the wave disturbance to be important. The steepening stops when the nonlinear effects inducing the steepening come into balance with the competing effects of viscous dissipation and heat conduction. These latter two effects depend strongly upon spatial gradients, and thus grow in importance as the wave steepens. Although the effects of viscosity and heat conduction are important inside the shock region, the usual procedure for analysis is to evaluate the mass, momentum, and energy conservation equations in regions where the dissipation terms can be ignored. The shock "jump conditions" thus do not involve viscosity or heat conduction explicitly.

First, pure hydrodynamic shocks will be discussed. The analysis is generally carried out in the shock frame of reference, with the region ahead of the shock referred to as region one, and that behind the shock referred to as region two. The steady state equations of mass, momentum, and energy conservation are then integrated across the shock boundary. Regions one and two are taken

to be uniform, and so viscosity and heat conduction make no contribution in these regions. The results may be expressed as follows:

$$\rho_2 v_2 = \rho_1 v_1 \tag{2.35}$$

$$p_2 + \rho_2 v_2^2 = p_1 + \rho_1 v_1^2 \tag{2.36}$$

$$\frac{\gamma p_2}{(\gamma - 1)\rho_2} + \frac{1}{2} v_2^2 = \frac{\gamma p_1}{(\gamma - 1)\rho_1} + \frac{1}{2} v_1^2 \tag{2.37}$$

These equations are known as the Rankine-Hugoniot relations. Their nontrivial solutions are

$$\frac{\rho_2}{\rho_1} = \frac{(\gamma + 1) M_1^2}{2 + (\gamma - 1) M_1^2} \tag{2.38}$$

$$\frac{v_2}{v_1} = \frac{2 + (\gamma - 1) M_1^2}{(\gamma + 1) M_1^2} \tag{2.39}$$

$$\frac{p_2}{p_1} = \frac{2\gamma M_1^2 - (\gamma - 1)}{\gamma + 1} \tag{2.40}$$

where $M_1 = v_1 / c_{s1}$ is the Mach number. Subscripts 1 and 2 refer to region one and two quantities, respectively. Thus c_{s1} is the sound speed in the upstream region, etc.

Note that the LHS's of (2.38)-(2.40) are all 1 when $M_1^2 = 1$. These LHS expressions may be either less than or greater than 1 for different values of M_1^2; so, for example, the density change across the shock interface (going from region one to region two) can be either from high to low or low to high. However, the addition of the entropy condition

$$s_2 \geq s_1 \tag{2.41}$$

restricts the allowed solutions to those consistent with

$$M_1^2 \geq 1. \tag{2.42}$$

This means that $\rho_2 \geq \rho_1$, $p_2 \geq p_1$, and $v_2 \leq v_1$. Details of the deduction of these results can be found in Ferraro and Plumpton (1961) and Priest (1982).

The work in the upcoming chapters actually involves shocks propagating parallel to magnetic field lines. In this case, the basic features of the hydrodynamic shocks are retained, but it turns out that the entropy condition (2.41) must be replaced by a stronger, so called "evolutionary," condition. A non-evolutionary shock tends to break up into multiple shocks. Satisfying the evolutionary condition insures that this does not occur. The evolutionary condition for the shocks of interest in this thesis is (see e.g., Landau, Lifshitz, and Pitaevskii 1984)

$$v_{A1} > v_1 > c_{s1} \tag{2.43a}$$

and

$$\min (c_{s2}, v_{A2}) > v_2 \tag{2.43b}$$

This condition is satisfied by the shocks to be encountered in the following chapters. (Shocks satisfying the condition 2.43 are referred to as "slow shocks.")

As indicated earlier, the shocks in this thesis develop in the numerical models to be explored in the upcoming chapters. The problem of handling shocks numerically is nontrivial. Problems occur in most conventional finite difference numerical schemes, since they rely on expansions of quantities in terms of expressions such as $\delta\rho/\rho$, in the case of the mass conservation equation (2.4). If $\delta\rho \approx \rho$, as is the case near steep gradients and shocks, the truncation errors in the code are as large as the solutions, thus precluding the effective use of such schemes.

The code in this thesis uses a different approach to the problem of modeling shocks. The code, named SHASTA, was developed by Boris and Book (1973,1976; see also Book, Boris, and Hain 1975). It is also a finite-difference algorithm, but utilizes a technique called "flux correction," and the resulting code is one of the FCT codes referred to above. Such codes circumvent the steep gradient problems by utilizing other, physical, properties of the

quantities of interest. A description of SHASTA's operation will be given using the example of the mass conservation equation.

The algorithm is composed of two stages, the first being a transport stage and the second a corrective, or antidiffusive, stage. The first stage implements a transport of mass subject to the requirement that, in addition to conservation of mass at the given timestep, the value of the mass remain positive. This positivity is forced on (the initially positive) system at all locations, including those where steep gradients or severe evacuations occur. A by-product of this first stage is the introduction of systematic numerical errors into the newly calculated quantity. This is corrected in the second stage. The correction is carried out in a fashion which prevents generation of new maxima or minima in the solution, or the accentuation of existing extrema; such new or accentuated extrema might induce negative values into the solution. The correction is nonlinear in that its value depends on the value of the mass from point to point. The FCT codes are capable of supporting steep gradients and shocks. Specifically, large jumps in quantities over one grid point can be maintained.

In the equations of this thesis, there are no explicit dissipative terms such as viscosity or heat conduction even though, as indicated earlier, such terms are important in true shock formation. The shocks which form in the numerical models can be thought of in one of two ways. The first is that the shock results from an effective viscosity: Implementation of the antidiffusion

stage of the FCT code yields a nonlinear residual term, which can be interpreted as this effective viscosity. The second way to interpret the shocks is that they are representations of actual solutions to the Rankine-Hugoniot relations. Such discontinuous solutions exist and are known as weak solutions (see Jeffrey and Taniuti 1964). In a physical system such as the solar atmosphere, however, the shocks would result from the dissipative effects of viscosity and heat conduction.

The particular FCT code used in the calculations of this thesis is explicitly based on the "conservation forms" of the mass, momentum, and energy equations. Thus equations (2.5), (2.13), and (2.20) are the ones used in all the forthcoming numerical calculations.

CHAPTER 3

LINEAR EVOLUTION OF ACOUSTIC GRAVITY WAVES ON STRONG FLUX TUBES

Introduction

As a first analysis of the MHD equations and their possible connection with spicules and fibrils, a linearized, analytical study will be pursued in this chapter. As discussed in the Introduction, spicules and fibrils are nonlinear phenomena, thus a true mathematical description of these features is expected to require a full nonlinear treatment. Such a treatment will be carried out in Chapters 4 and 6, utilizing numerical techniques. It will turn out that the analytical linearized work of this chapter will yield considerable insight into those forthcoming numerical nonlinear studies.

Analysis

The problem to be examined is formulated as follows. A magnetic flux tube will be taken to be vertical and have constant cross section in a stratified atmosphere. An impulsive force is to be imparted at the base of the flux tube, and the resulting motions of the atmosphere will be deduced. The analysis will lend insight into the rebound shock model for producing spicules introduced in

Chapter 1 (Section h) and to be analyzed in detail in Chapter 4. The results are also applicable to the fibril model of Chapter 6.

The magnetic flux tube will be taken to be ridged, consequently, cross-field motions will be prohibited. The atmospheric plasma, to be viewed as an MHD fluid, will then be channelled along the magnetic flux tube. This is a result of the frozen in assumption. The initial atmosphere is isothermal and in hydrostatic equilibrium under a constant gravitational acceleration, g. The transition region is omitted from the analysis. The equation of state is taken to be

$$p = \rho R T, \tag{3.1}$$

where p is the gas pressure, R is the gas constant, and T is the temperature. These assumptions imply a vertical atmospheric density profile described by

$$\rho(z) = \rho_0(0)\, e^{-zg/RT} \tag{3.2}$$

where $\rho_0(0)$ is the atmospheric density at the base of the flux tube.

In order to linearize the MHD equations, small amplitude disturbances will be assumed so that it is sufficient to take

$$p = p_0(z) + \delta p(z,t) \tag{3.3a}$$

$$\rho = \rho_0(z) + \delta\rho(z,t) \tag{3.3b}$$

$$v = 0 + \delta v(z,t) \tag{3.3c}$$

The subscript '0' denotes zero order quantities and the prefix 'δ' denotes first order perturbation quantities. The initial vertical velocity, v, is taken to be zero. The linerarized MHD mass, momentum, and energy equations are then

$$\frac{\partial}{\partial t}\delta\rho + \rho_0 \frac{\partial}{\partial z}\delta v + \delta v \frac{d\rho_0}{dz} = 0 \tag{3.4}$$

$$\rho_0 \frac{\partial}{\partial t}\delta v = -\frac{\partial}{\partial z}\delta p - g\,\delta\rho + f(z,t) \tag{3.5}$$

$$\frac{\partial}{\partial t}(\delta p - c_s^2\,\delta\rho) + \rho_0^{\gamma}\,\delta v \frac{d}{dz}\left(\frac{p_0}{\rho_0^{\gamma}}\right) = 0 \tag{3.6}$$

where $c_s = (\gamma p_0/\rho_0)^{1/2}$ is the sound speed, with γ the ratio of specific heats. The term f(z,t) is an explicit representation for some volume force which drives the atmosphere from the base. Combining (3.4) - (3.6) yields the wave equation

$$\frac{\partial^2 Q}{\partial t^2} = c_s^2 \frac{\partial^2 Q}{\partial z^2} - \omega_{ac}^2\, Q + \rho_0^{-1/2}(z) \frac{\partial}{\partial t} f(z,t) \tag{3.7}$$

where $\omega_{ac} = \gamma g/(2c_s)$. Also,

$$Q = \rho_0^{1/2}(z)\, \delta v. \qquad (3.8)$$

Equation (3.7) is a Klein-Gordon equation with an additional driving force term. Since this is a wave equation, it can be concluded that a force imparted on to the MHD fluid will drive waves. The character of the waves will be similar to sound waves, since the characteristic speed in (3.7) is the sound speed. But the actual waves will differ since the effect of gravity makes a contribution via the second term on the RHS of (3.7) The resulting waves are known as acoustic gravity waves, and are discussed by several authors, including Priest (1982).

Some features of (3.7) may be deduced by taking f = 0 and looking at its Fourier transform. Take $Q \sim e^{ikz - i\omega t}$. One then has

$$c_s^2 k^2 = \omega^2 - \omega_{ac}^2 \qquad (3.9)$$

This is a dispersion relation. Wave propagation exists when $k > 0$, i.e. when $\omega > \omega_{ac}$. Evanescence occurs when $\omega < \omega_{ac}$. The frequency ω_{ac} is known as the acoustic cutoff frequency.

Equation (3.7) may be solved for a variety of input forces, f(z,t). In the work here, the following form will be chosen:

$$f(z,t) = f_0\, \delta(z)\, H(t), \qquad (3.10)$$

where f_0 is a constant, $\delta(z)$ is the dirac-delta function in z, and H(t) the Heaviside step function. With the initial conditions

$$\frac{\partial Q}{\partial t}(z,0) = Q(z,0) = 0, \tag{3.11}$$

equation (3.7) may be solved via Laplace transforms. The solution is

$$Q(z,t) = [f_0/2c_s\rho_0^{1/2}(0)]\, J_0\, [\frac{\omega_{ac}}{c_s}(c_s^2 t^2 - z^2)^{1/2}]\, H(t - \frac{z}{c_s}) \tag{3.12}$$

for z > 0. This solution is the same as that obtained by Rae and Roberts (1982) in a similar linear analysis. Note that their solution, as (3.12), is not the response localized to an impulsive force as they claimed, but rather corresponds to a force which is localized at z = 0, turns on at t = 0, and remains on at all subsequent times. The force (3.10) is only implicitly included in the calculation of Rae and Roberts via their derivative initial condition on Q (Rae and Roberts 1982, eq. 16).

A form of f(z,t) of more relevance to the rebound shock model is a pulse which turns on at time t = 0, remains constant for a short time, b, and then turns off:

$$f(z,t) = a\, \delta(z)\, [H(t) - H(t - b)], \tag{3.13}$$

where a is the pulse amplitude. Since equation (3.7) is linear, the theorem for superposition of solutions holds. One may therefore

solve (3.7) using the two terms on the RHS of (3.13) separately. Then using (3.12), the solution to the pulse problem can be written down:

$$\frac{2c_s\rho_0^{1/2}(0)}{a}Q(z,t) = J_0\left(\frac{\omega_{ac}}{c_s}\sqrt{c_s^2t^2 - z^2}\right)H\left(t - \frac{z}{c_s}\right)$$

$$- J_0\left(\frac{\omega_{ac}}{c_s}\sqrt{c_s^2(t-b)^2 - z^2}\right)H\left[(t-b) - \frac{z}{c_s}\right] \qquad (3.14)$$

for $z > 0$.

Figure 3.1 plots the solution (3.14) at time t = 9 minutes as a function of height, z. The numerical values of the parameters are c_s = 8.12 km s^{-1} and $\omega_{ac} = 2.77 \times 10^{-2}$ s^{-1}. (These values correspond to the 'reference model' to be discussed in Chapter 4.) The value of b is 27 s, chosen for illustrative purposes only. Apparent in the figure is a wave front at z = 4400 km followed by the "pulse region" at the front of the solution between z = 4180 km and z = 4400 km, which was launched between time t = 0 and t = b. An oscillating wake appears at lower heights; it results from a superposition of the two Bessel functions in the solution (3.14).

The existence of the wake resulting from equation (3.7) may have been anticipated by examining the group velocity of the waves. Using (3.9), this is

$$v_g = \frac{\partial \omega}{\partial k} = \frac{k c_s}{\sqrt{k^2 + \omega_{ac}^2}} . \qquad (3.15)$$

This function indicates that information is propagated at all velocities less than the sound speed. This is characteristic of a wake behind a wave front traveling at the sound speed.

It is interesting to note the time development of the pulse region of the solution. This is depicted in Figure 3.2. (The example in Figure 3.2 is of the same solution as that of Figure 3.1.) In the first frame, 3.2a, the solution is shown at an early time, t = 2.26 min. The pulse region of the solution is positive and shows little structure. Oscillations appear in the region at a later time, t = 18 min. (Figure 3.2b). At an even later time, t = 72.2 min. (Figure 3.2c) internal structure dominates the region. As time advances, there is a piling up of oscillations in the "pulse region." This behavior can also be seen from equation (3.14) by noting the value of the first term at $z = c_s(t-b)$ (which is the height at which the second term becomes non-zero at time t). For large t, and thus large z, this value varies as $J_0[\omega_{ac}(2tb)^{1/2}]$, indicating that an increasing number of oscillations will occur in the "pulse region" as time increases.

It is also interesting to examine the behavior of the wake well behind the pulse region, i.e. at $z << c_s(t-b)$ and $\omega_{ac}(t-b) >> 1$. From the asymptotic behavior of the Bessel functions, it is readily deduced that the two Bessel functions in equation (3.14) can combine to reinforce or partially cancel the distant wake, depending on the

value of b. Reinforcement occurs when $\omega_{ac}b \approx \pi$, 3π, etc., i.e. for $b \approx$ 113, 340s, etc, if $\omega_{ac} = 2.77 \times 10^{-2}\ s^{-1}$. On the other hand, partial cancellation can occur when $\omega_{ac}b \approx 2\pi$, 4π, etc., i.e. for $b \approx 227$, 454s, etc. None of these special cases will occur in the models considered in this thesis.

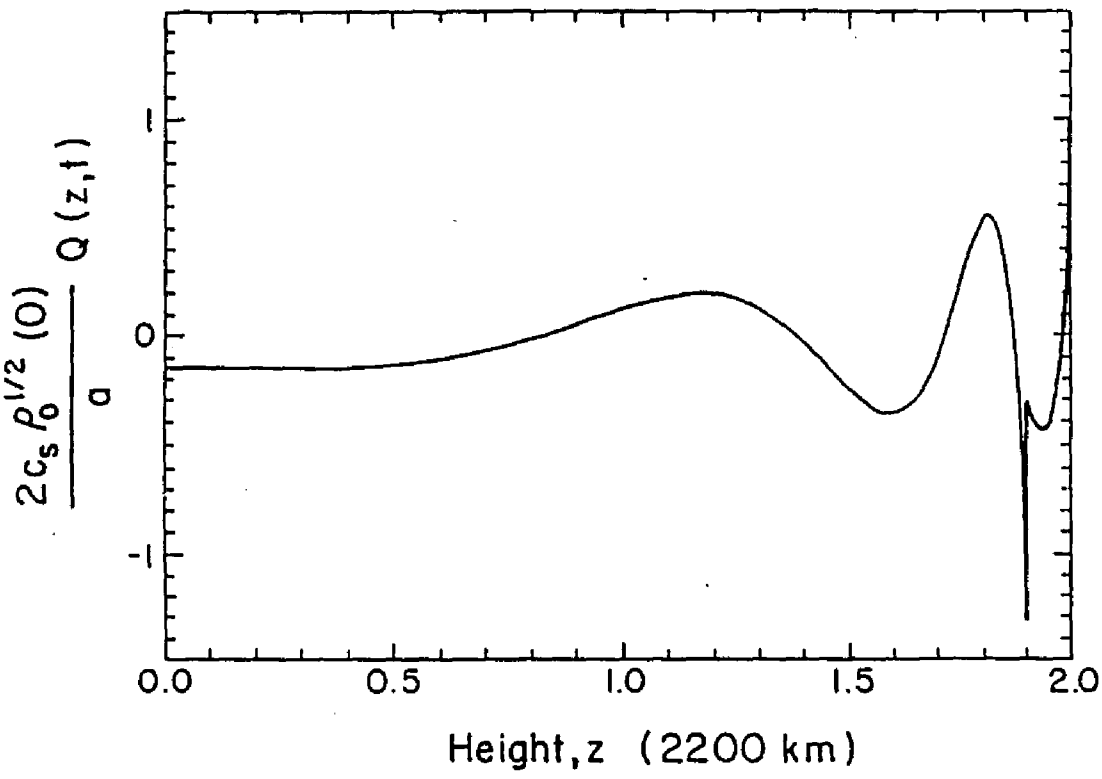

Fig. 3.1. Linear response of MHD fluid on a strong magnetic flux tube to an initial acceleration pulse as given by Equation (3.10) at t = 9 min. The pulse was turned on for a time b = 27s and has evolved into the 'pulse region' between z = 1.9 and z = 2.0 on the horizontal axis scale. The 'reference model' values for the sound speed and acoustic cutoff frequency; viz. c_s = 8.12 km s^{-1} and ω_{ac} = 2.77 x 10^{-2} s^{-1}, were chosen.

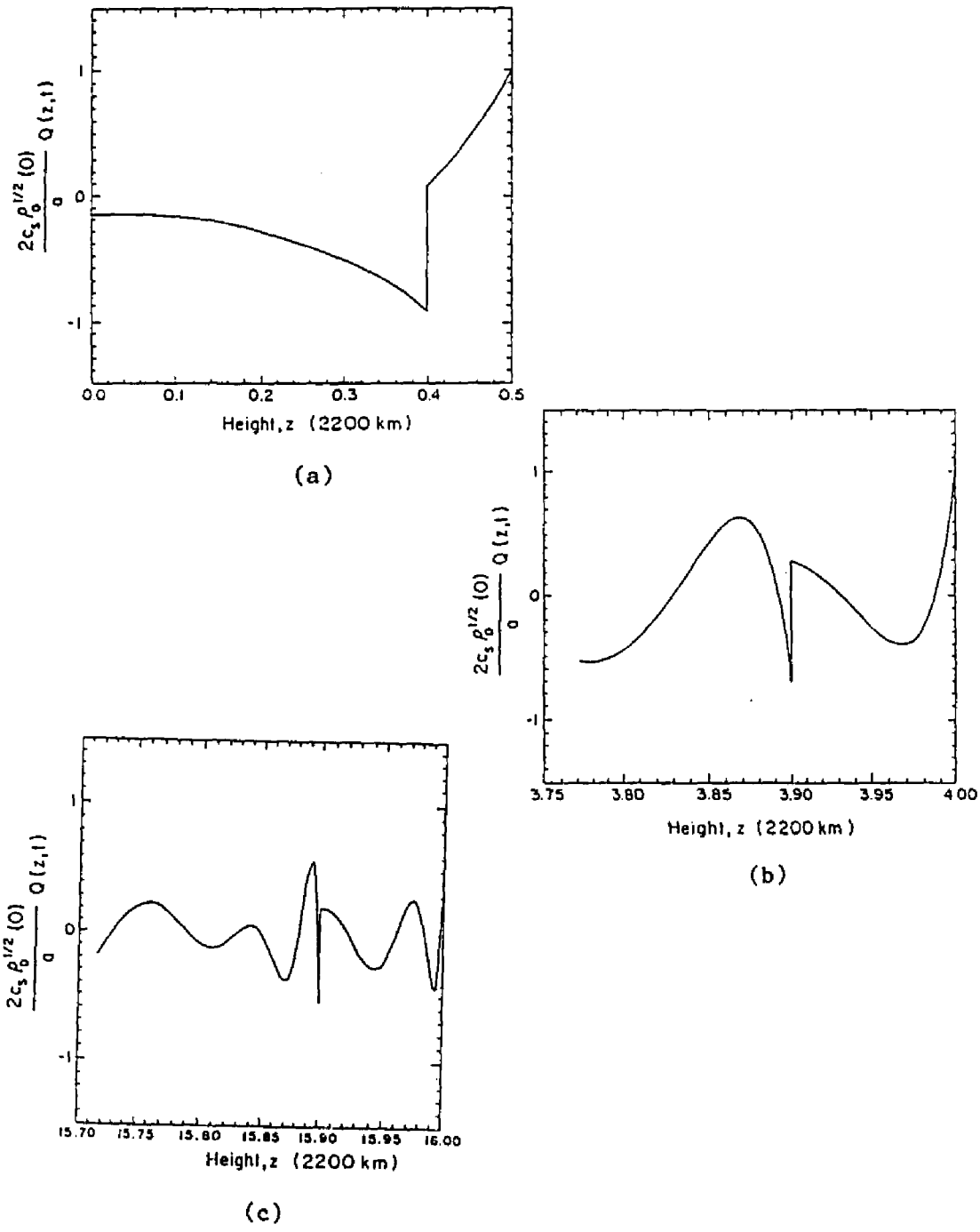

Fig. 3.2. Same as Fig. 3.1, except at a) t = 2.3 min, b) t = 18.0 min. c) t = 72.2 min. This figure illustrates the development of structure in the 'pulse region' of the solution (3.10) as a function of time.

CHAPTER 4

THE REBOUND SHOCK MODEL FOR SOLAR SPICULES: DYNAMICS AT LONG TIMES

Introduction

In this chapter the rebound shock model, introduced in Chapter 1 Section h, is extended and further developed. The model as presented by Hollweg (1982) is capable of explaining several key features of spicules. For example, the model offers an explanation for the the relatively constant upward velocity of spicules - in the model, a roughly constant spicule velocity results from the repeated interaction of the rebound shocks with the TR. Also, the model yields a hot spicule via the heat input from shock heating.

Some questions regarding the rebound shock model, however, still remain. The Hollweg (1982) study did not investigate the long-time behavior of the model; that study concluded with the model spicule still rising. But as pointed out in Chapter 1, the question of the spicule fate is important in understanding the dynamics of the solar atmosphere, and so the long term development of the model is a point of interest. Additionally, Hollweg (1982) did not investigate the variation of the model spicule's properties in response to input parameter variations. The objective of this chapter is to gain some insight into these outstanding issues.

The first question addressed in this chapter is that of the long-time behavior of the model. The original goal of this investigation was to learn how the model spicule material returns to the solar surface. However, as will be seen below, it was found that at long times the model predicts that the spicule material does not return to the surface. The transition region (TR) and the material below it remain raised and a new hydrostatic equilibrium at a higher temperature is approached. This result came as a surprise, and means that the question of the spicule fate is left unanswered by the model since, as demonstrated in Chapter 1, mass flux considerations require that most of the material in actual spicules return to the solar surface. It is now understood that the material in the model remains raised due to a transfer of energy from the initial impulse into other forms of energy. Since no dissipative terms are incorporated in the model, the only available channels for this energy are gravitational and thermal energy of the chromospheric gas which constitutes the spicule.

The new hydrostatic equilibrium approached by the model can be roughly characterized as consisting of three layers. In a representative example where the initial conditions are the same as those given in Hollweg (1982), these layers include: i) a region of nearly undisturbed chromospheric gas below some 1200 km; ii) an intermediate region of shock heated chromospheric gas which is identified with the spicule; and iii) nearly undisturbed coronal gas at heights greater than approximately 18,800 km.

Further investigations in this chapter involve the behavior of the model's characteristics as the initial input parameters are varied. Specifically, the variation of the TR's upward velocity, and of the spicule's final density, temperature, and height as functions of the magnitude of the initial impulse, its location, and the initial TR height is studied. It will be seen that a variety of final spicule characteristics can result from different input parameters. This is an important result in view of the low velocities and densities obtained by Hollweg (1982) in his model. The work of this chapter will lead to the conclusion that the low values he obtained are a consequence of the initial parameters chosen, and do not reflect an intrinsic failing of the rebound shock model. In particular, reasonable heights, densities and velocities can be obtained if the initial energy source is located a few hundred km below the height where $\tau_{5000} = 1$, and if the initial height of the TR is lower than in the models of Hollweg (1982).

As in the case of the Hollweg paper, the calculations here are very idealized; the effects of non-shock heating, heat conduction, radiation, and ionization are not included. Thus the emphasis is on the dynamics of the system. The results should be of value in understanding the dynamics of the solar atmosphere in various circumstances, but certainly a true model of spicules will have to await a more complete calculation including the above-mentioned factors. However, the term "spicule" will nonetheless be cavalierly used when describing the model results.

The following section reviews the rebound shock model, upon which the subsequent results are based. Also studied are the energetics of the model. Sections III and IV are devoted to the system's long time behavior and the variation of the system's characteristics as the input parameters are changed. The results are further discussed in Section V.

Rebound Shock Model

This section reviews the rebound shock model of spicules (Hollweg 1982). The model studies the evolution of a perturbed MHD fluid guided by a magnetic flux tube. Only vertical motions are considered. The flux tube is taken to be rigid. Hollweg pointed out that this approximation is valid for heights in excess of $\approx 10^3$ km above the $\tau_{5000} = 1$ solar surface. These heights are the most important regarding spicule formation, and so the rigid flux tube assumption was employed in the original model, and will be employed throughout this chapter.

The basic equations solved are the MHD mass (eq. 2.5), momentum (eq. 2.13), and energy (eq. 2.20) conservation equations of Chapter 2, expressed in the following form:

$$\frac{\partial}{\partial t}(\rho A) + \frac{\partial}{\partial z}(\rho v A) = 0 \qquad (4.1)$$

$$\frac{\partial}{\partial t}(\rho v A) + \frac{\partial}{\partial z}(\rho v^2 A) = -A\left(\frac{\partial P}{\partial z} + \rho g\right) + F \rho A h(z,t) \qquad (4.2)$$

$$\frac{\partial}{\partial t}(E A) + \frac{\partial}{\partial z}(E v A) = -\rho v g A - \frac{\partial}{\partial z}(p v A) + F \rho A v h(z,t) \qquad (4.3)$$

$$E = \frac{1}{2}\rho v^2 + \frac{p}{\gamma - 1} \qquad (4.4)$$

The acceleration of of gravity, g, is taken to be 2.7×10^4 cm s^{-2}. A perfect gas is assumed with $\gamma = 5/3$. The variable z is height in the solar atmosphere; this replaces the variable s which represents distance along the flux tube used in Chapter 2. The height where z = 0 in the models in this chapter coincides roughly with z = 0 in the HSRA/VAL model solar atmosphere (Gingerich et al. 1971; Vernazza, Avrett, and Loeser [VAL] 1973). However, the ambient chromosphere in the present models is isothermal, but it provides a reasonable fit to the height variation of chromospheric density in the HSRA/VAL model. The form of the cross-sectional area, A, chosen is indicated in figure 4.1, which displays $[A(z)/A(0)]^{1/2}$ in the range -880 km < z < 6600 km, where the greatest area variation occurs. At higher heights, A(z) remains constant. Figure 4.1 represents the area factor used by Hollweg (1982), and is a correction to Figure 1 which appears in that paper. Above z = 0, the cross sectional area expands by a factor of approximately 150, rather than 200 as stated in Hollweg (1982). Consequently, a field strength of 1500 gauss at z = 0 corresponds to a coronal field strength of 10 gauss. The reader is

referred to the original Hollweg (1982) paper for additional details of the initial solar atmosphere in the model. At time t=0, a quasi-impulsive vertical body force localized to the vicinity of a few grid points near z = 0 is imparted to the flux tube. This body force is represented by the final terms in equations (4.2) and (4.3). The localized spatial extent and the quasi-impulsive time variation of the force are contained in h(z,t). In this chapter's models, the time variation of h is one half of a sinusoidal cycle lasting 90.26 seconds. The factor F is the amplitude of the acceleration of the body force. (The effects of changing the location of the body force and the value of F are investigated in Section IV.)

Equations (4.1)-(4.3) are solved numerically using SHASTA - the fully nonlinear, flux-corrected transport code described in Chapter 2. The code published by Boris (1976) was used with the Eulerian grid option for all the original model calculations, as well as for the calculations in this thesis. Flow-through boundary conditions are also used for all calculations. These conditions are implemented by insisting that the value of a given quantity beyond the boundary equals the value of that quantity just inside the boundary. The value on the boundary is the average of these two, and is therefore the same as the value just inside the boundary. These boundary conditions allow for the free flow of plasma out of the numerical domain. These conditions have been tested by launching sound waves onto the upper and lower boundaries. The energy reflected by the boundaries was always found to be less than a few percent of the incident energy.

In the model calculations, the gravitational acceleration is constant throughout the region which represents the solar atmosphere. However, in the presence of gravity, the flow-through boundary conditions would allow material to continuously flow downward through the system, thus precluding a static equilibrium. This problem has been circumvented by introducing two regions, above and below the model atmosphere, in which the gravitational acceleration is smoothly tapered to zero. Tests have been applied to insure that these regions do not reflect more than a few percent of any incident energy, and that they are not sources of any significant drifts or energy fluxes. (In all figures in this chapter, the regions of varying gravity are excluded.)

The actual numerical computations used a convenient set of dimensionless variables. However, in presenting the results, everything has been converted back to physical (dimensional) quantities. This accounts for the unusual units which appear in all Figures of this chapter.

As demonstrated in Chapter 3, the response of the system to the imparted impulse at t = 0 is an upward propagating wave front, followed by an oscillating wake. Due to the nonlinear nature of the numerical calculations in this chapter, the wave front and wake evolve into a train of upward propagating rebound shocks. The shock train interacts with and repeatedly lifts the TR, which is modeled as a smoothly varying change over a narrow region in density, pressure,

and temperature. (This is a change from the Hollweg, 1982 work which represented the TR by discontinuous jumps.) The TR is regarded as the top of the spicule. Figure 4.2 shows the height of the TR as a function of time. The series of dashed lines indicates the trajectories of the rebound shocks. Each subsequent shock prevents the TR from following the ballistic path instigated by the previous shock. The result is a relatively smooth (compared to ballistic) upward trajectory of the TR at a velocity of some 16 km/s. Figure 4.2 is based on the system response to a body force localized in space to a few grid points near z = 110 km. The parameters used in producing Figure 4.2 are the same as those used to produce Figure 3 of Hollweg (1982). The slight differences in TR height vs. time in the two figures is accounted for by the inclusion of the force term in the energy equation (last term in equation 4.3); this term was inadvertently omitted in the Hollweg (1982) work.

The kinetic (E_{kin}), thermal (E_{ther}), and gravitational (E_{grav}) energies in the flux tube, normalized to the cross-sectional area at the top, A_{top}, are formulated as follows:

$$E_{grav}(t) = A_{top}^{-1} \int_{z_1}^{z_2} A(z)\, \delta\rho(z,t)\, \phi(z)\, dz + F_g(t) \qquad (4.5)$$

where ϕ is the gravitational potential (taken to be zero at z = 0), and

$$E_{ther}(t) = (\gamma - 1)^{-1} A_{top}^{-1} \int_{z_1}^{z_2} A(z)\, \delta p(z,t)\, dz + F_t(t) \qquad (4.6)$$

$$E_{kin}(t) = 0.5\, A_{top}^{-1} \int_{z_1}^{z_2} A(z)\, \rho(z,t)\, \delta v^2(z,t)\, dz + F_k(t) \qquad (4.7)$$

The quantities $\delta\rho$, δp, and δv represent the density, pressure, and velocity deviations from their initial values. The limits z_1 and z_2 are in the region of uniform gravity. Now any wave motions, shocks, or flows induced by the source (located in a localized region between z_1 and z_2) will yield a non-zero energy flux out of the region of integration. The terms $F_g(t)$, $F_t(t)$, and $F_k(t)$ are added to compensate for these fluxes, and are given by

$$F_g(t) = A_{top}^{-1} \sum_{i=1}^{2} (-1)^i A(z_i) \int_0^t \delta v(z_i,t')\, \rho(z_i,t')\, \phi(z_i)\, dt' \qquad (4.8)$$

$$F_t(t) = A_{top}^{-1}\, \gamma (\gamma - 1)^{-1} \sum_{i=1}^{2} (-1)^i A(z_i) \int_0^t \delta v(z_i,t')\, p(z_i,t')\, dt' \qquad (4.9)$$

$$F_k(t) = 0.5\, A_{top}^{-1} \sum_{i=1}^{2} (-1)^i A(z_i) \int_0^t \rho(z_i,t')\, \delta v^3(z_i,t')\, dt' \qquad (4.10)$$

The quantities given by equations (4.5) - (4.7) are plotted in Figure 4.3 for the case where $z_1 = 0$ and $z_2 = 19{,}400$ km. The two large amplitude oscillations represent the gravitational and thermal

energies per cross-sectional area, and the light solid curve represents the kinetic energy per cross sectional area. The thermal and gravitational energies oscillate out of phase with each other, and both, being first order quantities, dominate the second order kinetic energy term. Also indicated in Figure 4.2 is the time-behavior of the sum $E_{kin}(t) + E_{grav}(t) + E_{ther}(t)$ denoted by $E_{tot}(t)$. Note that $E_{tot}(t)$ is conserved to within a few percent. This gives one the confidence to extend the numerical calculation to study the long-time development of the model.

Long Time Behavior

The original work on the rebound shock model conducted by Hollweg (1982) concluded with the question of the model spicule's fate unresolved. The TR was still moving up after 18 minutes, at which time the calculation concluded. The model's long-time behavior will now be addressed.

The principal result is depicted in Figure 4.4, which is identical to the solid line in Figure 4.2, but continued out to t = 75 minutes. The TR continues to rise until a maximum height is reached - in this case, some 14,500 km. This occurs after about t = 26 minutes. At later times, the TR remains raised, oscillating about the average maximum height in response to continued interaction with the upward propagating train of progressively weaker rebound shocks.

The same general features are apparent in Figure 4.5, which shows density as a function of height. Each profile corresponds to the results at a different time, the lowest being at t = 180.54 seconds. Each subsequent plot occurs 180.54 seconds after the one immediately below it.

The spicule is approaching a new hydrostatic equilibrium. This is indicated most clearly by the energy vs. time plot in Figure 4.6. This figure is the time extended version of Figure 3, except here z_2, the upper limit of integration in equations (4.5) - (4.7), is at z = 34,100 km. The amplitudes of all the energy oscillations approach zero at long times. Note that $E_{tot}(t)$ is conserved to within some 20%; this is a measure of the inaccuracy of the long-time calculations.

As discussed in this chapter's Introduction, the new equilibrium state consists of three layers: i) nearly undisturbed chromosphere, ii) an intermediate layer which is to be associated with the spicule, and iii) nearly undisturbed corona. These layers are clearly visible in the temperature vs. height plot of Figure 4.7. The plot is at the time indicated by the arrow in Figure 4.4, i.e. t = 63.2 minutes. In this example, the spicule region has a temperature of 5-7 x 10^4 K if the molecular weight is 0.5. The heating is a consequence of the rebound shocks.

Ultimately, the shock heating explains why the spicule remains raised: a portion of the energy from the initial impulse is deposited into the spicule as thermal energy via the shock heating. Since the model contains no further dissipation mechanism for this energy, the thermal energy remains in the spicule and acts to balance the gravitational energy as the new hydrostatic equilibrium is approached.

It has been verified that, at long times, the density of the intermediate layer varies with height very nearly in the manner expected for a gas in hydrostatic equilibrium with the temperature shown in Figure 4.7. There are however, some small deviations from hydrostatic equilibrium due to the motions which are present even at long times. For example, the top of the spicule oscillates with a velocity amplitude of some 16 km s^{-1} (see Figure 4.4), which is small compared to the sound speed of 40 km s^{-1}. The velocities at lower heights are even smaller.

Examination of plots of density vs. time at a given constant height reveals that after the short time-scale oscillations are averaged out, there are no large systematic drifts ($\leq$10%, approximately) in average density after the TR has passed that given height (Figure 4.8a). Density fluctuations of around a factor of two on short time scales (a few hundred seconds) are seen at early times in response to the still relatively strong rebound shocks, but at later times the amplitude of the fluctuations decreases due to the progressive weakening of the rebound shocks. The temperature vs.

time plot at the same height (Figure 4.8b) shows some similar features. The change in average temperature from the time the TR passes until the end of the calculation is about 50%; the time average temperature is about 5×10^4 K. The temperature increases slowly due to the shock heating.

Figure 4.8 shows that the amplitudes of the fluctuations of density and temperature change with time. Most notable are the changes which occur in both Figure 4.8a and Figure 4.8b at $t \approx 900$s. This amplitude change corresponds to the passage of the TR at the height for which the plot was calculated, z = 11,200 km. Figure 4.8a also shows a discontinuous change in the amplitude of the density fluctuations at $t \approx 1985$s. (A change in the amplitude of the temperature fluctuations is also present in Figure 4.8b, but it is less apparent.) It has been found that these amplitude changes correspond to a decrease in the strength of the rebound shocks. It is not known why this transition occurs.

System Response to Input Parameter Variations

Of key interest is the variation of the spicule velocity, and the physical properties of the system in its new equilibrium state, as various input parameters are changed. For comparison purposes, the model run by Hollweg (1982) discussed in Sections II and III will be referred to as the "reference model."

Table 1 shows the results of varying F, the amplitude of the initial acceleration in equations (4.2) and (4.3). This amplitude is given in column 1, normalized to the corresponding amplitude in the reference model (denoted by subscript 'RM'). Negative values of F denote an acceleration in the negative direction; the initial force of the reference model was applied in the positive direction. Note that negative values of F are as effective in producing spicules as positive values. In the second column of Table 1, a representative density of the spicule material after the maximum height is achieved is given. The value was determined at the mid-height of the spicule. This height was determined from the temperature vs. height profile at late times using a visual estimate. Column 3 gives the spicule temperature at the mid-height. The average final height, column 4, was obtained from TR height vs. time plots similar to that of Figure 4.4.

The approximate average upward velocity of the TR is tabulated in the final column. This velocity was determined in a fashion analogous to that used by Hollweg (1982); i.e., the quoted figures represent a time-averaged upward velocity of the TR during roughly the first 15 minutes of the spicule development.

A comparison of the columns of Table 1 reveals some trends. The terminal height of the TR increases as the magnitude of the input force increases. Similarly, the temperature of the spicule increases with the input force magnitude. Although all of the temperature values in the table are substantially greater than those

observed in spicules, the amount of this energy which would be dissipated by other processes is not taken into account by the model. Further discussion of this point is included in the following section.

These trends reflect the fact that the increased input energy distributes itself in such a manner that the magnitudes of E_{grav} and E_{ther} both increase. The magnitude of E_{kin} also increases, but Table 1 indicates that the final densities, which are already low in the reference model case compared to observations, decrease as F is increased. This density decrease occurs because roughly the same amount of material is spread out over a larger height when F is increased. However, since the magnitude of E_{kin} increases with F, the wave velocities must be correspondingly larger. The increased velocities lead to stronger shocks which in turn produce higher TR velocities. The trend of increased TR velocity with increased force amplitude is borne out by Table 1.

The Table 1 results are useful vis-a-vis solar dynamics, but none of the specific cases conforms very closely to the properties of observed spicules. The densities and total mass contents of the model spicules are particularly low; observationally, spicule densities are of the order of 10^{-13} gm cm^{-3}. In order to produce high enough densities, the trends of Table 1 indicate that the input force amplitude would have to be somewhat lower than the reference model case, but such a model would have unacceptably low TR velocities.

The densities are increased substantially when the initial TR height is decreased. Table 2 gives the results for three cases of this type. The amount of reduction of the TR height from the reference model height of 2200 km is given in column 2 in terms of ambient (i.e. at t = 0) chromospheric scale heights, H; for these models, the ambient isothermal scale height $H = p_0/\rho_0 g = 147$ km. The remaining columns of Table 2 are determined in the same manner as the corresponding ones in Table 1. All other initial parameters remain unchanged. The spicule density increases in all cases, because the density on the lower side of the TR is increased when the initial height of the TR is lowered. Additional consequences are lower final TR heights and lower upward TR velocities. This behavior results from the increased spicule density. The same amount of energy imparted to the denser column of material will not raise the material as high as in the lower density case. Also, investigation of the distribution of energy in the model via plots similar to Figure 4.6 reveals that the same portion of the energy goes into kinetic energy in both the Table 1 and the Table 2 cases. Thus, since the density is higher in the latter case, the wave velocities must be lower than in the former. The result is weaker shocks and a lower upward TR velocity.

All the results presented so far were deduced with the initial force at a height of 110 km. There is, however, no a priori reason to rely on this height value. Thus, the consequences of varying the source location have also been investigated, and the results appear in Table 3. The source location is given in column 2 in km above the

τ_{5000} = 1 surface. The initial height of the TR is the same as in the reference model. The other columns in the Table are the same as the corresponding columns in the previous Tables.

For a constant input force, the spicule temperature and density show no clear trend as the source location is lowered. However, the final TR height and TR velocity both increase with the decrement of source location height (see next Section).

The calculations were continued moving the source location below the surface. The most interesting results from the standpoint of comparing with observed spicule properties were obtained when the initial TR height was also reduced. The results, given in Table 4, include the variation of the input source location for the case where the TR is lowered to 2.3H below that of the reference model case. All the column headings are the same as those in Table 3. The trends in TR height and velocity noted for the Table 3 results continue to hold true for the models runs in Table 4. The results tabulated in row 4 of Table 4 give densities (6×10^{-14} gm cm^{-3}) and velocities (24 km s^{-1}) which compare relatively well with those of observed spicules ($\approx 10^{-13}$ gm cm^{-3} and $\approx$ 25 km s^{-1}, respectively). From the results tabulated in Tables 1-4, the following generalizations of the behavior of the rebound shock spicule model can be made.

A: The final spicule densities

i. decrease as $|F|$ increases

ii. increase as the initial TR height decreases

iii. show no clear trend as the source height decreases

B: The upward velocity of the TR

i. increases as |F| increases

ii. decreases as the initial TR height decreases

iii. increases as the source height decreases

C: The terminal TR height

i. increases as |F| increases

ii. decreases as the initial TR height decreases

iii. increases as the source height decreases

D. The final raised spicule temperature

i. increases as |F| increases

ii. decreases as the initial TR height decreases

iii. shows no clear trend as the source height decreases.

Discussion

The goal of this chapter has been to present some new dynamical aspects of the spicule model due to Hollweg (1982). The model utilizes a series of rebound shocks to lift the TR and underlying chromosphere. The shocks result from a single quasi-impulsive source. The material below the raised TR is found to possess spicule-like properties. Chief among the new results involves the behavior of the model at long times; the TR, and

therefore the putative spicule, remains raised and a new three layer hydrostatic equilibrium condition is approached. A key problem which motivated these long-time studies remains unsolved: by what mechanism does the spicule material return to the solar surface? It has been determined that, when only shock heating and dynamics are considered, the spicules in the rebound shock model do not return to the surface, but rather a situation is reached whereby the energy input into the spicule from the shock heating balances the new level of gravitational energy. Nothing more concrete can be said about the fate of spicules using the rebound shock model without further modifications to the model. However, some speculations can be made. As suggested by Hollweg (1982), heating and ionization may lead to the fading of spicules from chromospheric lines, such as H_{α}, followed by emission in the UV. The model spicule's final temperature resulting from shock heating is generally around 5-7 x 10^4 K. The implied heating rates are probably not enough to fully ionize the spicule, especially when radiative losses are also considered.

There may, however, be additional heating mechanisms available. The three layer structure which results from the model calculations suggests a method by which Alfven waves trapped in a resonant cavity could lead to UV emitting temperatures inside the cavity. The resonance cavity would be formed by the spicule, with regions of differing Alfven speeds (the chromosphere and photosphere below and the corona above) forming the Alfven wave

reflecting regions. This mechanism will be presented and developed in the following chapter. (Also see Sterling and Hollweg 1984.)

However, it is difficult to see how further heating of the spicule could account for the ultimate tendency of the spicule to fall to lower heights; just the opposite would be expected. The return of the spicule material could conceivably be effected by the preferential radiation of thermal energy from the bottom portion of the spicule. Relatively uniform heating of the spicule (as indicated by Figure 4.7) could not balance the high radiation rate near the base of the spicule due to the higher radiative cooling rate there (Avrett 1981). The energy balance of the spicule indicated by Figure 4.6 would no longer hold near the spicule's base, and the elevated spicule could no longer be supported. The spicule material may then return in the form of the UV downflows observed in the TR (e.g., Pneuman and Kopp 1978; Gebbie et al. 1981; Roussel-Dupre and Shine 1982; Athay et al. 1983; Dere et al. 1984). It is again emphasized, however, that these considerations are wholly speculative at this point.

Also subject to speculation is the actual source of the spicules. Granular buffeting (Roberts 1979) of magnetic flux tubes has been suggested as a possible mechanism. An estimate of the velocities needed to generate spicules from photospheric motions has been made by Hollweg (1982). He found that the energy contained in 2 km s^{-1} velocities between z = 0 and z = 300 km is sufficient to generate a spicule with $\rho = 10^{-13}$ gm cm^{-3} and a height

of 8900 km. If the same velocities were imparted at lower levels, where the density is greater, even more energetic spicules could be produced. This was the case in models of this chapter: higher final TR heights and larger upward TR velocities were found when the source height was lowered (see Table 4). However, it is still unknown whether the required energy source exists at low levels, or what its nature is.

By running the rebound shock model with various input parameters, it has been found possible to produce a variety of spicules. A point of note is that downward forces are as well suited for producing spicules in the model as upward forces. Thus the possibility that falling chromospheric material induces spicules is left open. The falling material could be associated with the formation of the magnetic flux tubes in the network.

The case given in row 4 of Table 4 (source location -440 km, TR height 1860 km) gives densities and velocities closest to those observed. But there is no obvious reason to favor this particular case over any of the others. It can be said, however, that the rebound shock model is capable of generating spicules consistent with observations (with the exception of the temperature) when only the dynamics is considered.

Without the inclusion of the additional energy loss mechanisms of ionization and radiation, the study of the rebound shock model can in no way be construed as being complete; the

objective was to study some of the principal dynamics associated with the model. The radiative loss rate of spicules is not known. However, some estimates may be made. If spicules have properties similar to the upper chromosphere, then the thermal relaxation time is around 1000 seconds (Gibson 1972, p. 191). This is comparable to the lifetime of the spicule itself, and so the dynamics analyzed in this chapter would be as important as the thermal radiation effects. On the other hand, if the spicule is assumed to be optically thin, then the estimated thermal relaxation times can be less than a second. In such a case, the thermal radiation would be expected to dominate the dynamics discussed here. The estimated relaxation times for heat conduction are on the order of 10^6 seconds, and so the role of heat conduction on the spicule dynamics is expected to be small.

As an indicator of where future, more complete numerical work on the model may lead, one may note the results of the work on Alfvenic pulses in the solar atmosphere by Mariska and Hollweg (1985) which included the effects of heat conduction and radiation. In that study, Alfvenic pulses nonlinearly drove acoustic-gravity waves propagating along a magnetic flux tube. These acoustic-gravity waves were weaker than those in the rebound shock model, however, since they resulted from higher order processes. Consequently, spicule-like features did not develop in the Mariska and Hollweg (1985) work, even in the cases without heat conduction and radiation. Moreover, in the Mariska and Hollweg (1985) study, the source of the acoustic-gravity waves was propagating upward at the local Alfven speed, in contrast to the present work, where the

source is at a fixed height. It is believed that this qualitative difference also accounts for the absence of spicule-like features in Mariska and Hollweg's study. Nonetheless, the TR was found to undergo significant motions. The effect of the addition of radiative losses and heat conduction was to decrease the amplitude of these TR motions by about a factor of two. The Mariska and Hollweg (1985) results therefore suggest that the inclusion of additional loss mechanisms into the rebound shock model will lead to some differences in the details of the results, but probably not so significantly different as to discount the studies of the dynamics presented here. However, the effects of ionization have not been addressed in any study to date, and it is thus not clear to what extent ionization will affect the current chapter's results.

TABLE 1

Model Response to Input Source Magnitude Variation

F_o/F_{RM}	ρ (g cm^{-3})	T(K)	Final height(km)	TR Velocity (km s^{-1})
1 (Reference model)	5.1×10^{-15}	60,000	14,500	16
1.5	4.5×10^{-15}	64,000	21,000	18
2	2.3×10^{-15}	78,000	22,900	20
-1	3.2×10^{-15}	57,000	12,800	16
-2	2.6×10^{-15}	77,000	20,200	19

TABLE 2

Model Response to Initial TR Height Variation

F_o/F_{RM}	TR Height Reduced by	ρ(g cm^{-3})	T(K)	Final Height(km)	TR velocity (km s^{-1})
1	0.69H	1.4×10^{-14}	56,000	11,900	11
1	2.3H	6.3×10^{-13}	11,000	3,900	6
2	2.3H	5.9×10^{-14}	50,000	8,800	9

TABLE 3

Model Response to Input Source Location Variation

F_o/F_{RM}	Source Location, z(km)	ρ(g cm^{-3})	T(K)	Final Height (km)	TR Velocity (km s^{-1})
2	550	4.6×10^{-15}	62,000	11,200	9
2	110	2.3×10^{-15}	78,000	22,900	20
1	330	3.6×10^{-15}	63,000	11,200	10
1	110	5.1×10^{-15}	60,000	14,500	16
1	65	4.3×10^{-15}	55,000	15,000	16
1	0	7.6×10^{-15}	77,000	31,700	24

TABLE 4

Model Response to Input Source Location Variation with Lowered Initial TR Height

F_o/F_{RM}	Source Location, z(km)	ρ(g cm^{-3})	T(K)	Final Height (km)	TR Velocity (km s^{-1})
1	0	3.6×10^{-14}	52,000	12,000	10
1	-220	4.8×10^{-14}	57,000	17,200	16
1	-330	4.9×10^{-14}	67,000	21,200	18
1	-440	6.2×10^{-14}	73,000	24,200	24

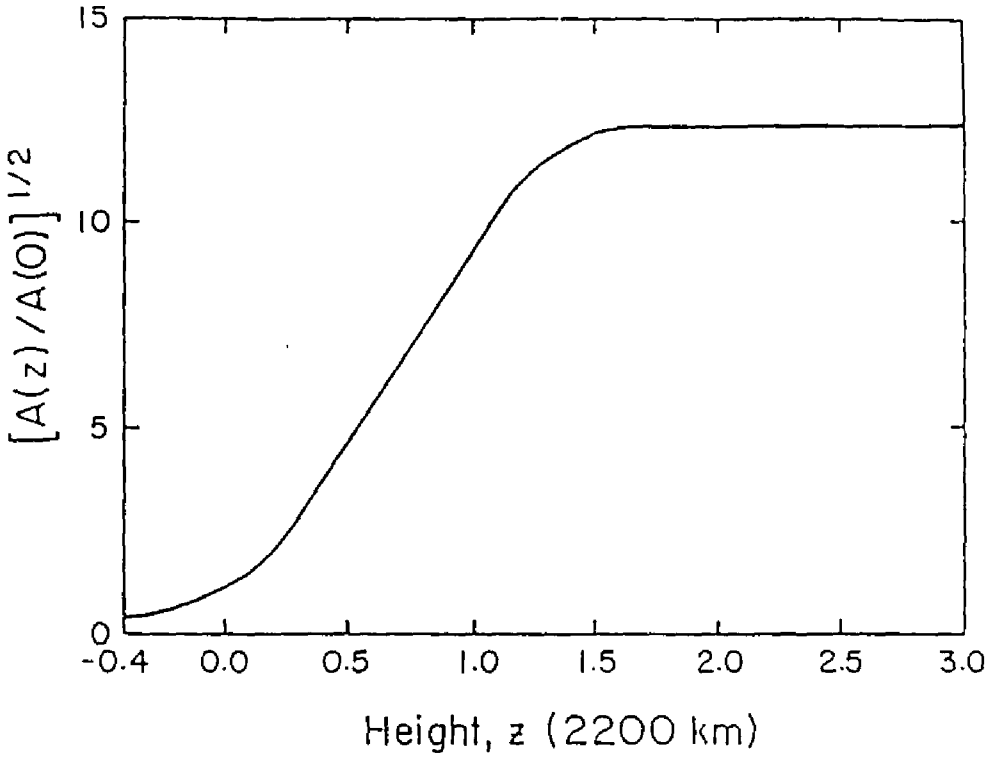

Fig. 4.1. The variation of the cross sectional area of the magnetic flux tube with height. The cross sectional area is normalized to its value at z = 0.

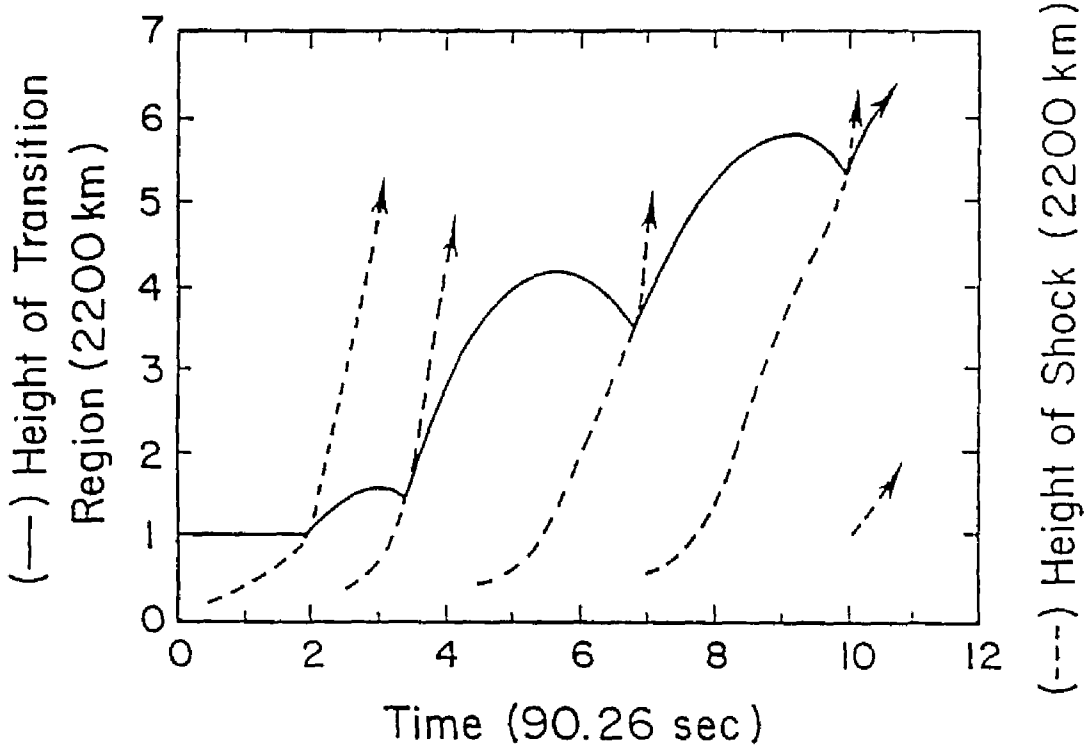

Fig. 4.2. Height of transition region vs. time (solid line) in the rebound shock model of spicules. The dashed lines represent trajectories of the rebound shocks. Figures 4.2-4.8 are all derived from the 'reference model' described in Section II.

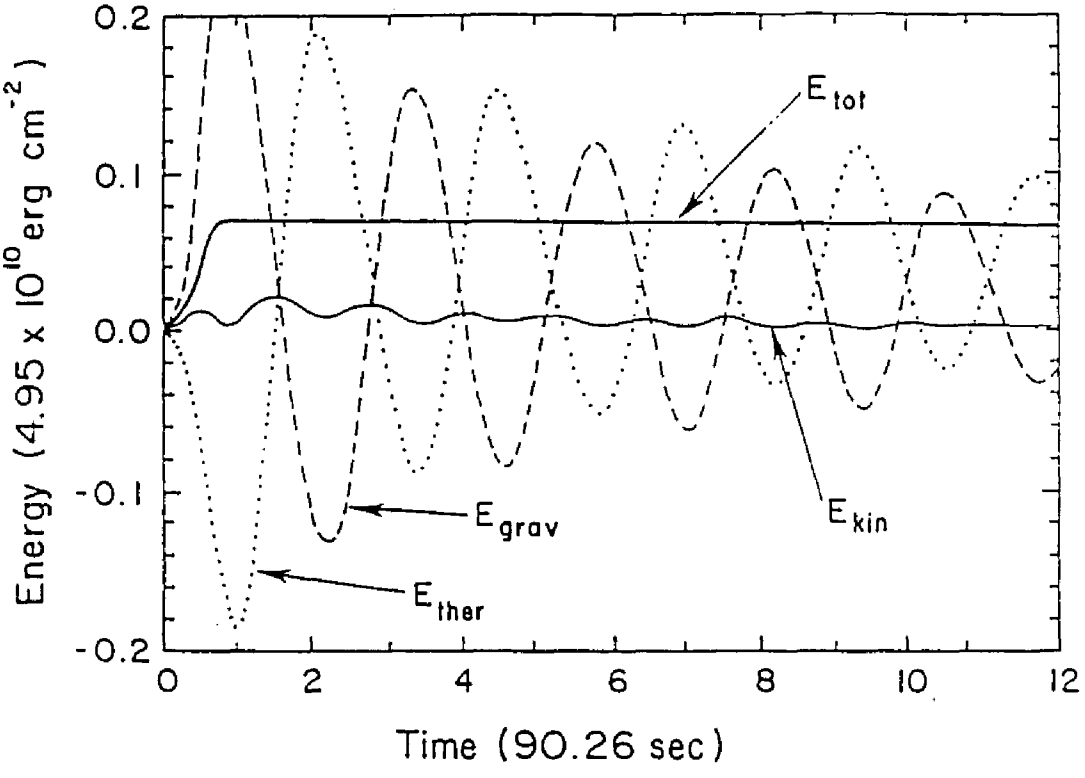

Fig. 4.3. Energy balance in the rebound shock model as a function of time, as described by equations 4.5 - 4.10. The dotted line represents the thermal, the dashed line the gravitational, and the light solid line the kinetic energy normalized to the cross-sectional area at the top of the flux tube in the model. Compensation has been made for fluxes out of the region of calculation (see text). The heavy solid line represents the sum of the other three quantities.

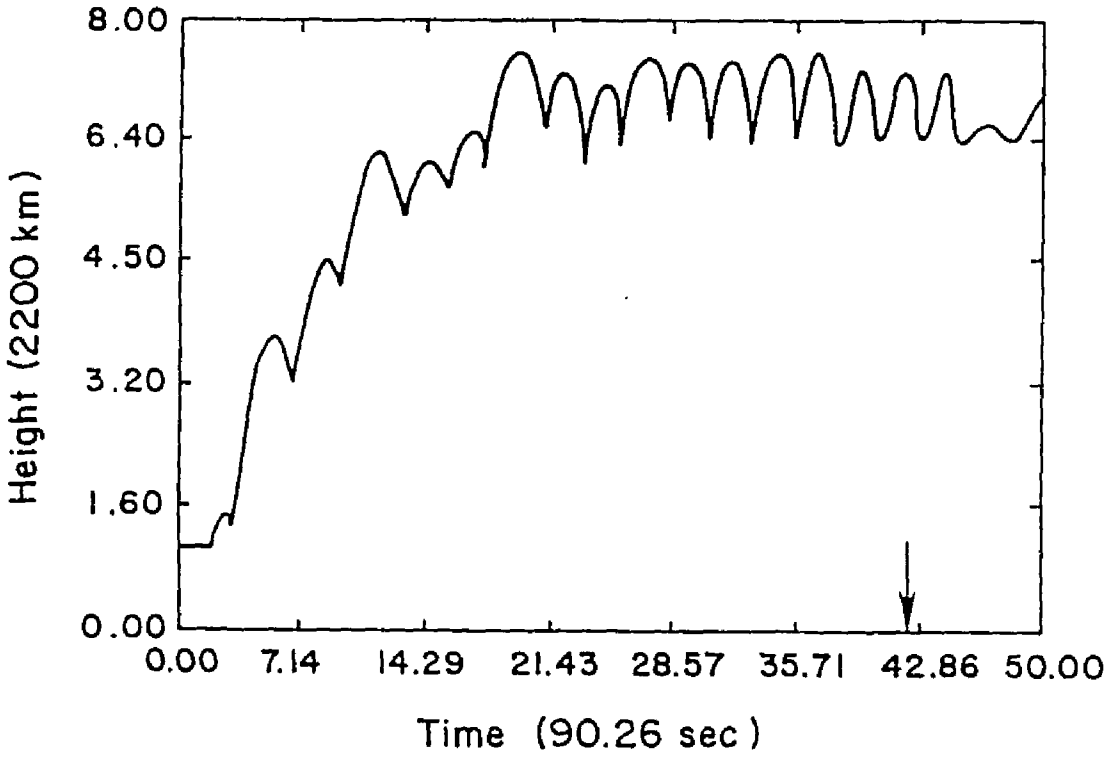

Fig. 4.4. Same as the solid line in Fig. 4.2; i.e., the height of the TR as a function of time in the rebound shock model. Here the calculation is continued until t = 75 min. The TR achieves and maintains a maximum height of some 14,500 km after approximately t = 26 min. The arrow indicates the time at which the calculation in Figure 4.7 is performed.

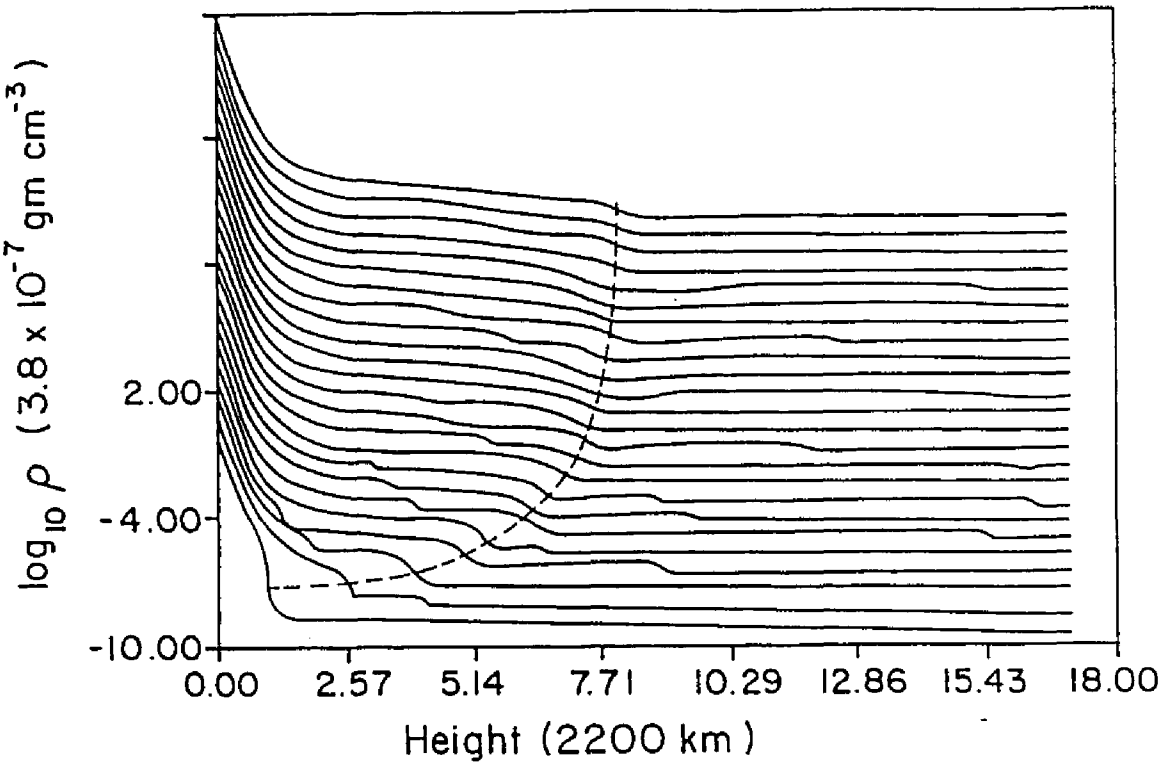

Fig. 4.5. Density vs. height at 24 different times. The lowest profile is at t = 180.54s. Each subsequent profile is 180.54s later than the profile immediately below it. The vertical scale corresponds to the lowest profile. Note that the profile remains roughly constant after the ninth profile. The dashed line indicates the TR.

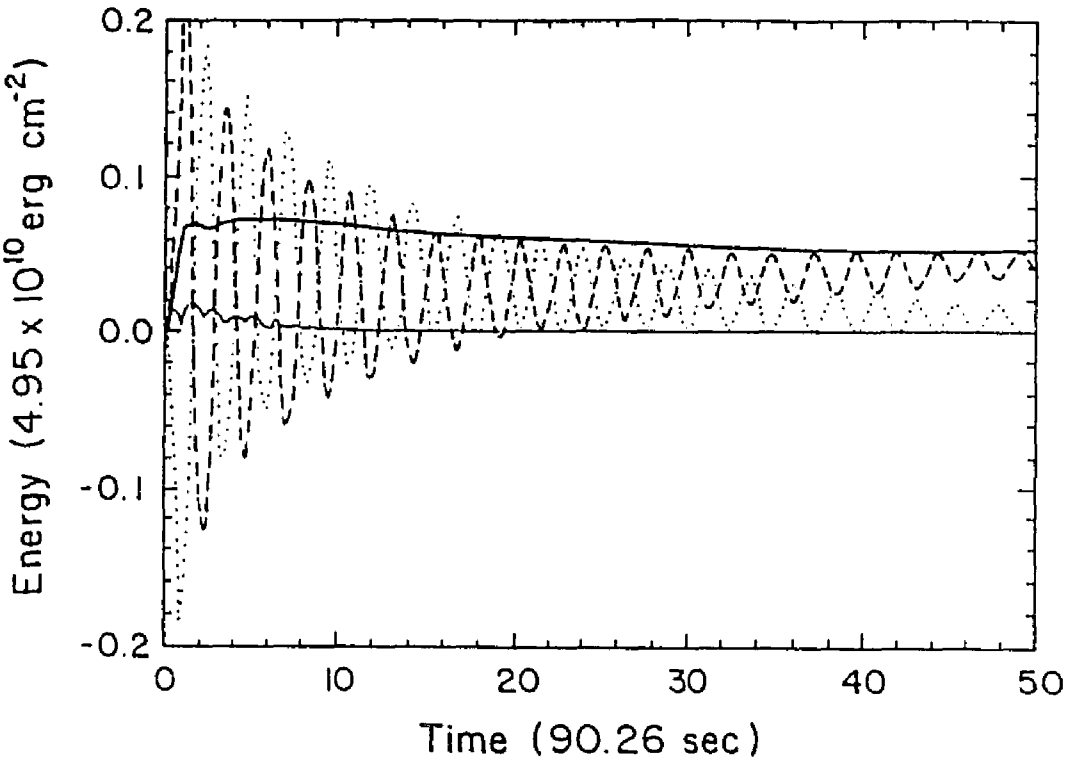

Fig. 4.6. Same as Fig. 4.3, except continued until t = 75 min. Note the decrease in amplitude of the oscillations at long times, indicating an approach to a new hydrostatic equilibrium.

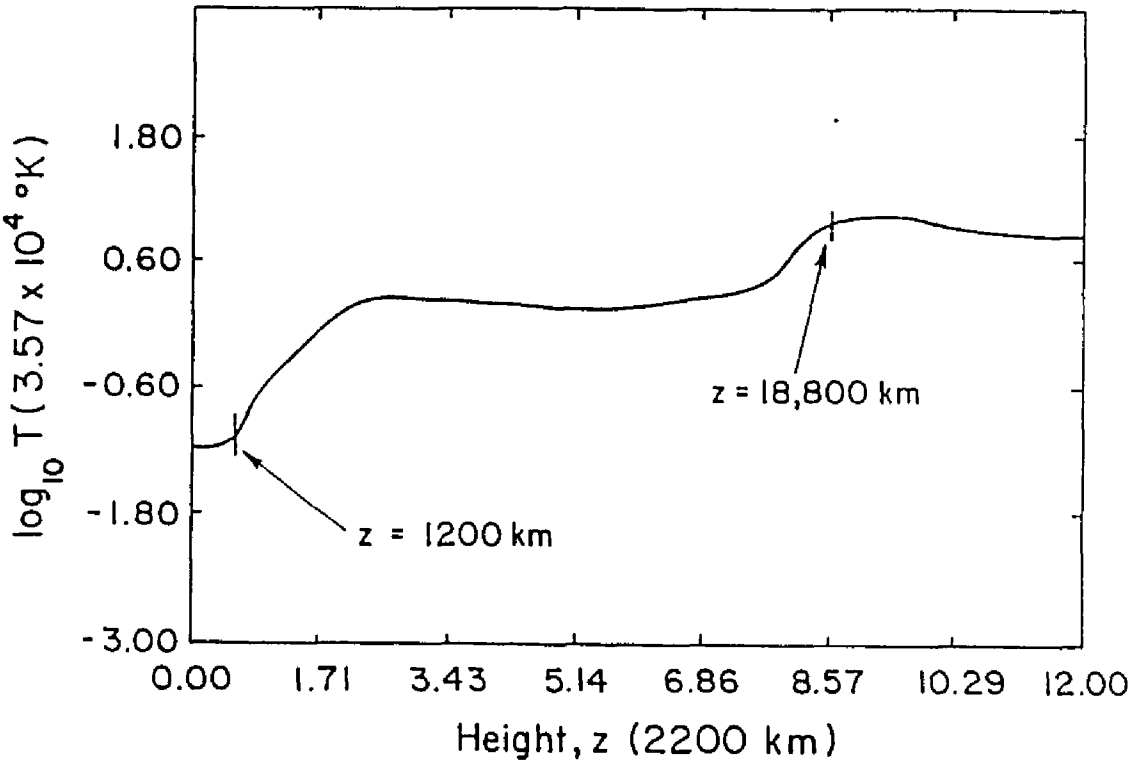

Fig. 4.7. Temperature vs. height at time indicated by arrow in Figure 4.4 (t = 63.2 min.). The TR has achieved its new height. Three layers are evident in the profile: chromosphere and photosphere below z = 1200 km; an intermediate shock-heated region associated with the spicule; corona above approximately z = 18,800 km.

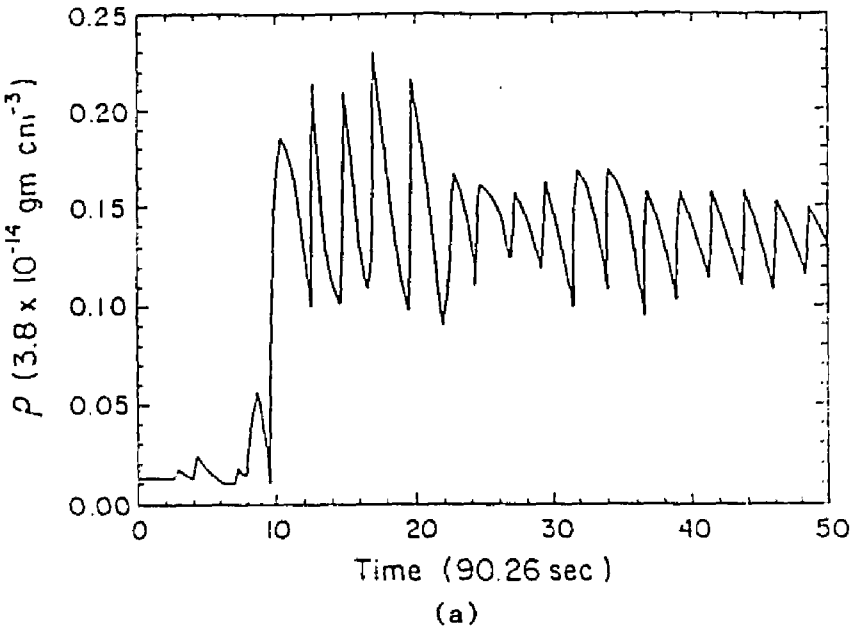

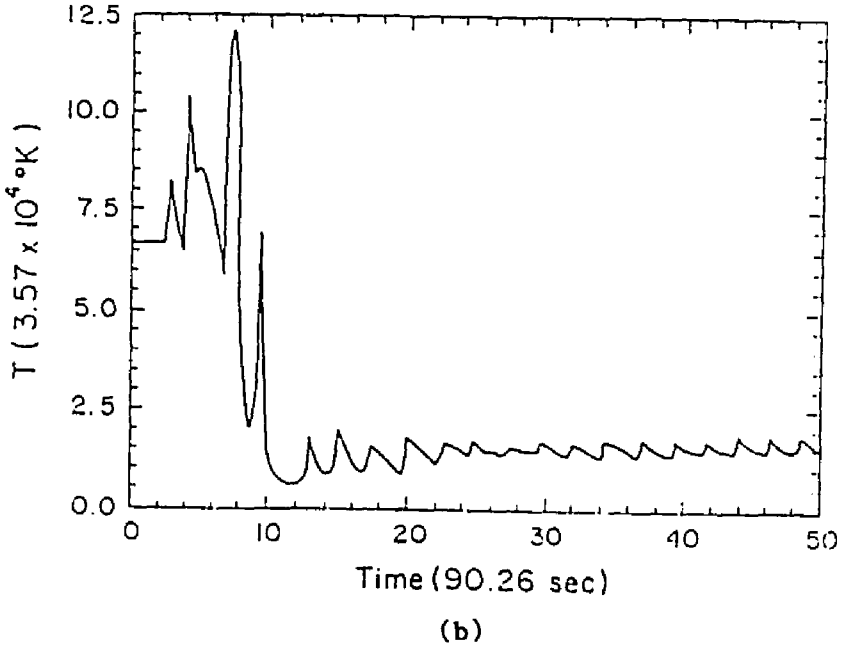

Fig. 4.8. Density (a) and temperature (b) as a function of time at z = 11,200 km. At times less than approximately 90s, the atmosphere at this height is basically coronal in nature. At later times, the TR has moved to higher heights; the densities and temperatures are then characteristic of the intermediate layer in Fig. 4.7.

CHAPTER 5

ALFVENIC RESONANCES ON SOLAR SPICULES

Introduction

The object of this chapter is to point out a new aspect of spicules which may account for some of their heating, and for their occasionally observed twisting motions (see Chapter 1). Specifically, it will be shown that spicules can be resonance cavities for Alfvenic twists. The resonance cavity forms because the spicule is bounded above by a region (the corona) where the Alfven speed is much larger than in the spicule, while it is bounded below by a region (the photosphere and low chromosphere) where the Alfven speed is a rapidly increasing function of height. Both of these regions can reflect Alfven waves, and trap wave energy in the spicule, forming a resonance cavity. It will be shown that the spicules act much like anti-reflection coatings on camera lenses, allowing photospheric disturbances of certain resonance frequencies to propagate through the chromosphere and into the spicule without undergoing substantial reflection. Moreover, it will be shown that this energy will heat the spicules, if a suitable wave dissipation mechanism is present in the spicule. It is suggested that the dissipation rate may be determined by the rate at which a turbulent cascade feeds energy to higher wavenumbers.

Resonance cavities have been of recent interest in other contexts, particularly in connection with heating coronal active region loops (Hollweg 1981, 1984a,b; Ionson 1982, 1984; Zugzda and Locans 1982). This chapter is similar to Hollweg (1984a) in that a three-layer model is used to represent the behavior of the Alfven speed. However, the behavior of the Alfven speed assumed in this paper is fundamentally different from that assumed in Hollweg (1984a), and thus the mathematical details require reevaluation.

The analysis of this chapter will be restricted by the simplifying assumption that the spicule is not changing in time. Thus L (the length of the cavity) will be taken to be constant, and plasma flows within the spicule will be ignored. In the case of a developing spicule, this turns out to be a marginal assumption for the fundamental (i.e. longest period) resonance, since the period of the fundamental is not very much shorter than the timescale over which the length of an actual spicule changes. For example, the period of the fundamental is approximately $4L/v_{A2}$, where v_{A2} is the Alfven speed inside the spicule. Taking L = 7000 km and v_{A2} = 357 km s^{-1} (appropriate for a spicular density of 10^{-13} gm cm^{-3} in a 40 Gauss field) yields a fundamental period of 78 seconds, which is to be compared to spicule lifetimes of a few hundred seconds. The approximation seems reasonable for the higher harmonics, however. For example, for the numerical values given above, the period of the first harmonic is only 26 s. However, if viewed in terms of the rebound shock model discussed in Chapter 4, the steady state

analysis of this chapter is not a severe approximation, since it was found that the spicules in that model reached a steady state after an initial period of growth.

Dissipationless Analysis

Resonances on spicules will be analyzed subject to the following simplifying assumptions:

1. The wave fluctuations are small amplitude. Hence, linearized theory will be used. The time-independent background quantities will be denoted by the subscript '0', and the wave quantities by the prefix 'δ'.

2. The magnetic flux tube on which the spicule is to occur will be taken to have constant cross section.

3. All quantities are taken to be axisymmetric. The symmetry axis is vertical. Hence $\partial/\partial\theta = 0$, where θ is the azimuthal angle about the symmetry axis.

4. The background magnetic field, $\mathbf{B}_0$, is untwisted, so $B_{0\theta} = 0$.

5. The only nonvanishing components of $\delta\mathbf{v}$ and $\delta\mathbf{B}$ are δv_θ and δB_θ, where $\mathbf{v}$ and $\mathbf{B}$ denote velocity and magnetic field respectively.

6. The effects of viscosity and electrical conductivity are not explicitly considered. However, some damping will be assumed at a later point.

Assumptions 3 and 5 together imply that the waves are non-compressive. Hence gravity and thermal pressure play no role in the momentum and energy of the system. Using basically the same assumptions, Hollweg (1984a) combined the MHD momentum equation (eq. 2.11), and the induction equation (eq. 2.24) into the following expression for the magnetic field fluctuation:

$$\frac{\partial}{\partial t}\delta B_\theta = \mathbf{B}_0 \cdot \nabla \delta v_\theta \tag{5.1}$$

and the following wave equation for the velocity fluctuations:

$$\frac{\partial^2}{\partial t^2}\delta v_\theta = v_A^2 \frac{\partial^2}{\partial s^2}\delta v_\theta \tag{5.2}$$

where the analysis has been restricted to near the symmetry axis.

Equation (5.2) is to be solved for three different regions of the solar atmosphere, each with a different expression for the Alfven speed, v_A. The geometry is given in figure 5.1. Note that s increases downward into the solar atmosphere.

Region 1 corresponds to the photosphere and chromosphere, where v_A is taken to be

$$v_A \propto \exp[-(s-L)/2h] \tag{5.3}$$

where h is a positive constant. Region 2 represents the spicule which will be taken to have constant Alfven speed. Region 3 represents the corona, which will also be taken to have a constant, but much higher, Alfven speed.

The source of the Alfven waves is assumed to be in the photosphere, so there will be upward- and downward-propagating waves in regions 1 and 2, but only an upward-propagating wave in region 3. For harmonic waves varying as exp(iωt), the solutions to (5.1) and (5.2) are easily verified to be:

Region 3 (s < 0):

$$\delta v_\theta = a \exp(i\omega t + i k_3 s) \tag{5.4}$$

$$\delta B_\theta = a \frac{k_3}{\omega} B_{0s} \exp(i\omega t + i k_3 s) \tag{5.5}$$

Region 2 (0 < s < L):

$$\delta v_\theta = (b e^{-i k_2 s} + c e^{i k_2 s}) e^{i\omega t} \tag{5.6}$$

$$\delta B_\theta = -\frac{k_2 B_{os}}{\omega}\left(b\, e^{-i k_2 s} - c\, e^{i k_2 s}\right) e^{i\omega t} \qquad (5.7)$$

Region 1 (s > L):

$$\delta v_{\theta'} = \left[d\, H_0^{(1)}(\xi) + e\, H_0^{(2)}(\xi)\right] e^{i\omega t} \qquad (5.8)$$

$$\delta B_{\theta'} = \frac{i B_{0s}}{v_A(s)}\left[d\, H_1^{(1)}(\xi) + e\, H_1^{(2)}(\xi)\right] e^{i\omega t} \qquad (5.9)$$

where $\xi \equiv 2h\omega/v_A(s)$; $\theta' = -\theta$, $k_2 = \omega/v_{A2}$, $k_3 = \omega/v_{A3}$, and a,b,c,d and e are complex constants.

The matching conditions at s = 0 and s = L require that δv_θ and δB_θ be continuous at those locations. Therefore

$$b = \frac{k_2 - k_3}{2 k_2} a \qquad (5.10)$$

$$c = \frac{k_2 + k_3}{2 k_2} a \qquad (5.11)$$

and

$$e = \frac{\pi\beta}{4i}\left[(b' + c')\, H_1^{(1)}(\beta) - i\,(b' - c')\, H_0^{(1)}(\beta)\right] \qquad (5.12)$$

$$d = -\frac{\pi\beta}{4i}\left[(b' + c')\, H_1^{(2)}(\beta) - i\,(b' - c')\, H_0^{(2)}(\beta)\right] \qquad (5.13)$$

where $\beta = 2h\omega/v_{A2}$ and

$$b' = b\, e^{-i k_2 L} \tag{5.14a}$$

$$c' = c\, e^{i k_2 L} \tag{5.14b}$$

Equations (5.10) - (5.13) completely specify four of the constants in terms of the fifth. Here four constants will be written in terms of a, the amplitude of the wave leaving the spicule resonance cavity and escaping into the corona. Equations (5.10) - (5.14) can be combined to yield

$$e = \frac{\pi \beta a}{4 i k_2} [(k_2 H_1^{(1)} + i k_3 H_0^{(1)}) \cos (k_2 L) - (k_2 H_0^{(1)} - i k_3 H_1^{(1)}) \sin (k_2 L)] \tag{5.15}$$

$$d = -\frac{\pi \beta a}{4 i k_2} [(k_2 H_1^{(2)} + i k_3 H_0^{(2)}) \cos (k_2 L) - (k_2 H_0^{(2)} - i k_3 H_1^{(2)}) \sin (k_2 L)] \tag{5.16}$$

where the argument of the Hankel functions is β.

Hollweg (1984a) showed that the time-averaged Poynting flux in region 1, in the negative-s direction (i.e. upward), is proportional to $|d|^2 - |e|^2$. He therefore identified the $H_0^{(1)}$ part of (5.8) as the wave which propagates upward from the photosphere, while the $H_0^{(2)}$ part of (5.8) was identified as the downward-propagating wave. Thus an energy reflection coefficient can be defined as

$$R = \frac{|e|^2}{|d|^2} \tag{5.17}$$

The transmission coefficient at the region boundary between regions 1 and 2 is

$$T = 1 - R \tag{5.18}$$

T and R can be calculated from (5.15) and (5.16). The analysis so far has only considered solutions to equation (5.2), which contains no dissipation. Therefore, the transmitted wave energy will flow thru the spicule and out into the corona.

Figure 5.2 plots the transmission coefficient T verses ω. The frequencies correspond to periods ranging from 7 to 500 seconds. The coronal density was taken to be $\rho_c = 3.3 \times 10^{-16}$ g cm^{-3}, which is a typical value for coronal holes, and the spicule density used was $\rho_s = 1 \times 10^{-13}$ g cm^{-3} (c.f. Beckers, 1972, Table 3). The chromospheric scale height, h, is 150 km, the spicule length L = 7000 km and B_0 = 40 G. The figure displays the aforementioned transmission resonances. The period of the fundamental resonance is about 90 seconds and the period of the first harmonic is about 30 seconds. The periods are closely approximated by equation (5.21), below.

Further insight into the properties of the resonances can be gained by simplifying the 'full' solutions (equations (5.15) - (5.18))

using appropriate approximations. It turns out that β is quite small for solar parameters, at least for the lower-order resonances, so the small argument approximations for Hankel functions, $H_1^{(1),(2)} \rightarrow \pm iY_1$, $H_0^{(1),(2)} \rightarrow 1 \pm iY_0$, and $|Y_1(\beta)| >> |Y_0(\beta)|$, may be employed. Also, since $\rho_s >> \rho_c$, one has $k_3 << k_2$. Using these, (5.15) and (5.16) can be reduced to give the following approximate expression for T:

$$T \approx \frac{-4 k_2 k_3 Y_1}{(k_2 - k_3 Y_1)^2 \sin^2(k_2 L) + k_2^2 Y_1^2 \cos^2(k_2 L)} \qquad (5.19)$$

where the argument of the Bessel function is again β. Note that the coefficient of $\cos^2(k_2 L)$ is large. Thus T is a maximum when $\cos(k_2 L) = 0$. Thus the resonances occur when

$$k_2 L \approx (2n - 1)\frac{\pi}{2} \qquad (5.20)$$

i.e.,

$$\omega_{res} \approx \frac{\pi}{2}\frac{v_{A2}}{L}(2n - 1) \qquad (5.21)$$

where n = 1, 2, 3...denotes the order of the resonance. An odd number of quarter-wavelengths must fit into region 2.

The heights of the resonance peaks are thus

$$T_{max} \approx \frac{-4 k_2 k_3 Y_1}{(k_2 - k_3 Y_1)^2} \qquad (5.22)$$

Using the small argument approximation $Y_1(\beta) \approx -2/\pi\beta$, and defining

$$L_n \equiv \frac{\pi^2 h}{2}(2n - 1)\frac{k_2}{k_3} \qquad (5.23)$$

(5.22) may be rewritten as

$$T_{max} \approx \frac{4 L/L_n}{(1 + L/L_n)^2} \qquad (5.24)$$

Note that $T_{max} = 1$ when $L = L_n$. In that case waves can propagate from the photosphere into the spicule without undergoing any reflections. However, for the spicule parameters used in Figure 5.2, $k_2/k_3 = v_{A3}/v_{A2} = (\rho_2/\rho_3)^{1/2} = 17.4$ and $L_n = 12900\ (2n - 1)$ km if $h = 150$ km. Thus $L_n > L$ for all n and T_{max} is always less than unity for these parameters; this can be seen in Figure 5.2. T_{max} could approach unity on longer spicules, however.

The approximate full width at half maximum of the transmission resonance peak, $\Delta\omega$, can be found from (5.19) by noting that the coefficient of $\cos^2(k_2 L)$ is large, and by expanding the denominator about $\cos^2(k_2 L) = 0$. There results, in terms of L_n,

$$\Delta\omega \approx 2\, v_{A2} \frac{k_3}{k_2} \frac{L_n}{L^2} \left(1 + \frac{L}{L_n}\right) \qquad (5.25)$$

The quality of the resonance is defined to be

$$Q \equiv \omega_{res} (\Delta\omega)^{-1}$$

Combining equations (5.21) and (5.25) yields

$$Q \approx \frac{L_n L}{2\pi h (L_n + L)}$$

Taking L = 7000 km, h = 150 km, and L_n = 12900(2n-1) km gives Q = 4.8 for n = 1 and Q = 6.3 for n = 2. Even in the absence of dissipation, the spicule resonances are not very high quality.

The energy flux density, F, entering the spicule is calculated by assuming that the convective motions launch a net upward-propagating energy flux density, P, in a frequency bandwidth B_ω. After integrating over one resonance peak one obtains (see also Hollweg, 1984a)

$$F \approx P\, T_{max} \frac{\Delta\omega}{B_\omega} \frac{\pi}{2} \qquad (5.26)$$

where it is assumed that the spectral density is flat for simplicity. Using (5.24) and (5.25), (5.26) can be written

$$\frac{F}{P} \approx \frac{4\pi v_{A2}^2}{(1+L/L_n)\, v_{A3}\, L\, B_\omega} \qquad (5.27)$$

Take $B_\omega = 10^{-1}\ s^{-1}$; this corresponds to assuming that the power is spread between periods of 60 and 1000s. Using the same numbers as in the previous examples, viz. v_{A2} = 357 km s^{-1}, L = 7000 km, h = 150 km, v_{A3} = 6210 km s^{-1}, L_n = 12900 km (n = 1 resonance), gives F/P = 0.24. The flux P is calculated by assuming that the photosphere twists the field lines with an rms velocity δv_{ph}. Then

$$P = \rho_{ph}\, \delta v_{ph}^2\, B_0\, (4\pi\, \rho_{ph})^{-1/2} \qquad (5.28)$$

where the subscript 'ph' denotes photospheric values. Assume ρ_{ph} = 3 x 10^{-7} g cm^{-3}, δv_{ph} = 1 km s^{-1}, and B_0 = 40 G. Then for the first order resonance, P = 6.2 x 10^7 erg $cm^{-2}\ s^{-1}$. This implies a flux of F = 1.5 x 10^7 erg $cm^{-2}\ s^{-1}$ entering the spicule. It is important to note that this estimate of the flux is only approximate, and could easily be, say, increased by a factor of two or more by considering slightly larger photospheric motions, and/or slightly larger values for B_0, since F varies as the square of both these quantities. Additional energy also becomes available when the higher order resonances are excited.

The velocity fluctuations in the spicule can be calculated from (5.6), (5.10) and (5.11):

$$\delta v_\theta = \frac{a}{k_2}[k_2 \cos(k_2 s) + i\, k_3 \sin(k_2 s)]\, e^{i\omega t}. \qquad (5.29)$$

Since $k_3 << k_2$ and since $\cos(k_2 L) \approx 0$ at resonance, it can be seen that the amplitude of the fluctuations is greatest near the top of the spicule, where $s = 0$, at resonance. This is a reflection of the fact that the wave amplitudes are much larger in the corona than in the chromosphere due to the corona's much lower density. As a numerical example, suppose that a flux $F = 1.5 \times 10^7$ erg cm^{-2} s^{-1} flows through the spicule and into the corona in one of the resonances. Thus $(1/2)\, \rho_3\, v_{A3}\, a^2 = 1.5 \times 10^7$ and one can deduce $a = 121$ km s^{-1}, if $B_0 = 40$ G and $\rho_3 = 3.3 \times 10^{-16}$; this is the velocity amplitude at the top of the spicule. The velocity amplitude at the bottom of the spicule ($s = L$) is only 7.0 km s^{-1} if $k_2/k_3 = 17.4$. Thus the resonances are capable of inducing large twisting motions on spicules. In fact, the predicted velocities near the top of the spicule are much larger than the typical observed values (≈ 20 km s^{-1}; e.g. Pasachoff, Noyes and Beckers 1968; Beckers 1972). The contradiction can be resolved by taking wave damping into account. This is done in the next section.

Wave Damping

Once energy has entered a spicule via a resonance, it must be dissipated in order for heating to occur. Without such dissipation, the energy simply flows through the spicule and into the corona.

In this section, the effects of damping on the transmission coefficient of the Alfven waves entering the spicule from the chromosphere will be investigated. The damping mechanism is unspecified. Rather, some form of linear damping will be assumed. The effect of this is to change the spicule wave number, k_2, to a complex quantity. Thus write $k_2 = k_r + ik_i$, where k_i is negative if damping is to occur.

In redoing the analysis to determine the transmission coefficient of the Alfven wave entering the spicule from the chromosphere, it must be noted that the condition $k_2 = \omega/v_{A2}$ no longer holds. Equations (5.15) and (5.16) are now

$$e = \frac{\pi \beta a}{4 i k_2} [(k_2 H_1^{(1)} + i k_3 \frac{k_2 v_{A2}}{\omega} H_0^{(1)}) \cos (k_2 L)$$

$$- (k_2^2 \frac{v_{A2}}{\omega} H_0^{(1)} - i k_3 H_1^{(1)}) \sin (k_2 L)] \qquad (5.30)$$

$$d = \frac{\pi \beta a}{4 i k_2} [(k_2 H_1^{(2)} + i k_3 \frac{k_2 v_{A2}}{\omega} H_0^{(2)}) \cos (k_2 L)$$

$$- (k_2^2 \frac{v_{A2}}{\omega} H_0^{(2)} - i k_3 H_1^{(2)}) \sin (k_2 L)] \qquad (5.31)$$

with $k_2 = k_r + ik_i$. The argument of the Hankel functions is still β.

The transmission coefficient is again given by (5.18). The form of k_r is assumed to be

$$k_r^2 \approx \frac{\omega^2}{v_{A2}^2}\left(1 - 3\frac{k_i^2}{k_r^2}\right) \tag{5.32}$$

which is a fairly general expression valid when the damping is not too strong (Hollweg 1984a, equation 64).

Using (5.30) - (5.32), the transmission coefficient for various values of $|k_i/k_r|$ were determined (see Figure 5.3). The transmission peak heights are enhanced for the cases with a small amount of damping added. Note that the high-order resonances tend to blend together. This occurs in part because the damping increases $\Delta\omega$ (see below), and in part because the waves are so severely attenuated in propagating from s = L to s = 0 that effective contact with the transition region is lost. It is then no longer meaningful to talk about resonances, but it should be noted that T becomes very large in those cases.

The heights of the transmission peaks can be estimated from (5.32) and (5.31) by assuming that the peaks occur when $\cos(k_r L) \approx 0$. If also $\beta \ll 1$, $Y_1(\beta) \approx -2/(\pi\beta)$, $|Y_1| \gg Y_0$, $k_3 \ll k_2$, $|k_i/k_r| \ll 1$ and $|k_i|L \ll 1$, one can deduce

$$T_{max} \approx \frac{4\pi h k_3 k_r^2}{(k_3 + \pi h k_r^2)^2}\left(1 - \frac{k_r k_i L}{k_3}\right)\left[1 - \frac{k_r k_i L}{k_3 + \pi h k_r^2}\right]^{-2} \qquad (5.33)$$

The width of the resonance peak can be found in the same manner as before (see also eq. 56 of Hollweg 1984b). It is given by

$$\Delta\omega = \frac{2 v_{A2}}{L}\left(\frac{\pi h \omega_{res}}{v_{A2}} + \frac{k_3}{k_r}\right) - 2\omega_{res}\frac{k_i}{k_r} \qquad (5.34)$$

Note that dissipation ($k_i < 0$) broadens the resonance.

The energy flux density, F, entering the spicule can be calculated by combining (5.26), (5.33) and (5.34); the result will not be written down. This is the energy which flows out of the spicule into the corona, plus the energy which is deposited in the spicule as heat. Of this total, the fraction, f_H, which is deposited as heat is

$$f_H = \left[1 + \frac{k_3}{k_r}(k_r L)^{-1}\left(\frac{|k_i|}{k_r}\right)^{-1}\right]^{-1} \qquad (5.35)$$

(See eq. 58 of Hollweg 1984b.) For example, consider the fundamental resonance ($k_r L = \pi/2$) and take $k_r/k_3 = 17.4$; then f_H = 0.21, 0.50, 0.73 and 0.85 for $|k_i/k_r| = 0.01$, 0.037, 0.1 and 0.2 respectively. The average volumetric heating rate in the spicule can be obtained by dividing the energy flux density which goes into heat by L. Thus equations (5.26), (5.33), (5.34), and (5.35) yield

$$\frac{E_H}{P} = \frac{4\pi^2 h v_{A3} (k_r L)^2}{L^3 B_\omega} \frac{|k_i|}{k_r} \left[1 + (k_r L) \frac{k_r}{k_3} \left(\frac{\pi h}{L} + \frac{|k_i|}{k_r} \right) \right]^{-1} \quad (5.36)$$

For the spicule parameters used in this chapter (h = 150 km s^{-1}, L = 7000 km, v_{A2} = 357 km s^{-1}, v_{A3} = 6210 km s^{-1}, B_ω = 0.1 s^{-1}, and P = 6.2 x 10^7 ergs cm^{-2} s^{-1}), and for the n = 1 resonance ($k_r L = \pi/2$), one has E_H = 0.03, 0.04, and 0.045 ergs cm^{-3} s^{-1} for $|k_i/k_r|$ = 0.1, 0.2 and 0.3 respectively. The value 0.04 ergs cm^{-3} s^{-1} will be taken as representative. This value of E_H may provide significant spicule heating. For example, take

$$\frac{3}{2} n k \frac{\partial \tau}{\partial t} = E_H \quad (5.37)$$

where τ denotes spicule temperature, n denotes the particle concentration, and k is Boltzmann's constant. No allowance is made for losses due to ionization and radiation, and the adiabatic cooling due to the spicule expansion. For a fully ionized hydrogen spicule (molecular weight = 0.5), n = 1.2 x 10^{11} cm^{-3} and $\partial\tau/\partial t$ = 1600 deg s^{-1}, only 12 seconds would be required to heat the spicule by 20000 K. About 15 minutes (i.e. somewhat longer than a spicule lifetime) would be required to heat a spicule to coronal temperatures ($\approx$ 1.5 x 10^6 K), and only 120s are required to heat a spicule by 200000 K according to the above estimates. These estimates motivate the suggestion that H_α - emitting spicules fade from view as the hydrogen becomes fully ionized as the gas is heated, and that the spicules eventually attain EUV-emitting temperatures and become

EUV spicules. Observational evidence in support of this viewpoint can be found in a paper by Withbroe (1983).

However, it is important to note that radiation will be an important energy loss mechanism, which will severely limit the ability of waves (or any other process) to heat spicules to EUV-emitting or coronal temperatures. Unfortunately, the radiative energy budget of spicules is not known. If one were to treat an H_α spicule as typical of the upper chromosphere or lower transition region, then the conclusion would be that some 10^{-2} ergs cm^{-3} s^{-1} is needed to balance the radiative losses (Fig. 49 of Vernazza, Avrett and Loeser 1981). This is comparable to the above calculated value of E_H. At EUV-emitting temperatures (few x 10^5 K) the spicule can be assumed to be optically thin. The radiative losses are then $\approx 6 \times 10^{-22} n_e^2$ (in ergs cm^{-3} s^{-1} if n_e is in cm^{-3}) (see Figure 10 of Rosner, Tucker, and Vaiana 1978). If the heating occurs at constant density, then $n_e = 6 \times 10^{10}$ and the radiative losses are 2.2 ergs cm^{-3} s^{-1}. The predicted heating rate cannot sustain these losses, and so it is concluded that radiative losses prevent the resonances from heating spicules to EUV emitting temperatures at constant density. However, if the heating occurs at constant pressure, then n_e would decrease by a factor of about 10 as the spicule is heated from H_α emitting temperatures to EUV-emitting temperatures. The radiative losses are then 0.02 ergs cm^{-3} s^{-1} which is again comparable to the above estimates of the resonant heating. It can only be concluded that the resonances provide a good possibility to heat spicules to

EUV-emitting temperatures if the heating occurs at constant pressure, but the radiative losses represent a major unknown.

A cautionary note: Equations (5.33) - (5.36) are valid only if there is a distinct resonance peak, unblended with neighboring resonances. Figure 5.3c shows an example where this condition is satisfied for the n = 1 resonance, but it fails for the higher-order resonances. In such cases it is necessary to use the full result for the transmission coefficient, based on equations (5.30) and (5.31). Figure 5.3 indicates that the transmission coefficient becomes quite large at high frequencies, ω greater than or about equal to 0.2 s^{-1}. Thus most of whatever high-frequency power is generated by the convection zone can actually be available for spicule heating.

The velocities in the spicule can be computed in detail from equation (5.29), even for complex k_2. However, only a rough estimate will be given here. Since E_H refers to the heating averaged over the length of the spicule, one can write

$$E_H = \frac{2\,\omega\,|k_i|}{k_r}\,\rho_s << \delta v_\theta^2 >> \qquad (5.38)$$

where $<< \delta v_\theta >>$ represents an average over both time and over the length of the spicule; equation (5.38) assumes equipartition between magnetic and kinetic energies and the factor 2 arises when one considers energy which is a quadratic quantity. Taking E_H = 0.04

ergs cm^{-3} s^{-1}, $\rho_s = 10^{-13}$ gm cm^{-3}, and $\omega \approx 0.08$ s^{-1} (the n = 1 resonance) yields

$$<< \delta v_\theta >>^{1/2} = 15.8 \, (k_r / |k_i|)^{1/2} \text{ km s}^{-1} \qquad (5.39)$$

The predicted spicule velocities are compatible with the observed twisting velocities (Beckers 1972 quotes turbulent velocities of some 20 km s^{-1} while Pasachoff, Noyes and Beckers 1968 give 30 km s^{-1} as an upper limit on the twisting velocities) if $|k_i| / k_r > \approx 0.25$.

Heating Mechanisms

Hollweg (1984a) made speculations regarding the turbulent heating of coronal loops. Here similar arguments will be applied to the spicule heating problem.

Hollweg pointed out that Alfven waves in a resonant cavity can be unstable to the Kelvin-Helmholtz instability, in virtue of the shearing motions intrinsic to the Alfven wave. He further suggested that the Kelvin-Helmholtz instability could initiate and mediate a Kolmogorov turbulent cascade to higher transverse wavenumbers, where energy could be dissipated via microscopic processes, such as viscosity. The turbulent heating rate is, approximately,

$$E_H \approx \rho_s k_{t0} \langle \delta v^2 \rangle^{3/2} \qquad (5.40)$$

where k_{t0} is the 'outer' transverse wavenumber, i.e. the wavenumber at which energy is injected.

Unfortunately, k_{t0} must be guessed. A conservative guess is $k_{t0} = 2\pi/$(spicule diameter). Thus $k_{t0} = 6.3 \times 10^{-8}$ cm^{-1} for a spicule diameter of 1000 km. If Beckers' (1972) value for the turbulent velocities in spicules is taken, viz. $\langle \delta v^2 \rangle^{1/2} = 20$ km s^{-1}, then $E_H = 0.05$ ergs cm^{-3} s^{-1}. This value of E_H is sufficient to heat spicules to EUV-emitting temperatures, as discussed in the previous section. It is also comparable to the value of E_H deduced from equation (5.36). It is concluded that Kolmogorov turbulence can dissipate the Alfven wave fluxes which are predicted to enter spicules, and that the dissipation is consistent with the observed nonthermal motions on spicules. Note that equation (5.40) predicts more heating per particle near the top of the spicule, where the velocities are predicted to be largest. The resonance model may therefore account for observations indicating that spicules are hotter near their tops (e.g. Athay 1976, page 440). However, the rebound shock model (Chapter 4) and the model due to Suematsu et al. (1982) also yield higher temperatures near the spicule tops.

It should also be mentioned that ion-neutral frictional heating (Piddington 1956; Osterbrock 1961) may also play a role in heating spicules.

Discussion

In this study, a possible explanation for the heating and rotational motions of spicules has been suggested. The transition region with the corona forms the upper boundary of the spicule, while the photospheric and chromosphere forms the lower boundary. In this way the spicule can be thought of as a cavity. It has been shown that torsional Alfven waves generated in the lower regions of the solar atmosphere can enter this cavity and that the transmission amplitude of these waves into the spicule can be large at certain selected resonant frequencies. Large fluxes of energy enter the cavity and thereafter heat the spicule if dissipated. One possible dissipation mechanism is as follows: the torsional twists introduced at the base of the spicule induce shearing motions susceptible to Kelvin- Helmholtz instabilities, which in turn generate Kolmogorov turbulent rolls that cascade to ever-higher transverse wave numbers and are subsequently dissipated via microscopic processes.

An interesting by-product of this work is a suggested explanation for the presence of EUV spicules and the fading of H_α spicules. It is predicted that spicules can be heated by Alfvenic twists at a rate of some 20000 degrees in about 10 seconds. This rate is too high to conform to observed values, but it has been assumed that all the energy goes into heat, where in fact some losses due to ionization and radiation would be expected. In any

case, the suggested scheme indicates that the spicule could continue to be heated even after its maximum height has been obtained. As the temperature continues to increase, the degree of ionization will increase. The intensity of the H_α radiation will correspondingly decrease and the spicule will fade from view if observed in H_α. If the spicule continues to be heated and attains a temperature of 1-2 x 10^5 degrees, emission in the EUV can be expected.

It is interesting to note that Dere et al. (1983) observed "chromospheric jets" in the EUV which have properties similar to those of spicules, but with much shorter lifetimes ($\approx$ 40 seconds). The ideas presented here could be consistent with these observations, since it is suggested that the EUV emissions only occur when the spicule is near the end of its life. It is also interesting to note that Withbroe (1983) has called attention to some statistical similarities between EUV and H_α spicules. His results are consistent with the suggestion that H_α spicules can be Alfvenically heated to temperatures at which they eventually become EUV spicules.

Several aspects of the spicule phenomenon have not been addressed in this chapter's study. It was assumed from the start that the spicule has been raised to a given height. Several of the spicule generating theories discussed in Chapter 1 could perhaps lead to structures resembling spicules, but which are not of spicular temperature. For example, it is conceivable that a process such as the rebound shock mechanism could initiate spicule formation, while

the resonant processes discussed in this chapter heat the spicule, and superpose additional twisting motions on the spicule cavity.

There is some question as to the origin of the twists on the flux tubes. Here their existence was merely postulated. However, some workers have suggested that twisted and untwisting flux tubes are fairly ubiquitous on the sun (see e.g. Piddington 1981; Parker 1982). A testable prediction of this chapter is that the motions undergo torsional oscillations at the preferred resonant frequencies. The periods of the fundamental resonances turn out to be ≈ 100 seconds, and so several complete oscillations would be expected in a spicule lifetime. Whether or not such motions have been observed is not clear. Pasachoff et al. (1968) did report some time dependence of the inclinations of some spicule chromospheric spectral lines, but more detailed observations are needed before any conclusive statements can be made in this regard. Cook et al. (1984) observed tilts in the spectral lines of ultraviolet, spicule-like structres. They report that "at least some examples" from their data set do not appreciably slow or reverse tilt. However, it is not clear what oscillation periods are expected from the Cook et al. data since the densities of the features they observe are unknown, and consequently it is difficult to estimate the appropriate Alfven speed.

The strength of the magnetic field in the spicule was also postulated. A value of 40G was chosen, corresponding roughly to average field strengths in the network. But this value is really a

guess, since no data exist concerning the actual field strengths on spicules. However, it should be noted that a smaller value of B_0 would result in longer resonant periods. If this were the case, the assumption that the spicule can be treated as quasi-steady would have to be abandoned, since that assumption requires that the resonant periods be small compared to the spicule lifetime. Such long period resonances may still play a role, however, if spicules reach a new equilibrium where they remain raised (for a period of time long compared to the period of the resonances) as suggested by the rebound shock model discussed in Chapter 4.

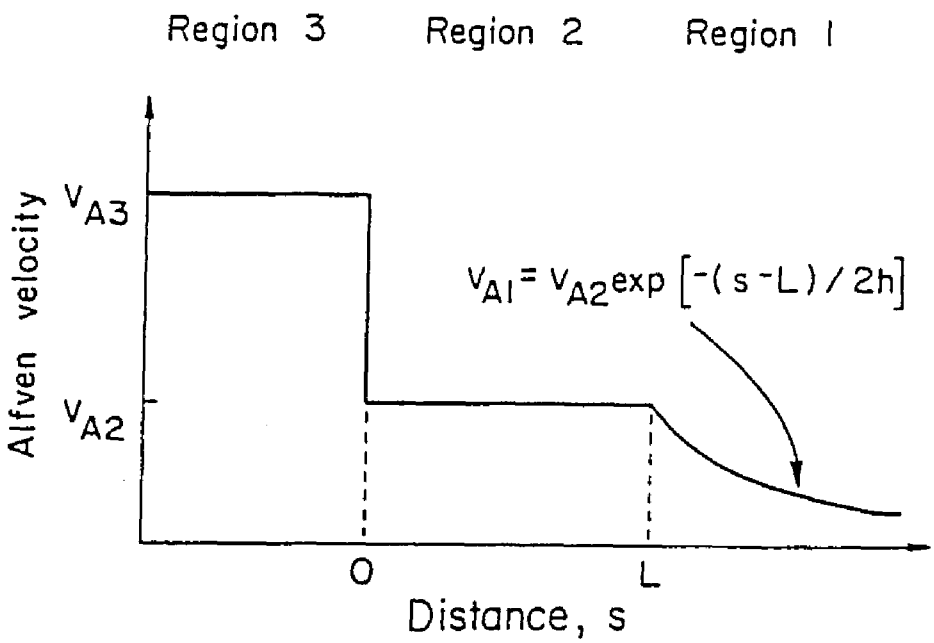

Fig. 5.1 The Alfven velocity as a function of distance in the solar atmosphere. Regions 1,2, and 3 represent the photosphere and chromosphere, the uplifted spicule, and the corona, respectively.

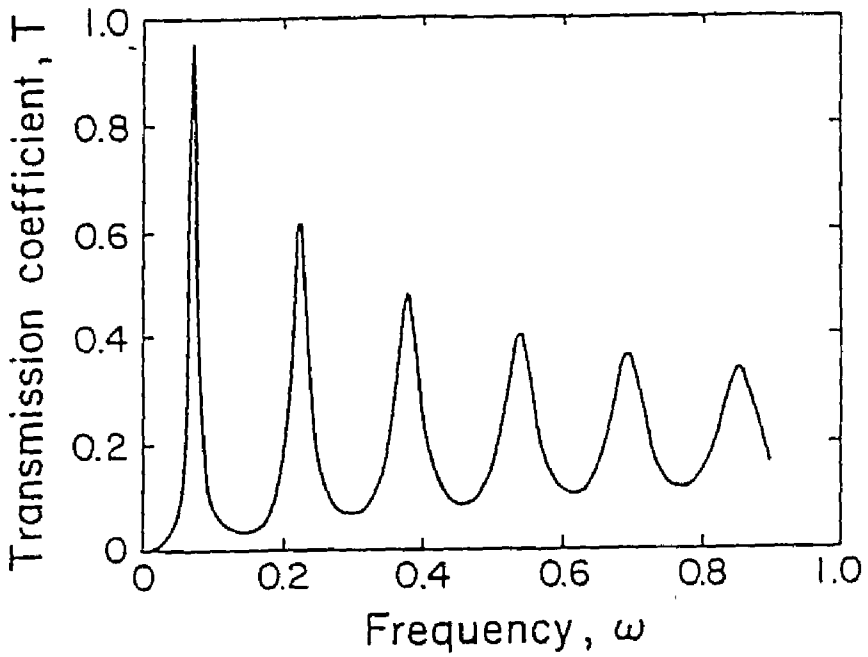

Fig. 5.2 The transmission coefficient T vs. angular frequency ω. The parameters used were L = 7000 km, v_{A2} = 357 km s^{-1}, v_{A3} = 6210 km s^{-1}, and $k_i/k_r = 0$.

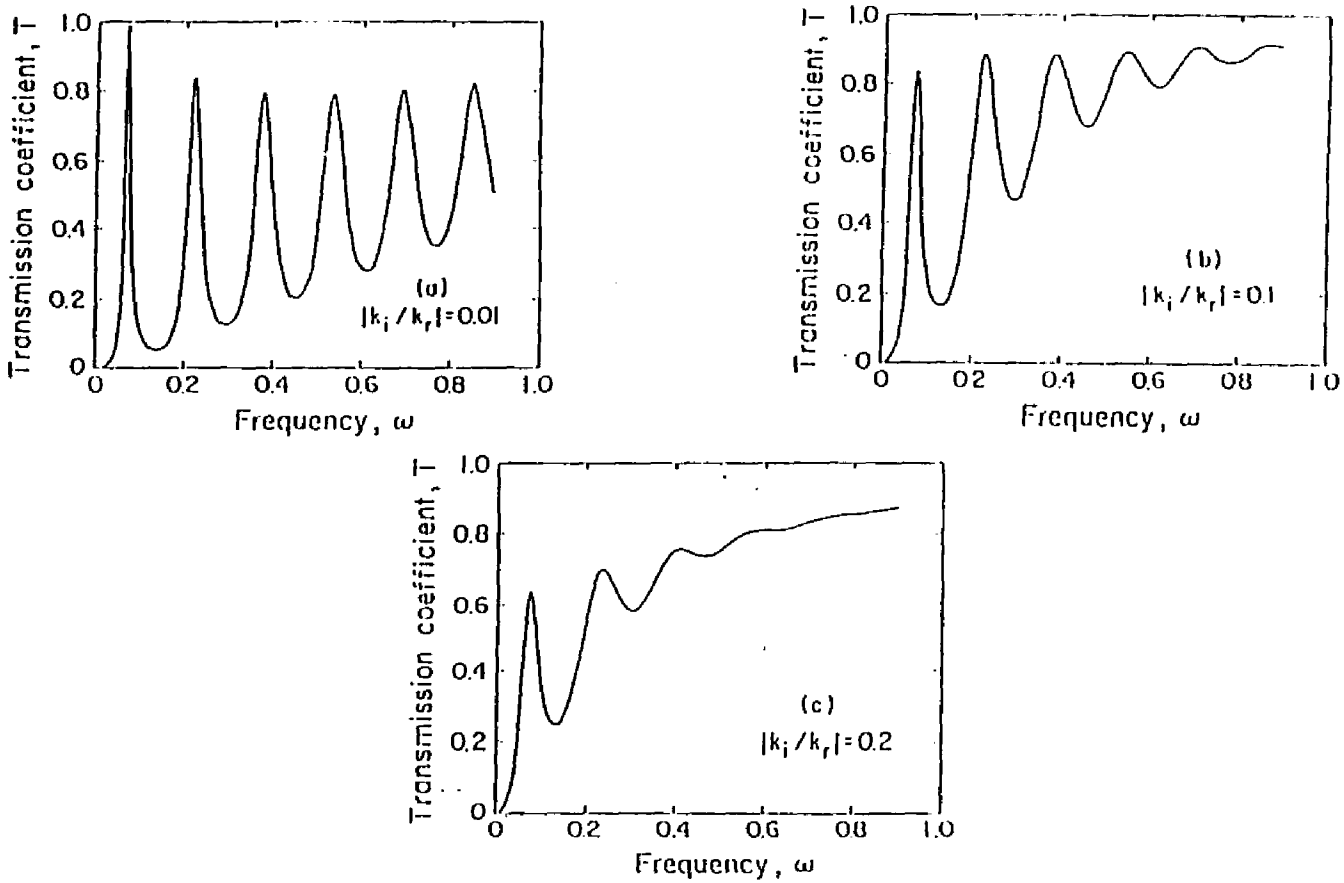

Fig. 5.3 The transmission coefficient vs. angular frequency with damping for the same parameters as in Fig. 5.2. In (a) $|k_i/k_r| = 0.01$; (b) $|k_i/k_r| = 0.1$; (c) $|k_i/k_r| = 0.2$. Note that in Fig. 5.3c the fundamental peak is distinct, whereas the higher order peaks blend together.

CHAPTER 6

A REBOUND SHOCK MODEL OF FIBRILS

Introduction

The solar fibrils reportedly take on the appearance of low-lying spicules (e.g. Foukal 1971a,b). Therefore it is tempting to investigate the possibility that both features have a common driving mechanism, but are channeled along different magnetic field geometries. This chapter numerically examines the consequences of applying the rebound shock model (discussed in Chapter 4) to a magnetic field geometry which contains a substantial horizontal component. Specifically, the magnetic field to be considered originates in the photosphere and extends vertically upward through the chromosphere and transition region, turns horizontal for 11,000 km (roughly a supergranule radius), and finally turns vertical again and extends out into the outer solar atmosphere. Such magnetic field structures may exist in solar quiet regions or coronal holes. Motivation for attempting to develop fibrils on the proposed magnetic field configuration can be gained from remarks of Athay (1986), who notes that the fibrils do not appear as complete loops. Rather, they appear to emanate from the chromospheric network at one end, but the location of their other end is unknown.

The following will show that features which may be identifiable with fibrils evolve on the horizontal segment of the flux tube, and that spicules of the nature of those in Chapter 4 do not develop. Some upward fluid motions are, in fact, induced on the vertical flux tube following the horizontal segment, but the heights reached by the fluid will be seen to be substantially less than those in the spicule model. It should be mentioned that any comparison of the following results with fibrils is necessarily cumbersome, since the fibril data are not yet complete enough to generate a standard observed fibril model with which to compare. However, as was the case with the term "spicule" in Chapter 4, the following will utilize the vernacular "fibril" to refer to the material which flows along the horizontal segment of the magnetic flux tube.

The following work is carried out under the same simplifying assumptions used in Chapter 4; thus the effects of heat conduction, radiation, and ionization are omitted. However, shock heating still contributes to the system's evolution. An immediate consequence of these factors is that the energy deposited at the base of the flux tube to initiate the calculation will remain in the system at the end of the calculation as gravitational and thermal energy. Again, the long-time behavior of the system is to approach a new hydrostatic equilibrium.

The numerical calculations show that oscillations of the gas in the flux tube develop after the fibril and a "short spicule" become established. By considering an analytical solution to a relevant but

simplified problem, it will be demonstrated that the oscillation is due to a standing wave on the flux tube.

Analysis

The attempt to model motions on solar magnetic flux tubes with a horizontal component will be restricted to one-dimension. The magnetic field geometry described above may be represented by a one-dimensional flux tube, but with the gravitational acceleration zero in the region which is to represent the horizontal segment. The equations to be solved are then identical to equations (4.1)-(4.4), but with the following two exceptions: i) the height variable, z, is replaced with the variable s, which represents distance along the flux tube (c.f. Chapter 2); ii) the gravitational acceleration is now a function of s, and is given by

$$g = g(s) = \begin{cases} 0 & \text{if } d_1 < s < d_2 \\ 2.7 \times 10^4 \text{ cm s}^{-2} & \text{otherwise} \end{cases}$$

where the horizontal segment of the flux tube begins at d_1 and ends at d_2. These values will be taken to be 3300 km and 14300 km, respectively. Note that this places the horizontal segment above the TR, which is again at 2200 km as in the 'reference model' of Chapter 4. Several other conditions are also the same as the corresponding ones in Chapter 4. These include the area variation factor, A (now =

A(s)), which is therefore given by Figure 4.1. The distribution in distance and time of the input body force, h(s,t), is the same as h(z,t) in equations (4.2) and (4.3), and the height of the input force will be s = 110 km, which was the height of the input force in the reference model of Chapter 4. Note that the source location is at the base of the vertical portion of the flux tube. The force magnitude is also taken to be the same as in the Chapter 4 reference model, and the boundary conditions on the system are the same as those in Chapter 4.

The fundamental results of the calculations can be seen in Figure (6.1a), which plots the density of the system as a function of distance, s, at 24 different times. The lowest curve is at time 180.54s, and each subsequent plot is at time 180.54s later than the preceding plot. The locations where the flux tube bends, s = d_1 and s = d_2, are indicated. The third vertical line indicates the average final position of the TR. The response to the input force is to eject photospheric and chromospheric material below the TR onto the horizontal section of the flux tube. The density on the horizontal segment of the flux tube is increased substantially over its initial value. It is suggested that this density enhancement corresponds to a fibril.

Figure 6.2a displays the density variation as a function of time at the location s = 8250 km, which is inside the horizontal segment of the flux tube. The density is initially at the coronal value of 5 x 10^{-16} g cm^{-3}, but rises to an average value of 1.1 x 10^{-14} g cm^{-3}.

This density increase corresponds to a temperature decrease from 220,000 K to 10,400 K for a molecular weight of 0.5, as indicated in Figure 6.2b. Note that the temperature of the fibril material is higher than that of the initial undisturbed photosphere and chromosphere, which was at 6230 K for a molecular weight of 1.3. The gas is heated by rebound shocks which develop on the vertical segment of the flux tube at heights lower than $s = d_1$.

Consider the density versus distance plot in Figure 6.1b at late times, where the system is again nearly in hydrostatic equilibrium. The density profile is nearly constant on the horizontal portion of the flux tube. Now at $s = d_2$, the flux tube again turns vertical, and so the effects of gravity are again felt. Thus the density resumes decreasing with distance. The TR has reached its average terminal extent somewhat beyond $s = d_2$, at approximately $s = d_2 + 2050$ km = 16,350 km, corresponding to a height of 5350 km, as evidenced by Figure 6.3. This plug of gas extending beyond the horizontal section and onto the vertical flux tube is a short spicule.

Figure 6.3, which displays the TR location versus distance, gives some insight as to why a full spicule does not develop. The rebound shocks only interact with the TR in two places before the TR reaches d_2; these two places are indicated by arrows in the Figure. Additionally, the shocks lose energy to heat while traveling on the horizontal section of the flux tube. The result is a smaller spicule than that of Chapter 4. Recall that in that case, the TR's motion was characterized by systematic falls in response to gravity before

being pushed upward again by one of the rebound shocks. The smooth motion of the TR in Figure 6.3 results from the zero gravity of the horizontal flux tube section. (Note, however, the TR's velocity is slowed somewhat on the horizontal segment by the rarefaction which develops behind the TR.) During its developing period, ranging between about 5 minutes and 13 minutes, the average velocity of the model fibril is some 25 km s^{-1}. The velocity imparted by the only rebound shock which strikes the TR during the model fibril's development at t = 5 minutes is 60 km s^{-1}.

The velocity of the model fibril's material as a function of time at the height of 8250 km is depicted in Figure 6.4. Note that both positive and negative velocities are present. At long times, there are two oscillation frequencies apparent in the figure. The higher frequency wiggles are at approximately the acoustic cutoff frequency of the chromosphere and photosphere; this frequency has a corresponding period of $2\pi(2c_s)/\gamma g$ = 227s. This value is based on a photospheric and chromospheric temperature of 6230 K and a molecular weight of 1.3; these are the standard conditions used in this model, and that of Chapter 4 (see Hollweg 1982). So the higher frequency wiggles are the response in the horizontal segment to the ringing of the photosphere and chromosphere (i.e., the wake discussed in Chapter 3) induced by the initial impulse in the vertical segment at the base of the flux tube.

The lower frequency variations in Figure 6.4 coincide in frequency and magnitude with density drifts. These density drifts

are most easily noticed by following the oscillations of the density jump indicated by the arrow in Figure 6.1b. The question of why this feature develops is unknown and will not addressed here - it will merely be used as a tracer for the motions of the gas on the flux tube. The fact that the velocity of the tracer coincides with the gas velocity in Figure 6.4 indicates that the tracer is not propagating relative to the gas but is rather a convected contact surface in pressure equilibrium. By following the tracer in Figure 6.1b, or by examining Figure 6.4, a period of approximately 23 minutes can be inferred.

The described motion is believed to occur because the magnetic flux tube supports a standing wave. The following simplified analysis will demonstrate that such a standing wave has the appropriate period. Consider a density profile as a function of distance (denoted by w) consisting of four regions as depicted in Figure 6.5. The bottom region represents photosphere and chromosphere with an exponentially increasing (with depth) density. The region labeled region 1 consists of nearly uniform density; it is taken to represent the horizontal flux tube region. Region 2 is the "short spicule" region, where again the density falls exponentially with height at constant temperature. The final region consists of the hot, tenuous corona. The function of the first and last regions is essentially passive in that they serve to support boundary conditions for the calculations. Specifically, the base region will be taken to be a zero velocity region (because of its high density), and the coronal region is taken to have negligible pressure fluctuations

(because of its low density); thus two conditions are $\delta v(w=0) = 0$, and $\delta p(w=L) = 0$. Regions 1 and 2 are taken to have the same temperatures. The analysis further assumes low frequency waves so that $\omega/\omega_{ac} << 1$, where ω_{ac} is the acoustic cutoff frequency in region 2. There are two propagating waves in region 1 and two evanescent waves in region 2 (since $\omega < \omega_{ac}$ there).

The problem is now one of standard wave reflection analysis. The solutions for the wave velocities, δv, are written down for regions 1 and 2, and the boundary conditions of velocity and pressure continuity are imposed at $w = 1$. The two wave numbers in region 2, given by the dispersion relation for acoustic gravity waves, take on a particularly simply form for the low frequency case being considered. One wavenumber is approximately zero, and the other is approximated by $ik_2 \approx \rho_0 g/p_0$. The equations are then solved to yield the following expression for the wave number in region 1, k_1:

$$-\frac{c_s^2}{g} k_1 \cot k_1 l = \frac{e^{\alpha} - 1}{e^{\alpha} + (\gamma - 1)^{-1}}$$

where

$$\alpha = \frac{g \rho_0}{p_0} (L - l)$$

Now for the oscillations indicated by the tracer in Figure 6.2b, this turns out to be

$$-k_1 l \cot k_1 l \approx 8.8$$

or

$$k_1 l \approx 2.83$$

Taking l = 11000 km, the wavelength of the standing wave is λ = 24,400 km. Using the temperature in the fibril indicated by Figure 6.2b, the period of this wave can be calculated from its wave length and the sound speed. The result is t = 23.6 minutes, which is very close to the measured value.

Discussion

The general concept of the work performed in this chapter is similar to that of the spicule rebound shock model discussed in Chapter 4. Before the input body force response reaches location s = d_1 the results of the two studies are identical. An initial impulse launches an upward propagating wave front followed by an oscillating wave train. Nonlinearly, these waves steepen into a series of upward propagating shocks which impart an upward momentum on the TR. In the Chapter 4 work, the TR continued to rise until the effects of gravity initiated the return of the TR to lower heights. This fall was, however, interrupted by subsequent rebound shocks which again induced an upward velocity to the TR.

This process continued until the TR achieved a new steady state with the TR remaining raised and the material below it resembling a spicule. In the work of this chapter, the displaced TR enters a horizontal magnetic field region at $s = d_1$. The gas moving horizontally does not feel the effects of gravity. Nonetheless, there is some slowing of the gas via the relatively weak process of partially adiabatic (there is some heat input into the gas via shocks) expansion. The TR reaches the end of the horizontal segment of the flux tube ($s = d_2$) before the third shock (the second rebound shock) can catch up to it. (The first rebound shock strikes the TR before the TR reaches $s = d_1$ - this can be seen in Figure 6.2.) During the expansion phase, the average velocity of the TR (25 km s^{-1}) is greater than that of the reference model spicule (16 km s^{-1}) of Chapter 4.

A motivation for the studies of this chapter is to see if the mechanisms of the rebound shock model for spicules can produce fibril-like features on horizontal flux tubes. Unfortunately, the properties of fibrils are not well known, as pointed out in Chapter 1. Thus it is not possible to give a firm correlation between the model results and observations. Some points of comparison will merely be noted. The velocity of the TR in the model is 25 km s^{-1} while it is moving on the horizontal segment. Velocities of the material remaining on the horizontal segment after the TR has left it vary from about -4 to 4 km s^{-1}. The observed velocities on fibrils range from about 20 to 34 km s^{-1}. Fibril densities are observed to be greater than 10^{-13} g cm^{-3} by Foukal (1971b), while Pikelner (1971b)

gives much lower densities (8×10^{-15} g cm^{-3}). The model fibril has a density of about 10^{-14} g cm^{-3}. The model fibril's temperature is about 11000 K, which is somewhat lower than observed fibril temperatures of 18000 to 25000 K.

Full sized spicules due not form on the vertical (third) section of the flux tube in this model. Note that this result is may be consistent with the observations suggesting an absence of spicules in supergranule cell centers, where the third section of the flux tube in the model may exist. A factor in the production of only short spicules is that the rebound shocks must travel a greater distance before reaching the TR than in the Chapter 4 spicule case. The shocks lose some of their energy to heat in transit, and are therefore too weak to generate a larger spicule.

The numerical fibril model of Suematsu (1985) differs from that presented here chiefly in that Suematsu utilizes a loop geometry. A nice feature of his loop model is that it provides for a mechanism by which the fibril material returns to the end of the loop from which it originates. The fibril forms via a pressure pulse at the base of one end of the loop. Material identified with the fibril moves along the loop behind a displaced TR. The return mechanism results from the existence of a TR and chromosphere at the far end of the loop. The coronal gas compressed between the displaced TR and the TR at the far end of the loop eventually leads to the retraction of the fibril. Additional factors leading to the retraction of the material are gravity and shock waves traveling opposite to

the motion of the developing fibril. These shocks result from the partial reflection of shocks off the TR at the far end of the loop.

In contrast, the fibril model of this chapter remains extended at long times a la the spicule in Chapter 4. This occurs because a situation is reached where the gravitational potential energy is balanced by the thermal energy input by shock heating, and there is no dissipation in the system. The fibril retraction could presumably be caused by the addition of radiative loss, heat conduction, and ionization terms in the calculations, in a manner similar to that discussed for spicules in Chapter 4. It should be pointed out that the long time behavior of the Suematsu (1985) model, which also neglects dissipation losses, is unknown. That calculation concluded after the retracted model fibril rebounded off the lower solar atmosphere, and began to extend again.

It is worth noting that observed fibrils do not consistently retract; they are also observed to merge with other fibrils, or fade. Moreover, it is not uncommon for some fibrils to fade without changing their length (Marsh 1976).

The loop fibril model due to Suematsu (1985) did not produce strong rebound shocks. This is because the effect of gravity on the fibril material decreases as the material evolves along the loop. As indicated in Chapter 4, gravity is responsible for the formation of the oscillating wake, and therefore for the rebound shocks, which develop on vertical flux tubes. A consequence of the absence of

strong rebound shocks is that not much heating is supplied to the evolved fibril in the loop model. Thus Suematsu (1985) only obtained temperatures of about 1000 K in his model fibril. The geometry of the flux tube used in the work of this chapter contains a long enough vertical segment above the source location to allow for the generation of strong rebound shocks which eventually heat the fibril material. Thus this model yields temperatures of 11000 K in the fibril. However, partial reflections of the shocks at the $s = d_1$ boundary help prevent shocks from heating the fibril to as high a temperature as the model spicule in Chapter 4. The heating problem would be made more extreme with the inclusion of dissipative losses. Apparently, additional heating must be added to the model to reproduce the observed temperatures of fibrils.

Another limitation on the work here vis-a-vis fibrils is that fibrils on magnetic flux tubes of the suggested geometry would be susceptible to the Rayleigh-Taylor instability, since the model predicts dense material overlying less dense material. The instability question is avoided in this work since it is restricted to one-dimension.

This study has also afforded an opportunity to study oscillations of the gas on the flux tube. The motion is clearly visible in Figure 6.1b, by virtue of a jump in density that develops on the horizontal flux tube. The oscillations extend outward to include the TR also. These oscillations can be understood in terms of standing wave analysis. The procedure involves a study of plane

waves in a four-layer mock density profile selected to represent the density profile of the evolved fibril. The analysis leads to a standing wave with a period of 23 minutes, which corresponds well with the numerical results. It turns out that the "short spicule" component of this profile is quite important in the standing wave analysis. To see this, note that an analysis ignoring the short spicule, i.e. region 2 of Figure 6.6, leaves one with a closed organ pipe problem. In such a case, the fundamental mode is one quarter of a wavelength in region 1, implying a wavelength of 44,000 km. The corresponding wave period would then be 43 minutes. Thus the addition of the "short spicule" layer, even though it is only 2050 km in extent, reduces the period of the standing wave on the flux tube by almost a factor of two.

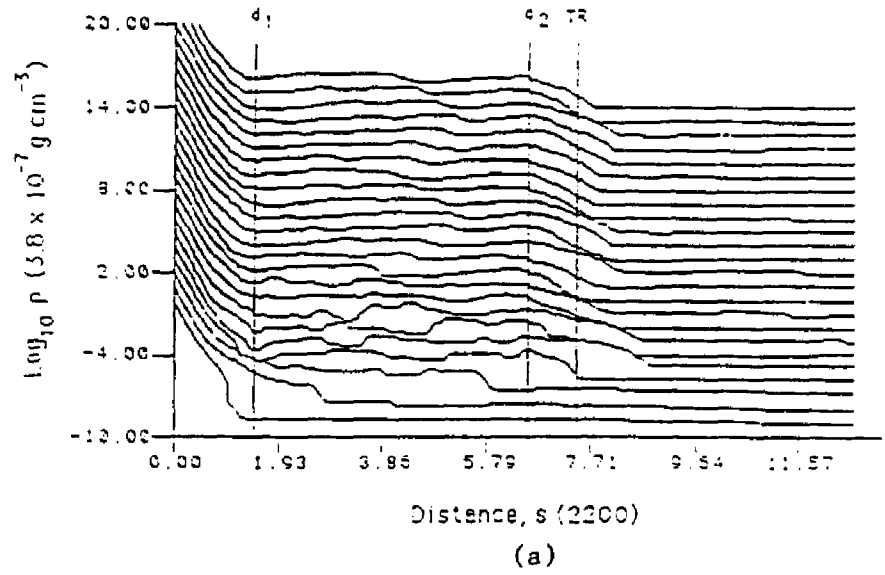

(a)

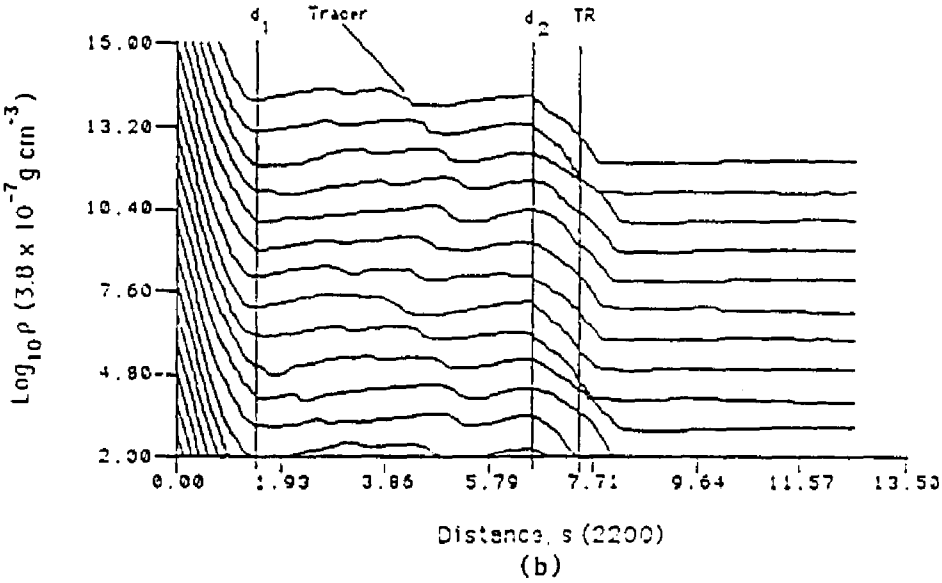

(b)

Fig. 6.1 (a). Density vs. height at 24 different times in the rebound shock model for fibrils. The lowest profile is at t = 180.54 s. Each subsequent profile is 180.54 s later than the profile immediately below it. The vertical scale corresponds to the lowest profile. The calculation is based on a magnetic field geometry which is vertical at its base, horizontal between d_1 and d_2, and vertical beyond d_2. The line labeled TR denotes the average height of the TR after the fibril has achieved its maximum extent. (b). Same as (a), but only at the 13 latest times. Indicated is a blob of gas which acts as a tracer for fluid motions on the flux tube.

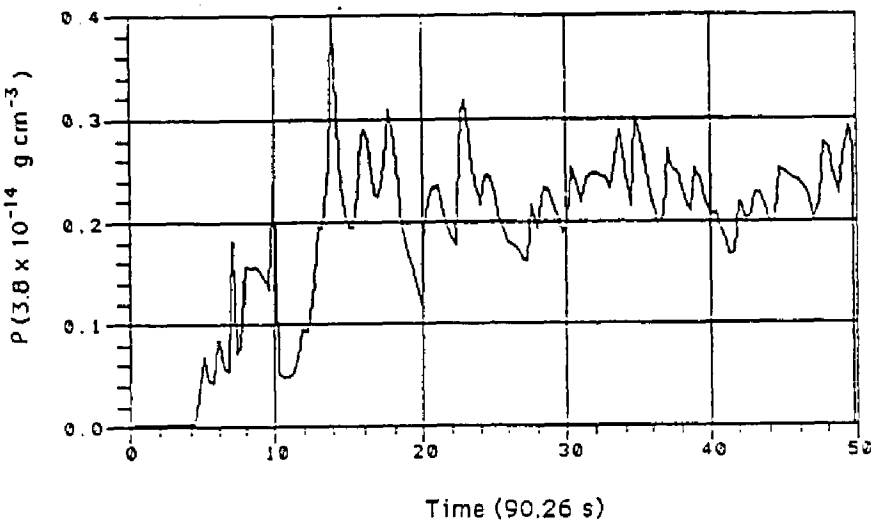

(a)

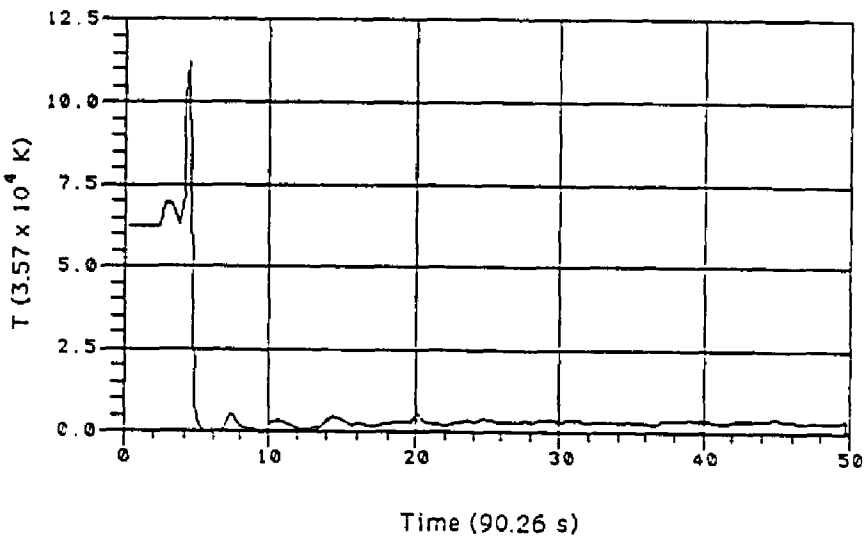

(b)

Fig. 6.2. Density (a) and temperature (b) as a function of time on the horizontal segment of the flux tube (height of 8250 km) in the rebound shock model of fibrils.

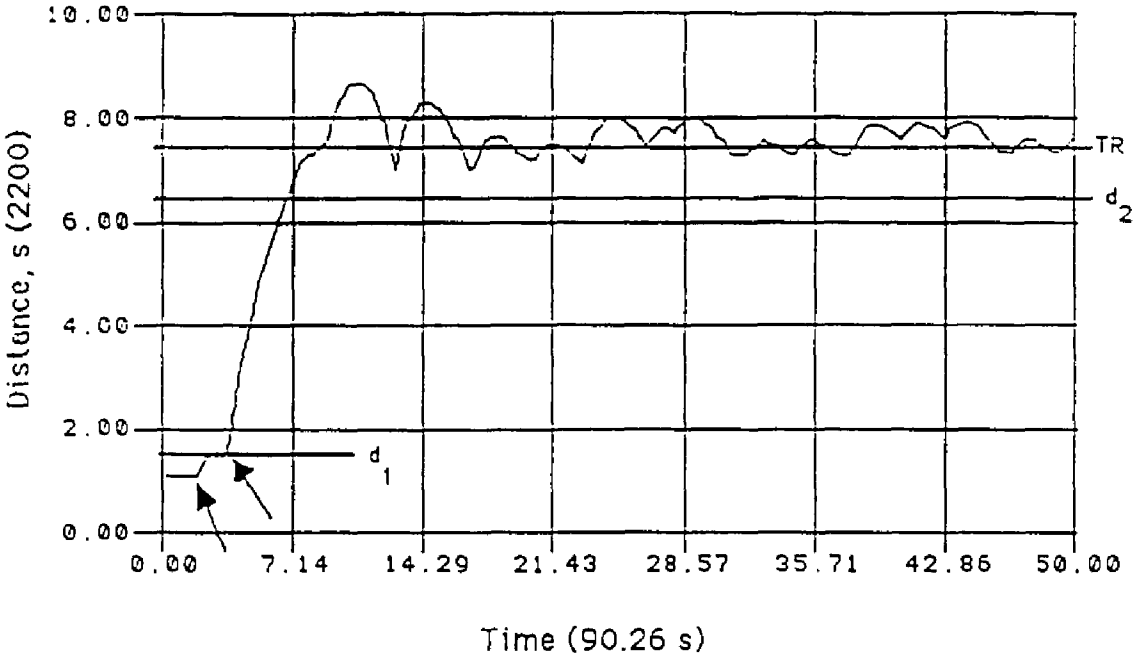

Fig. 6.3. Transition region height as a function of time in the rebound shock model of fibrils. The locations d_1, d_2, and TR are the same as in Fig. 6.1. The arrows indicate the locations where the first two shocks strike the TR.

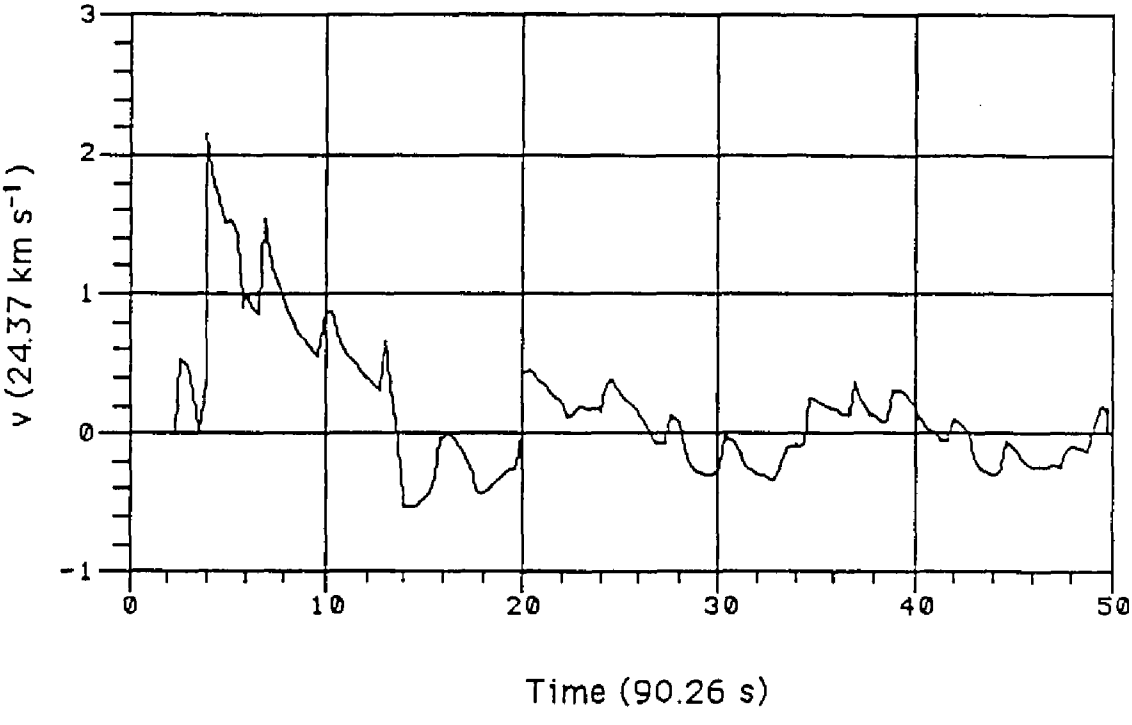

Fig. 6.4. Velocity as a function of time at the same location as in Fig. 6.2.

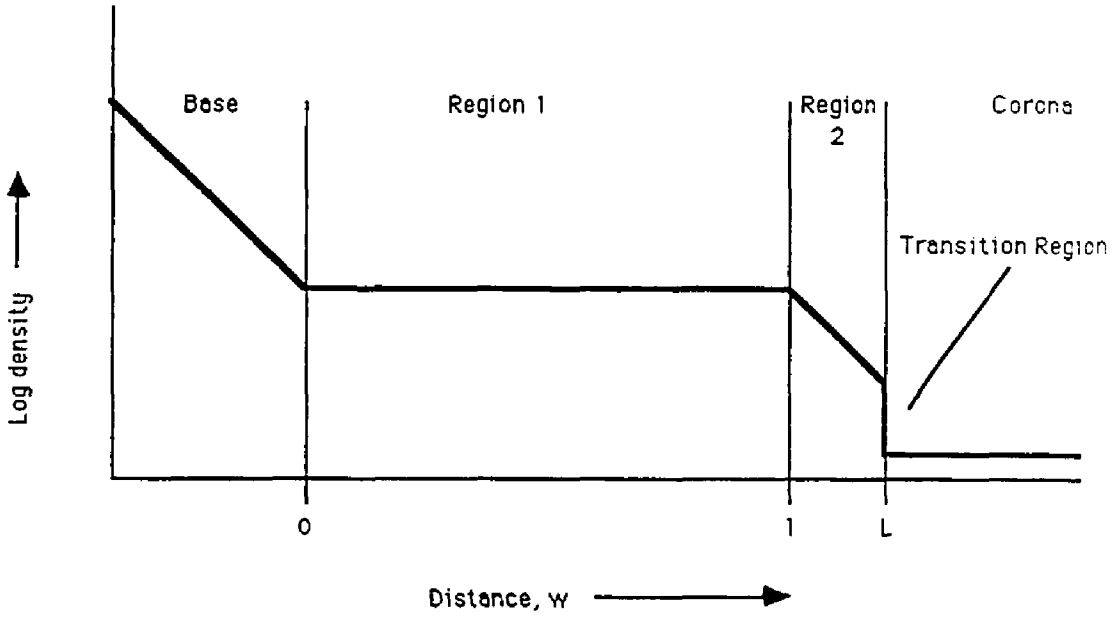

Fig. 6.5. Log density, r, as a function of distance, w, for the standing wave analysis of Chapter 6. The density falls exponentially in the base region, region 2, and in the corona. The scale height in the corona is much larger than that of the base region and region 1, hence the density fall off with height is much slower in the there. Region 1 represents the horizontal section of the flux tube in the rebound shock model of fibrils.

CHAPTER 7

CONCLUSION

Motivations for Studies

One of the primary objectives of solar physics is to understand the sun's atmosphere. Specifically, attempts are being made to understand the energization of and interaction between the various atmospheric regions. This goal is important in terms of the more general objectives of understanding the entire sun, and the sun's effect on the earth and other planets. Furthermore, it is now clear that many stars have solar-like atmospheres, and undergo activity similar to that which occurs on the sun (see Noyes 1985). Study of the solar atmosphere is of great importance in the quest to understand such stars, since the sun is the only star which can be investigated in great detail.

This thesis has concentrated on theoretical aspects of the solar chromosphere. The chromosphere is intimately connected with the other atmospheric regions of the sun. For example, the lower chromosphere is probably heated via waves from the photosphere, while the heating in higher regions may result from processes similar to those which energize the hot corona. Thus the studies carried out in this thesis really relate to the entire solar atmosphere.

Spicules and fibrils play a major role in the dynamics of the chromosphere. There are several reasons why these features are important. Perhaps most notably, the chromosphere appears to be largely (if not entirely) composed of discrete features of the nature of spicules and fibrils. Moreover, spicules and fibrils appear to be magnetically controlled - and this seems to be a common thread between various features throughout the solar atmosphere above the photosphere. Spicules are also important because they apparently play a role in the mass balance of the solar atmosphere, since their upward mass flux is much greater than the outward mass flux of the solar wind (see Chapter 1). Also, the energy requirements of spicules are comparable to those of other regions of the solar atmosphere. Spicules and fibrils are also of interest since they are nonlinear phenomena - such phenomena are probably common in the solar atmosphere, and in other astrophysical contexts.

Summary of Results

This thesis consists of three main sections in which new work is presented. The major work and results may be summarized as follows.

In the first segment (Chapter 4), a model for spicule generation, originally presented by Hollweg (1982), is extended and analyzed. In the model (Hollweg 1982), a spicule results from a

single impulsive body force imparted near the base of a rigid magnetic flux tube in the solar atmosphere. The impulse generates an upward propagating wave train. The wave train subsequently evolves into a series of rebound shocks due to the nonlinear nature of the calculation. The shocks interact with and lift the transition region, and the material below the raised transition region is identified with the spicule. Among the results of the work on the model in this thesis, it was found that at long times the model spicule achieves and maintains a maximum height, and a new hydrostatic equilibrium is approached. This occurs because the model neglects channels of energy dissipation (with the exception of shock heating), such as heat conduction, radiation, and ionization. Thus the energy input into the system via the initial impulse remains in the system at long times as gravitational and thermal energy. Further investigations into the model involved a study of the properties of the resulting spicule as the initial input parameters were varied. It was determined that the model is capable of reproducing observed spicule characteristics, with the exception of temperature, when only the dynamics is considered. The deduced temperatures are higher than those observed in actual spicules. However, if additional energy dissipation effects are taken into account, the final temperatures would be expected to be reduced.

The new equilibrium approached by the spicule in the model suggests a three layer structure in the system consisting of a region of relatively high, but exponentially decreasing density (the photosphere and chromosphere), a region of intermediate density

identified with the spicule, and a region of nearly undisturbed low density corona. Such a structure would have a corresponding three layer Alfven wave speed versus height profile - exponentially increasing in the bottom region, constant in the spicule region, and constant but higher in the corona. In the second part of this thesis, (Chapter 5) the consequences of launching torsional Alfven waves at the base of the flux tube in such a three-layer model were studied. Although partial reflections of the waves occur at the boundary between the bottom and spicule regions, and at the boundary between the spicule and corona, it was found that large energy transmission through the spicule could be achieved when specific resonance frequencies are excited. Thus the spicule can be thought of as a resonance cavity for Alfven waves. When some form of damping of the waves inside the spicule cavity is assumed, the Alfven waves can heat the spicules. It was postulated that the wave dissipation is mediated by a Kelvin-Helmholtz instability, with a subsequent turbulent cascade of the wave energy to higher wave numbers following a Kolmogorov spectrum. Moreover, it was shown that such a Kolmogorov turbulence is consistent with the observed nonthermal motion in spicules. An important aspect of the Alfven wave resonance concept is that the torsional Alfven waves offer an explanation for the reported twisting motions of spicules. The energy entering the spicule via the resonances may lead to additional heating of the spicule, and its subsequent fading in the H_{α}.

The third segment of this thesis (Chapter 6) attempts to investigate fibrils using the spicule model of Chapter 4. The magnetic field geometry in this case is different; it consists of a vertical segment at the base, a horizontal segment above the transition region, and a second vertical segment which heads out into the outer solar atmosphere. It was found that fibril type features can develop on the horizontal segment of the flux tube. The evolving material on the horizontal segment of the flux tube does not feel the effects of gravity. This results in the smooth (compared to the case of the spicule of Chapter 4) motion of the transition region while developing as a fibril. However, the shocks which led to the full spicule in the original spicule model are weakened by dissipation of a portion of their energy on the horizontal segment of the flux tube in the fibril model, and thus only a "short spicule" results on the final vertical segment of the flux tube. Another result, found by studying the long-time behavior of the model, is that a standing wave develops on the fibril flux tube which induces oscillations of the fibril gas. The period of these oscillations is highly influenced by the existence of the "short spicule" on the vertical portion of the flux tube.

Future Prospects

As is often the case in scientific pursuits, the work completed suggests more projects worthy of study. Perhaps the most pressing is the suggestion to reproduce the numerical calculations of

Chapters 4 and 6 with the addition of energy dissipation terms. Although some speculations of the consequences of the addition of these terms were made in Chapter 4, a true spicule or fibril model must await the actual nonlinear numerical calculations with which to compare observations. Another potential project suggested by this thesis is to run the Chapter 4 spicule model calculation with the energy loss terms, plus a uniform heating term in the spicule region. Such a heating term could be fashioned to represent the heating due to Alfven wave resonances of Chapter 5. The author plans to pursue these calculations in the near future.

Any theoretical work provokes the query, are the results related to reality? As far as the projects of this thesis are concerned, there is no definitive answer at this time. The answers can only be found via observations. Unfortunately, current earth based observations of chromospheric fine structure features, such as spicules and fibrils, are of insufficient resolution to unambiguously differentiate between the multitude of theories attempting to describe these features. However, discussions of a space based, high resolution solar observatory are now underway. Eventually, the observations will come to corroborate or refute the theories. In the meantime, the sun will continue to shine.

List of References

Antiochus, S.K. 1984, *Bull. Amer. Astr. Soc.*, **16**, 928.

Athay, R.G. 1976, *The Solar Chromosphere and Corona: Quiet Sun* (Dordrecht: Reidel).

_____. 1984, *Ap. J.*, **287**, 412.

_____. 1985, *Solar Phys.*, **100**, 257.

_____. 1986, in *Physics of the Sun*, Vol. II (P.A. Sturrock et al., eds.), (Dordrecht:Reidel).

Athay, R.G., Gurman, J.B., Henze, W., and Shine, R.A. 1983, *Ap. J.*, **265**, 519.

Athay, R.G. and White, O.R. 1978, *Ap. J.*, **226**, 1135.

_____. 1979, *Ap. J.*, **229**, 1147.

Avrett, E.H. 1981, *Solar Phenomena in Stars and Stellar Systems*, (Bonnet, R.M., and Dupree, A.K., eds.), p. 173 (Dordrecht: Reidel).

Axford, W.I. 1985, *Solar Phys.*, **100**, 575.

Bahcall, J.N. 1985, *Solar Phys.*, **100**, 53.

Beckers, J.M. 1968, *Solar Phys.*, **3**, 367.

_____. 1972, *Ann. Rev. Astr. Ap.*, **10**, 73.

Bessey, R.J., and Kuperus, M. 1970, *Solar Phys.*, **12**, 216.

Bhavilai, R. 1965, *M.N.R.A.S.*, **130**, 411.

Blake, M.L., and Sturrock, P.A. 1985, *Ap. J.*, **290**, 359.

Book, D.L., Boris, J.P., and Hain, K. 1975, *J. Comput. Phys.*, **18**, 248.

Boris, J.P. 1976, *NRL Memorandum Rept.* 3237.

Boris, J.P., and Book, D.L. 1973, *J. Comput. Phys.*, **11**, 38.

_____. 1976, *J. Comput. Phys.*, **20**, 397.

Bray, R.J., and Loughhead, R.E. 1974, *The Solar Chromosphere* (London:Chapman and Hall).

Bruner, E.C. Sr. 1978, *Ap. J.*, **226**, 1140.

Campos, L.M.B.C. 1984, *M.N.R.A.S.*, **207**, 547.

Chen, F.F. 1974, *Introduction to Plasma Physics* (New York:Plenum).

Cook, J.W., Brueckner, G.E., Bartoe, J.-D.F., and Socker, D.G. 1984, *NRL Publication No.* 41-84-119.

Defouw, R.J. 1970, *Solar Phys.*, **14**, 42.

Dere, K.P., Bartoe, J.-D.F., and Brueckner, G.E. 1983, *Ap. J. (Letters)*, **267**, L65.

_____. 1984, *Ap. J.*, **281**, 870.

_____. 1986, *Ap. J.*, **310**, 456.

Dowdy, J.F. Jr., Rabin, D., and Moore, R.L. 1986, *Solar Phys.*, **105**, 35.

Ferraro, V.C.A, and Plumpton, C. 1961, *An Introduction to Magneto-Fluid Mechanics* (London:Oxford).

Foukal P. 1971a, *Solar Phys.*, **19**, 59.

_____. 1971b, *Solar Phys.*, **20**, 298.

Gabriel, A.H. 1976, *Phil. Trans. Roy. Soc. Lond.*, **A. 281**, 339.

Gaizauskas, V. 1984, *Solar Phys.*, **93**, 257.

_____. 1985, in *Chromospheric Diagnostics and Modelling*, (B.W. Lites, ed.) National Solar Observatory Conference Proceedings (NSO/Sacramento Peak, Sunspot, NM).

Gebbie, K.B., Hill, F., Toomre, J., November, L.J., Simon, G.W., Gurman, J.B., Shine, R.A., Woodgate, B.E., Athay, R.G., Bruner, E.C., Rehse, R.A., Tandberg-Hanssen, E.A. 1981, *Ap. J. (Letters)*, **251**, L115.

Gibson, E.G. 1972, *The Quiet Sun*, NASA SP-303 (Washington D.C.).

Gingerich, O., Noyes, R.W., Kalkofen, W., and Cuny, Y. 1971, *Solar Phys.*, **18**, 347.

Giovanelli, R.G. 1974, *Solar Phys.*, **37**, 301.

_____. 1975, *Solar Phys.*, **44**, 299.

_____. 1984, *Secrets of the Sun* (Great Britain:Cambridge)

Hollweg, J.V. 1981, *Solar Phys.*, **70**, 25.

_____. 1982, *Ap. J.*, **257**, 345.

_____. 1984a, *Ap. J.*, **277**, 392.

_____. 1984b, *Solar Phys.*, **91**, 269.

_____. 1985 in *Chromospheric Diagnostics and Modelling*, (B.W. Lites, ed.) National Solar Observatory Conference Proceedings (NSO/Sacramento Peak, Sunspot, NM), p. 235.

Hollweg, J.V., Jackson, S., and Galloway, D. 1982, *Solar Phys.*, **75**, 35.

Hollweg, J.V., and Sterling, A.C. 1984, *Ap.J. (Letters)*, **267**, L65.

Hood, A.W., and Priest, E.R. 1980, *Astron. and Ap.*, **87**, 126.

Ionson, J.A. 1982, *Ap. J.*, **254**, 318.

_____. 1984, *Ap. J.*, **276**, 357.

Jeffrey, A., and Taniuti, T. 1964, *Non-Linear Wave Propagation* (New York: Academic).

Jordan, S. 1981, ed., *The Sun as a Star*, NASA SP-450 (Washington D.C.).

Kopp, R.A. and Kuperus, M. 1968, *Solar Phys.*, **4**, 212.

Krat, V.A., and Krat T.V. 1971, *Solar Phys.*, **17**, 355.

Kuperus, M., and Athay, R.G. 1967, *Solar Phys.*, **1**, 361.

Landau, L.D., Lifshits, E.M., and Pitaevskii, L.P. 1984, *Electrodynamics of Continuous Media* (Elmsford, New York:Pergamon).

Livshits, M.A. 1967, *Soviet Astr.*-AJ, **10**, 570.

Lynch, D.K., Beckers, J.M., and Dunn, R.B. 1973, *Solar Phys.*, **30**, 63.

Mamedov, S.G. and Orudzhev, E.Sh. 1978, *Sov. Astron.*, **22**(4) 451.

_____. 1983, *Sov. Astron.*, **27**(6), 692.

Mariska, J.T. 1986, *Ann. Rev. Astron. Ap.*, **24**, 23.

Mariska, J.T., and Hollweg, J.V. 1985, *Ap. J.*, **296**, 746.

Marsh, K.A. 1976, *Solar Phys.*, **50**, 37.

Michard, R. 1974, *IAU Symp.*, **56**, 3.

Moore, R.L. 1986, private communication.

Morse, P.M., and Feshbach, H. 1953, *Methods of Theoretical Physics*, (New York: McGraw-Hill), Section 11.1.

Muller, R. 1985, *Solar Phys.* **100**, 237.

Newman, M.J. 1986, in *Physics of the Sun*, Vol. III (P.A. Sturrock et al., eds.), (Dordrecht:Reidel).

Nikolskii, G.M. 1970, *Solar Phys.* **12**, 379.

Noyes, R.W. 1985, *Solar Phys.*, **100**, 385.

Osterbrock, D.E. 1961, *Ap. J.*, **134**, 347.

Parker, E.N. 1964, *Ap. J.*, **134**, 347.

_____. 1979, *Cosmical Magnetic Fields* (England:Oxford).

_____.1982, *Geophys. Ap. Fluid Dyn.*, **22**, 195.

Pasachoff, J.M., Noyes, R.W., Beckers, J.M. 1968, *Solar Phys.*, **5**, 131.

Piddington, J.H. 1956, *M.N.R.A.S.*, **116**, 314.

_____. 1981, *Space Sci.*, **75**, 273.

Pikel'ner, S.B. 1969, *Soviet Astron.*, 13, 259.

_____. 1971a, *Comm. Ap. and Space Sci.*, **3**, 33.

_____. 1971b, *Solar Phys.* **20**, 286.

Pneuman, G.W., and Kopp, R.A. 1978, *Solar Phys.*, **57**, 49.

Pneuman, G.W., and Orrall, F.Q. 1986, in *Physics of the Sun*, Vol. II (P.A. Sturrock et al., eds.), (Dordrecht:Reidel).

Priest, E.R. 1982, *Solar Magnetohydrodynamics* (Dordrecht:Reidel).

Rabin, D., and Moore, R.L. 1980, *Ap. J.*, **241**, 394.

_____.1984, *Ap. J.*, **285**, 359.

Rae, I.C., and Roberts, B. 1982, *Ap. J.*, **256**, 761.

Roberts, B. 1979, *Solar Phys.*, **61**, 23.

_____. 1983, in *Solar and Magnetic Fields: Origins and Coronal Effects* (J.O. Stenflo, ed.), IAU, p. 61.

Roberts, P.H. 1967, *An Introduction to Magnetohydrodynamics* (London:Longmans).

Roberts, W.O. 1945, *Ap. J.*, **101**, 136.

Rosner, R., Tucker, W.H., and Vaiana, G.S. 1978, *Ap. J.*, **220**, 643.

Roussel-Dupre, D. and Shine, R.A. 1982, *Solar Phys.*, **77**, 329.

Schatten, K.H., and Mayr, H.G. 1986, *Ap. J.*, **309**, 864.

Secchi, P.A. 1877, *Le Soleil*, Vol. 2, Chap. II (Paris:Gauthier-Villars).

Solar Physics 1985, **100** (Dordrecht:Reidel).

Stein, R.F., and Schwartz, R.A. 1972, *Ap. J.*, **177**, 807.

Sterling, A.C., and Hollweg, J.V. 1984, *Ap. J.*, **285**, 843.

Sturrock, P.A., Holzer, T.E., Mihalas, D.M., and Ulrich, R.K. (eds) 1986, *Physics of the Sun*, Vol. I, II, and III (Dordrecht:Reidel).

Suematsu, Y. 1985, *Solar Phys.*, **98**, 67.

Suematsu, Y., Shibata, K., Nishikawa, T., and Kitai, R. 1982, *Solar Phys.*,**75**, 99.

Title, A., Tarbell, T., and the SOUP Team 1987, in *Theoretical Problems in High Resolution Solar Physics* II (Athay, G. and Spicer, D.S., eds), NASA Conference Publ. 2483 (Washington D.C.).

Tsirul'nik, L.B. 1983, *Sov. Astron.*, **27**(4), 411.

Uchida, Y. 1961, *Publ. Astron. Soc. Japan*, **13**, 321.

_____. 1969, *Publ. Astron. Soc. Japan*, **21**, 128.

Unno, W., and Kawabata, K. 1955, *Publ. Astr. Soc. Japan*, **7**, 21.

Vernazza, J.E., Avrett, E.H., and Loeser, R. 1973, *Ap. J.*, **184**, 605.

Weart, S.R. 1970, *Solar Phys.*, **14**, 310.

Wentzel, D.G., and Solinger, A.B. 1967, *Ap. J.*, **148**, 877.

Withbroe, G.L. 1976 in *IAU Colloquium 36, Energy Balance and Hydrodynamics of the Solar Chromosphere and Corona*, ed. R.M. Bonnet and P. Delache (Paris:Clermont-Ferrand), p.263.

_____. 1983, *Ap. J.*, **267**, 825.

Withbroe, G.L., and Noyes, R.W. 1977, *Ann. Rev. Astron. Ap.*, **15**, 363.

Zirin, H. 1966, *The Solar Atmosphere*, (Waltham, Mass:Blaisdell).

Zirker, J.B. 1967, *Solar Phys.*, **1**, 204.

Zirker, J.B. (ed.) 1977, *Coronal Holes and High Wind Streams, Skylab Workshop I* (Colorado Associated University Press).

Zugzda, Y.D., and Locans, V. 1982, *Solar Phys.*, **76**, 77.